SYNTHESIS AND COORDINATION CHEMISTRY OF NOVEL LIGANDS FOR METALLOSUPRAMOLECULAR ASSEMBLY

ROBERT ALAN FAULKNER

University of HUDDERSFIELD

A thesis submitted to the University of Huddersfield in partial fulfilment of the requirements for the degree of Doctor of Philosophy

The University of Huddersfield

September 2016

Copyright Statement:

Acknowledgements

A little over four years ago in a packed lecture theatre at the University of Huddersfield, I sat and listened to my PhD supervisor give a public lecture entitled ‘From the bottom up: Self-assembly in Chemical Systems’. As the lecture drew to a close, Professor Craig Rice began his acknowledgements with the phrase ‘We stand on the shoulders of giants’. Whilst the phrase is usually used by many people across the world to reference the greats or geniuses of a field (such as Newton in physics, Mozart in music or Turing in computing), at this moment it was meant differently. The next few minutes were used to highlight and thank the people Craig considered giants and he unpretentiously referred to his project, placement and PhD students. It was the mark of an individual who recognised the position he had reached, yet who also fully acknowledged the assistance and work ethic of those around him that had contributed to his achievements.

Now it is my turn to say thank you to the giants whose shoulders I have stood on or leant on over the years, who have each in their own significant way contributed to the completion of this PhD thesis.

To begin with I would like to thank my supervisor Professor Craig R. Rice for his constant support both inside and outside of the laboratory throughout my time at Huddersfield. Without his support, assistance and wisdom, none of the work detailed within would have been possible.

Secondly, I would like to say thank you to all current and previous members of the Rice research group. Whether a project student (Mark, Gage, Pavlina, Liam and Josh), a placement student (Jasmine, John, Ben and Ross) or a PhD student (Becca, Samantha and Josh) I am indebted to them for their support, teaching, contributions and friendship. I would like to say a special thank you to Francesca Davidson and Christopher Slater whose tolerance and support in the closing stages of this research, and the writing up period of this thesis in particular was outstanding.

Further to this I would like to thank my family for their support both financially and emotionally. Without their continual support and tolerance of me, the completion of this thesis would have been far from a foregone conclusion. In particular, I would like to say a special thank you to my mum Lynn and my sister Helen. Thank you for keeping me (in)sane.

I would also like to thank the people who I am lucky enough to call friends. Alessandro, Ben, Catherine, Gareth, Jasmine, Lorna, Ruth, Vanessa and the greatest non-scientific proof reader in the world, Sarah. They have picked me up, motivated me and kept me laughing throughout the last four years. Thank you!

I give my final thanks to my Lord and saviour Jesus Christ for leading me through all of the difficulties of life and research and guiding me through to the completion of this thesis. I shall forever be thankful that through some of my hardest and darkest times, I found my way to faith and back to the light. To you be glory and praise forever.

Abstract

Described herein is the synthesis and coordination chemistry of several novel polydentate ligand strands **L^1** – **L^7**. Upon reaction with transition metal ions, these ligand strands form various metallosupramolecular assemblies ranging from mononuclear species to an infinite honeycomb-like structure comprised of circular helicates.

Described in chapter two is the potentially hexadentate, ditopic ligand strand **L^1** (Fig. 1). Reaction of **L^1** with copper (II) metal ions results in the formation of the dinuclear complex $[Cu_2(\mathbf{L^1})(ClO_4)_2(MeCN)_4]^{2+}$. However, adjusting the metal to ligand stoichiometry gives rise to the dinuclear complex $[Cu_2(\mathbf{L^1})_3]^{4+}$. Reacting **L^1** with cadmium (II) and europium (III) metal ions results in the formation of the complexes $[Cd(\mathbf{L^1})_2]^{2+}$ and $[Eu(\mathbf{L^1})_2(CF_3SO_3)]^{2+}$ respectively. However, reacting **L^1** with europium (III) and silver (I) metal ions results in the creation of the tetranuclear dimetallic assembly $[Eu_2Ag_2(\mathbf{L^1})_3(CF_3SO_3)_8]$. Reacting **L^1** with rhenium (I) pentacarbonyl chloride gives the *ter*-$\mathbf{L^1}ReCl(CO)_3$ complex in which the rhenium (I) metal centre coordinates to the terminal pyridyl-pyrimidine bidentate domain of the ligand. However, through the use of a lanthanide ion as a template, the position the rhenium (I) metal centre is coordinated to can be controlled and this allows for the creation of the *cent*-$\mathbf{L^1}ReCl(CO)_3$ species. In this complex, the rhenium (I) metal ion coordinates to the central bipyrimidine domain, leaving the remaining tetradentate site uncoordinated and suitable for the binding of transition metal ions.

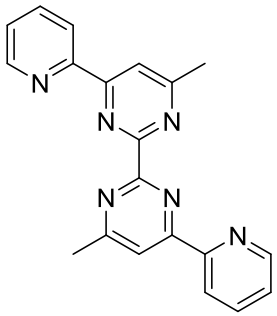

L^1

*Fig. 1: A schematic representation of the ligand strand **L^1** whose synthesis and coordination chemistry will be reported and discussed in chapter two.*

Described in chapter three are the polydentate ligand strands **L²** – **L⁴** (Fig. 2) whose reaction with transition metal ions result in the formation of various circular helicate assemblies. Reaction of **L²** with zinc (II) metal ions results in the formation of the tetranuclear circular helicate species $[Zn_4(\mathbf{L^2})_4]^{8+}$.[1] Reaction of **L³** with zinc (II) metal ions results in the formation of the pentanuclear circular helicate species $[Zn_5(\mathbf{L^3})_5]^{10+}$. The change in nuclearity between the two complexes is attributed to the replacement of the –OH group on the central aromatic spacer in **L²**, with an –OMe group in **L³**. This prevents the hydrogen bonding observed in the core of the tetranuclear assembly and results in the formation of the larger pentanuclear circular helicate. Reaction of **L⁴** with copper (II) metal ions gives a pentanuclear circular helicate assembly, $[Cu_5(\mathbf{L^4})_5]^{10+}$, but due to the unsymmetrical nature of the ligand strand, a head-to-tail binding conformation is achieved.

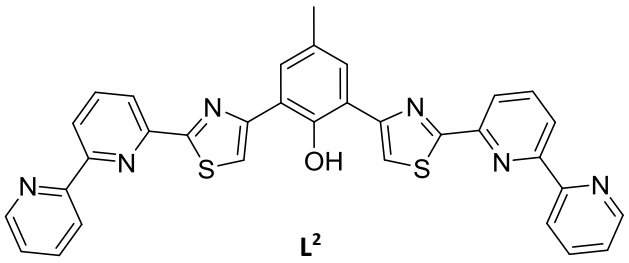

L²

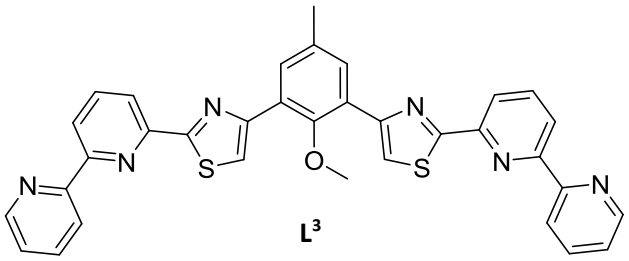

L³

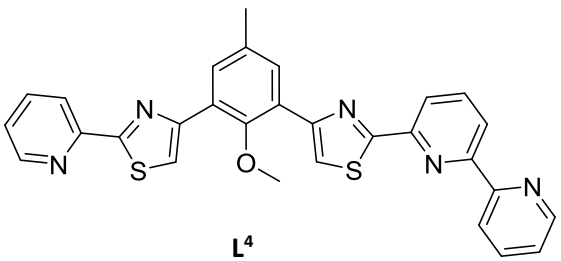

L⁴

*Fig. 2: Schematic representations of the ligand strands **L² – L⁴** whose synthesis and coordination chemistry will be reported and discussed in chapter three.*

Described in chapter four are the polydentate ligand strands **L^5** – **L^7**, which form various metallosupramolecular assemblies upon reaction with silver (I) metal ions. Reaction of **L^5** with silver (I) metal ions results in the formation of the dinuclear mesocate species $[Ag_2(\mathbf{L^5})_2]^{2+}$. The mesocate species is believed to be a result of the hydrogen bonding from the –OH group of the aromatic spacer to the nitrogen atom of the uncoordinated thiazole domain. Reaction of **L^6** with silver (I) metal ions forms the one-dimensional helical polymer species $[Ag_n(\mathbf{L^6})_n]^{n+}$ and the phenyl ring substituent on the aromatic spacer promotes the polymeric species through π-stacking interactions. Reaction of **L^7** with silver (I) gives the three-dimensional infinite honeycomb-like polymer $[Ag_6(\mathbf{L^7})_6]^{6+}]_n$ made up of individual hexanuclear circular helicate units all connected together via inter-assembly Ag···Ag interactions. However, reaction of **L^7** with copper (I) metal ions gives the hexanuclear circular species $[Cu_6(\mathbf{L^7})_6]^{6+}$ and no polymeric effects are observed.

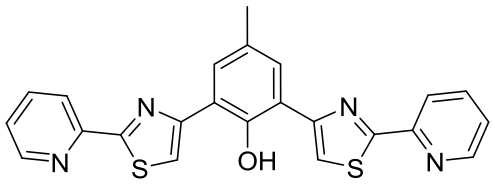

L^5

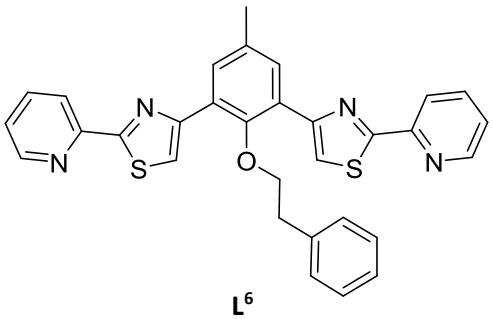

L^6

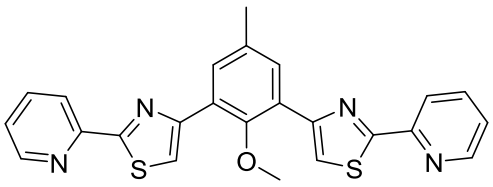

L^7

*Fig. 3: Schematic representations of the ligand strands **L^5** – **L^7** whose synthesis and coordination chemistry will be reported and discussed in chapter four.*

Contents

List of Abbreviations

Å	Angstrom
ar	Aromatic
°C	Degrees Celsius
cent-	Central
d	Doublet
DCM	Dichloromethane
ddd	Doublet of doublets of doublets
DMF	Dimethylformamide
dt	Doublet of triplets
EDTA	Ethylenediaminetetraacetic acid
ESI-MS	Electrospray ionisation mass spectrometry
EtOH	Ethanol
g	Gram
HCl	Hydrochloric acid
HI	Hydroiodic acid
HRMS	High resolution mass spectrometry
Hz	Hertz
J	Coupling constant
K	Degrees Kelvin
m	Multiplet
m/z	Mass/charge ratio
mg	Milligram
MHz	Megahertz
mL	Millilitre

mmol	Millimole
mol	Moles
MS	Mass spectrometry
NMR	Nuclear magnetic resonance
ph	Phenyl
ppm	Parts per million
py	Pyridyl
pyr	Pyrimidine
RT	Room temperature
s	Singlet
sp. gr.	Specific gravity
td	Triplet of doublets
ter-	Terminal
THF	Tetrahydrofuran
TLC	Thin layer chromatography
TOF MS	Time of flight
TOF-q MS	Time of flight/triple quadrupole hybrid mass spectrometry
tz	Thiazole
δ	Delta (chemical shift)

List of Figures

1 Introduction

1.1 In the beginning. . .

The genesis of supramolecular chemistry can arguably be traced back to the discovery of the molecular structure of deoxyribose nucleic acid (or DNA) by Watson, Crick, Franklin and Gosling. Being possibly the most famous supramolecular structure of all time, the double helix of DNA is a visually stunning example of how the natural world has shown its ability to create beautiful molecular architectures. The structure itself possesses incredibly intricate levels of design and functionality and as a result, a virtually infinite amount of chemical information is stored within the self-assembled system so that it is able to store the code of life.[2] Discovery of the molecular structure allowed the inner workings of the double helix to be explored. Each ribbon-like strand of the helix is comprised of phosphate sugars, providing a backbone for the base pairs adenine (A), thymine (T), guanine (G) and cytosine (C). These base pairs undergo hydrogen bonding to the base pairs of another ribbon of phosphate sugars, connecting the ribbons together and giving rise to the entwined double helix (Fig. 4).

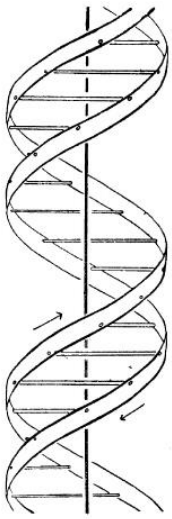

Fig. 4: An image of the molecular structure of deoxyribose nucleic acid suggested by Watson and Crick in 1953. Each helical ribbon represents a backbone of phosphate sugars and the horizontal rods represent the base pairs connecting each strand of the double helix together. The vertical line passing down the centre indicates the axis of the structure.[3]

However, on closer inspection it was observed that the purine base pairs, adenine (A) and guanine (G), would hydrogen bond specifically to the pyrimidine base pairs, thymine (T) and cytosine (C), and also exclusively to one another in the order A to T and G to C. This was attributed to the complementary nature of the donor and acceptor functional units within the base pairs e.g. adenine and thymine form two hydrogen bonds between one another and guanine and cytosine form three (Fig. 5). This 'lock and key' principle seemed simple yet showed an astonishing level of selectivity and specificity in a self-replicating and entirely self-assembled supramolecular structure.[3–7]

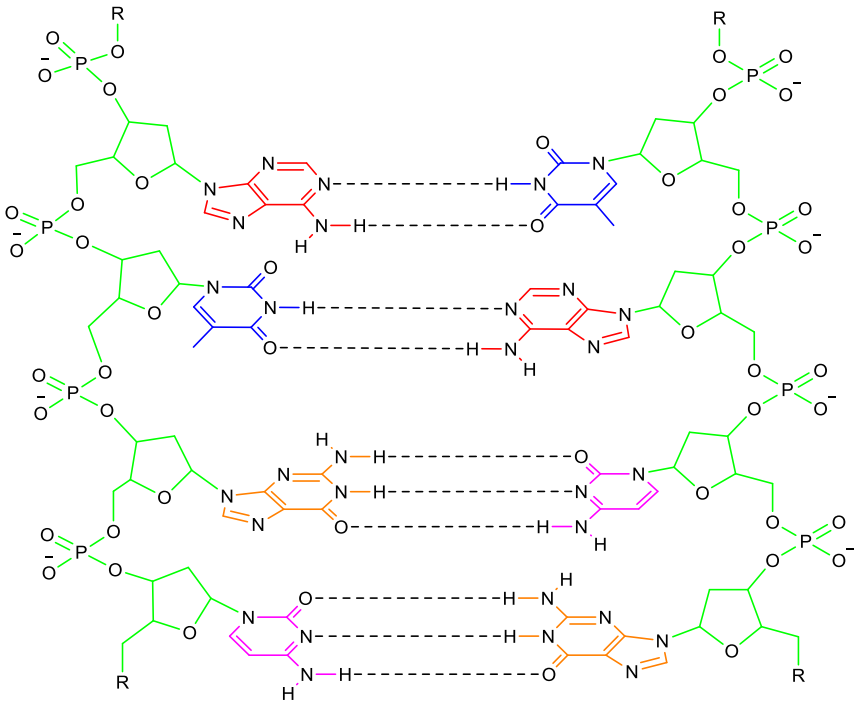

Fig. 5: Schematic representation of the molecular structure of a partial section of deoxyribose nucleic acid, showing the complementary nature of hydrogen bonding between the nucleic acid base pairs. This representation shows how the hydrogen bonding (dashed lines) between the base pairs is selectively between certain base pairs, as only two hydrogen bonds can form between adenine (red) and thymine (blue) whilst three can form between guanine (orange) and cytosine (pink). R = the continuation of the phosphate backbone (green).

Discoveries of molecular structures from the natural world, such as that of DNA, have inspired scientists all over the world into first understanding and then manipulating the forces that control their formation in attempts to create their own synthetic super structures.[8,9] Three such scientists were the chemists Donald J. Cram, Jean-Marie Lehn and Charles J. Pedersen who were jointly

awarded the Nobel Prize in 1987 for "their development and use of molecules with structure-specific interactions of high selectivity". Whilst their research and findings collectively contributed to the dawn of supramolecular chemistry as a major field, their individual works were significantly different.

1.2 Be my guest. . .

Cram *et al.* were responsible for the initial developments into an area of supramolecular chemistry which they called 'Host-Guest Chemistry'.[8,10] Host-guest chemistry is based upon the notion that a highly structured molecular species will have at least one host module and one guest module within it. Cram defined that the host constituent would be "an organic molecule or ion whose binding sites *converge* in the complex", whilst the guest constituent would be "any molecule or ion whose binding sites *diverge* in the complex" (Fig. 6).[11]

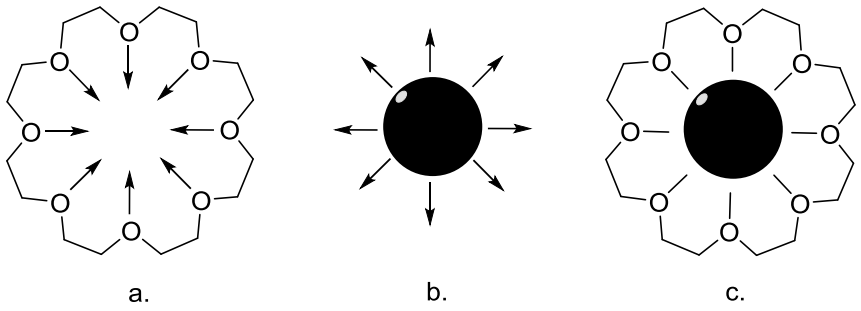

Fig. 6: A schematic representation showing the convergence and divergence of binding sites in host and guest components. a. A host molecule with binding sites converging to a singular point, b. a guest molecule whose binding sites are diverging away from a singular point and c. an organic host molecule with a guest bound in its centre due to a complementary convergence and divergence of binding sites.

Due to the nature of the binding sites of hosts being convergent, they have to be designed and synthesized to possess higher levels of organization so that the binding sites can converge in on a singular point (such as a complementary guest) and generally this contributes to hosts being bigger than their guest counterparts.[8]

1.3 Crowns from the ether

Pedersen reported the creation of thirty-three different cyclic polyethers (or crown ethers) ranging from molecules with nine to sixty atoms and including three to twenty oxygen atoms in the ring (Fig. 7). With the oxygen atoms positioned facing into the ring, the potential for these crown ethers to bind positively charged alkali metals through ion-dipole interactions in their centres became apparent and complexes were formed with many different cations. The assortment of metal ions that were bound ranged from the relatively small lithium (I) and sodium (I) cations, through to the much larger mercury (II) and cerium (III) ions and even on to ammonium and alkyl ammonium cations. It had not only been demonstrated that it was possible to bind metal ions into these crown ether molecules but by changing the size of the ring and the number of oxygen atoms in the ring, it was possible to accommodate different sized cations in the complexes.[12]

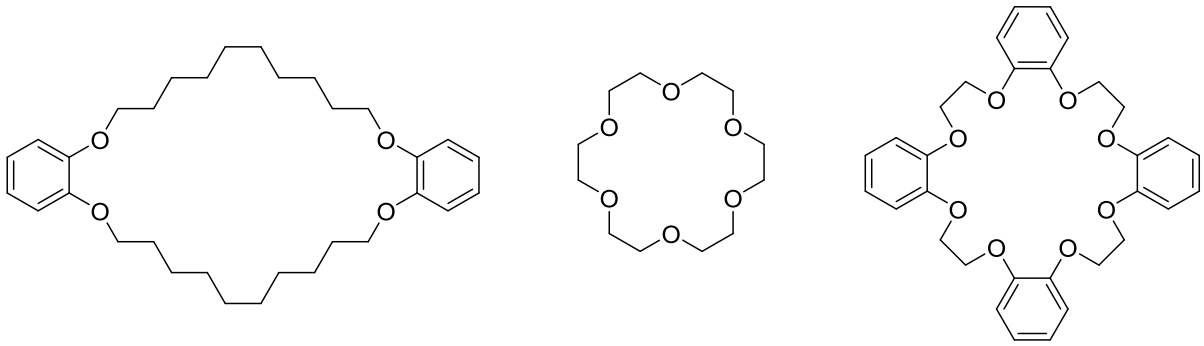

Fig. 7: Schematic representations of a selection of cyclic polyethers, or crown ethers, reported by Pedersen in 1967.[12]

1.4 Specifically Selective Spherands

As well as developing Pedersen's work further by creating chiral crown ethers[13–17], Cram *et al.* also developed a type of host molecule known as a spherand (Fig. 8). Spherands are rigid host molecules that are heavily preordered so that the binding pairs of electrons from their donor atoms line the spherical cavity in the centre and provide an environment for the guest to bind in.[8]

By being such a completely preorganised and rigid motif, the crystal structures of the host spherand on its own and then bound with a guest as part of a complex were virtually identical except for the obvious presence of the guest component in the centre. This stringent preorganisation and inflexibility gives spherands the higher level of organisation they require for a host molecule to converge its binding sites on a central point and successfully bind a guest.[8]

Kaneda *et al.* demonstrated how such strict control over the structure of a spherand could result in "perfect selectivity". They created a spherand which only formed a complex with lithium (I) ions by restricting the size of both the entrances and the central cavity itself to only marginally larger than those of lithium ions. On complexing with this cation a colour change from yellow to violet took place yet there was no evidence of complexation with any of the other fifty-eight different metal ions and salts they experimented with, suggesting a definitive selectivity solely to lithium (I) ions (Fig. 8 c.).[18]

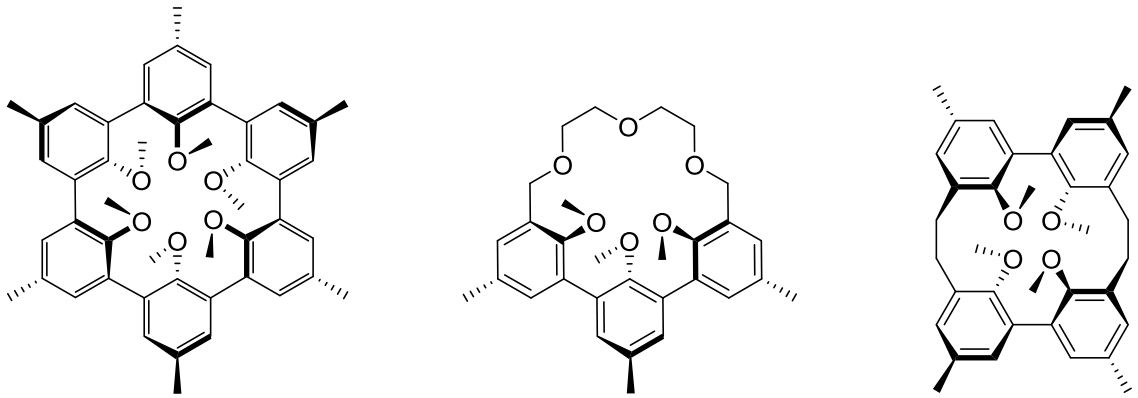

a. b. c.

Fig. 8: Schematic representations of a. a spherand and b. a hemispherand reported by Cram et al.[7] c. The spherand reported by Kaneda et al. that demonstrated "Perfect selectivity" with lithium ions.[17]

1.5 Tales from the Cryptates

Similar to spherands are a class of host molecules called cryptates and these were first reported in a seminal paper by Lehn *et al.* in 1969.[19] Cryptates bear similarities to spherands in that they are highly ordered host molecules that possess a domain within them intended to bind a guest component. However, whilst spherands have an almost entirely spherical and rigid motif, cryptates are generally more flexible. The first cryptate reported by Lehn *et al.* possessed three chains comprised of ether linkages (similar to those observed in crown ether compounds) connected to nitrogen atom bridgeheads resulting in a cavity in the centre (Fig. 9 a.).[19] Since then various other derivatives of cryptates have been designed and synthesised increasing the number and the lengths of the chains of ether linkages and replacing the connecting nitrogen atom bridgeheads with other atoms (Fig. 9 b. and c.).[20]

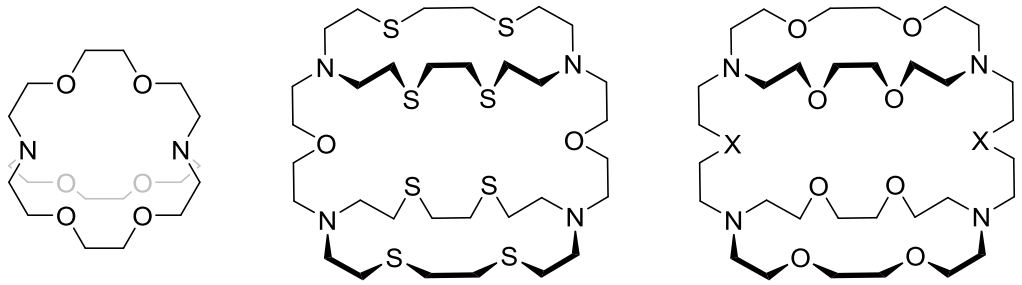

Fig. 9: Schematic representations of several cryptates reported by Lehn et al. a. The original cryptate reported by Lehn et al. in 1969,[19] b. and c. variations upon the original cryptate showing different atom types within these linkages and different group types at the bridgehead. In c. X = O, CH_2, σ-phenylene or NH.[20]

Changing the size of the cavity inside the cryptate by changing the number of ether linkages in a chain and/or increasing the number of chains in the molecule, provided a pathway to study interactions between cations by enabling the cryptates to bind more than one cation. If the distances between the cations were sufficient then substrates could even bridge the cations. This flexibility for the structure to be adjusted so that more than one guest could be bound within, ultimately resulted in cryptates being used as molecular reaction vessels to study various aspects of chemistry ranging from catalysis to molecular receptors.[20]

The previous examples discussed here all use ion-dipole interactions to form the host-guest assembly and these interactions use a polarised atom or species such as an ether or amine, to interact with a cation, such as an s-block metal ion or an ammonium ion. However, host-guest interactions are not limited to just ion-dipole interactions as other forms of attractive intermolecular interactions can be employed. One example of such an interaction is π-π stacking.

1.6 Anyone for π. . . stacking?

π-π stacking interactions are a non-covalent attraction interaction that is observed between aromatic rings in molecules. When the geometries of the aromatic systems bring them into a face-to-face contact with one another, their π-systems align, thereby creating an attraction. Whilst perfect alignment between ring-planes is quite rare, an offset or slipped stacking alignment is more common and still entirely capable of forming the interaction. This interaction is also notably observed between the base pairs in the centre of DNA and helps influence its characteristically compact structure.[21–23]

A powerful example of the influence of π-π stacking interactions was demonstrated by Sygula *et al.* when they reported a 'Buckycatcher' capable of binding a molecule of C^{60} Buckminsterfullerene. (Fig. 10).[24]

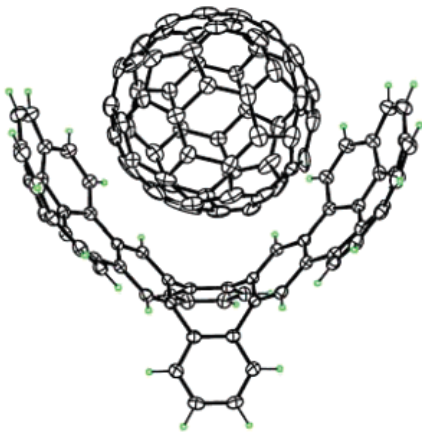

Fig. 10: The crystal structure of the 'Double Concave Hydrocarbon Buckycatcher' that could hold a C_{60} Buckminsterfullerene molecule by π-π stacking interactions reported by Sygula et al. [24]

They produced a type of molecular tweezer (Fig. 11 a.) comprised of sixty carbon atoms which included two corannulene sub-units capable of forming a concave pocket for the C_{60} to bind in via π-π interactions. With the two branches of corannulene subunits present, different conformations of the proposed molecule were possible as both sub-units could adopt a concave, a convex or an alternate concave-convex geometry (Fig. 11 b. - d.). However, through the binding strength of the π-π interactions between the convex 'buckyball' and the concave faces of the appropriately aligned corannulene sub-units of the 'buckycatcher', the concave-concave conformation proved to be the preferred arrangement and was successful in binding the fullerene molecule (Fig. 10).[24]

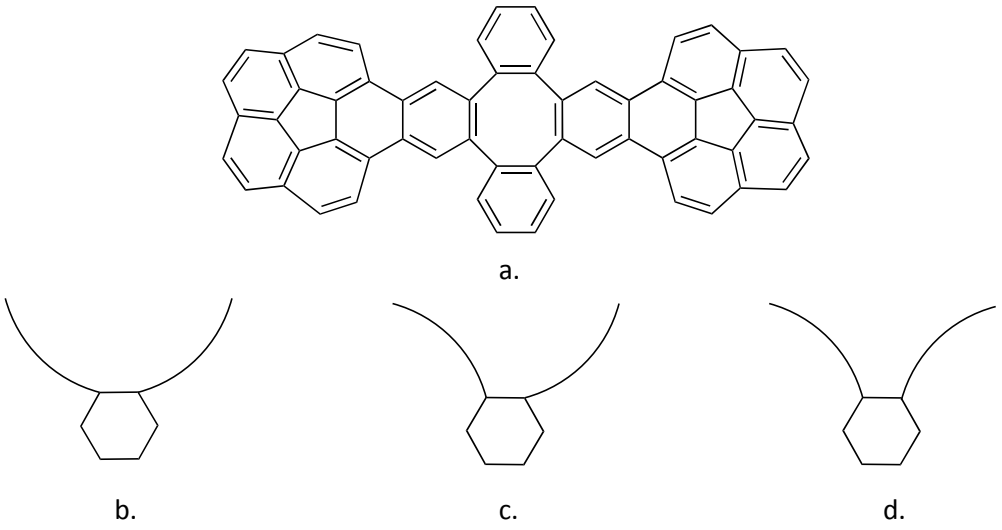

Fig. 11: a. The molecular tweezer developed by Sygula et al capable of binding Buckminsterfullerene in its centre via π-π stacking interactions and schematic representations of b. the molecules concave-concave, c. concave-convex and d. convex-convex conformations.[24]

Whilst all previous examples reported here focus on the formation of complexes through 'host-guest' chemistry, an alternative method of complex formation called molecular self-assembly is also well documented and has seen significant advances in recent years.[25]

1.7 Self-assembly: ". . .so it just does it itself?"

Molecular self-assembly is the general term for a process in which a disordered system spontaneously forms a larger organized molecular unit from smaller subunits. Generally the smaller sub-units are sufficiently programmed so that through directed interactions between themselves (such as hydrogen bonding, electrostatic interactions, π-π stacking, van der Waals forces, etc.), a single, larger supramolecular species is generated. The assembling process of these systems is kinetically fast, replicable and at the same time completely reversible. The reversibility and reproducibility of these reactions allows for the structures to assemble, disassemble and then reassemble depending on the conditions the structure and its components are in. This allows these systems to achieve the most thermodynamically stable product possible.[26,27]

There are many examples of self-assembly throughout the sciences ranging from biological systems using peptides and proteins for nano-technological applications,[28,29] to the design of organic materials[30] and even the assembly of the recently discovered wonder-material graphene[31] into nanostructures[32] and helical nanotubes[33]. However, all of these assemblies are examples of the self-assembly that forms between organic molecules by generally relying on π-π stacking interactions and electrostatic interactions such as ion-dipole and dipole-dipole. Yet there is another form of self-assembly that involves a specific type of interaction between a ligand (a molecule which contains an energetically accessible lone-pair of electrons; e.g. Fig. 12)[34] and a metal ion (most commonly a transition metal ion. However, there are instances of main group metal ions being used[35]) and this is termed metallo-supramolecular self-assembly.

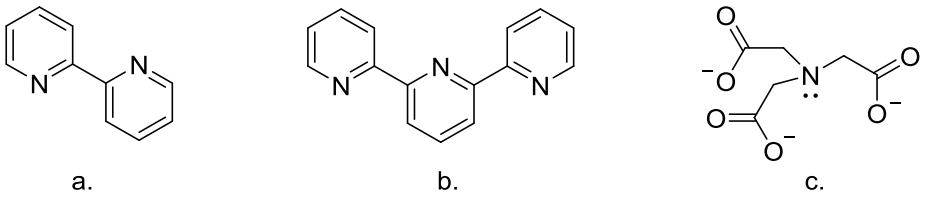

Fig. 12: Examples of various ligands with energetically accessible lone-pairs of electrons. a. The bidentate ligand bipyridine, b. the tridentate ligand terpyridine and c. the tetradentate ligand nitrilotriacetate.[34]

1.8 Metallo-supramolecular self-assembly: Supramolecular glue. . .

In metallo-supramolecular chemistry, ligands use their ability to coordinate metal ions to bind together and give rise to assemblies larger than their initial subunits. In contrast to 'host-guest chemistry' where host binding molecules are generally big enough to envelop the guest entirely within themselves, in metallo-supramolecular chemistry the self-assembled structures tend to be comprised of multiple ligands and/or other sub units, instead of just a sole host and guest. This results in the possibility of assemblies with no size limit being designed and created from the ground up or through a 'bottom-up' approach.[26,27]

Whilst supramolecular structures are rarely comprised of one non-covalent interaction on their own (they're usually assembled through a combination or series of non-covalent interactions), in metallo-supramolecular chemistry the nature of the binding strands within the ligand and the coordination geometry of the metal ion are the main determining factors in the formation of the resulting self-assembled species.[26,36]

For example, reaction of the ligand quaterpyridine (qtpy) with a divalent metal ion (such as nickel (II) or zinc (II) ions which generally prefer an octahedral coordination geometry) results in the mononuclear species $[M(qtpy)]^{2+}$. In this complex the ligand acts as a tetradentate donor, coordinating the four equatorial positions of the metal ion and leaving the two axial sites uncoordinated (Fig. 13).[37]

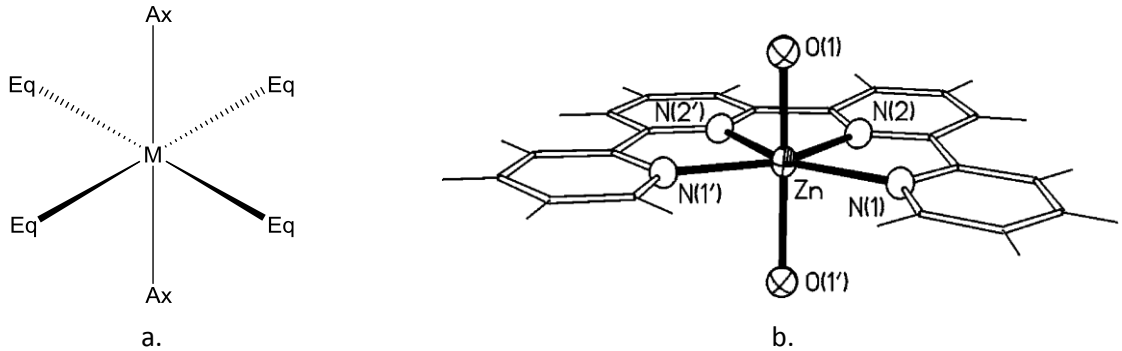

Fig. 13: a. A schematic representation of a typical octahedral geometry around a divalent metal ion. Eq denotes the equatorial positions of the metal ion and Ax denotes the axial positions. b. The quaterpyridine ligand (qtpy) coordinating the four equatorial positions of the divalent metal ion Zn^{2+} when reacted in a 1:1 metal to ligand stoichiometry. The axial positions are occupied by oxygen atoms from water molecules.[37]

However, reaction of the same ligand with a metal ion that has a preference for a tetrahedral geometry such as copper (I), results in the formation of a dinuclear double helicate $[M_2(qtpy)_2]^{2+}$. In this complex the copper (I) ion is coordinated by two nitrogen atoms at the end of the ligand strand but, due to the steric constraints of the ligand, the remaining two coordination sites of the metal ion cannot be coordinated via the same ligand. Instead, the remaining bidentate domain of the ligand coordinates a second copper (I) ion and a further ligand coordinates both metal ions resulting in a molecule with two ligands and two metal ions. Each ligand has a substantial twist about the two bidentate units giving rise to the term transition metal helicate (Fig. 14).[37]

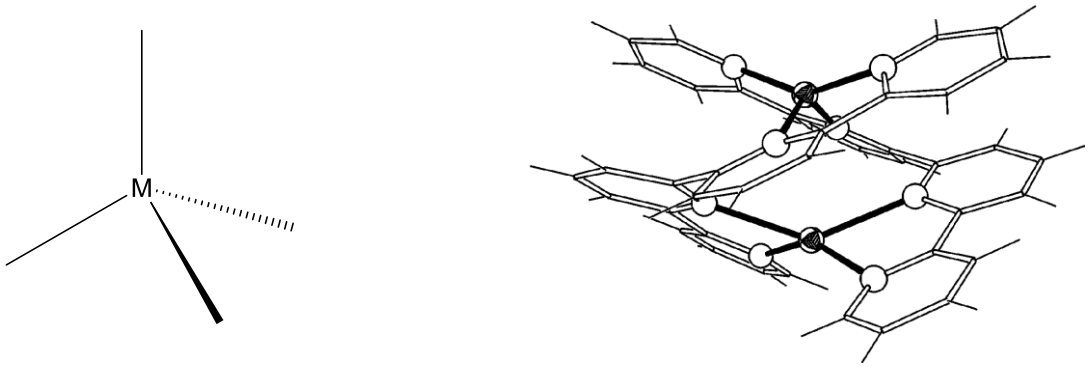

a. b.

Fig. 14: a. Schematic representation of a typical tetrahedral geometry around a metal ion such as copper (I) (M). b. The dinuclear double helicate structure formed by the reaction of quaterpyridine with copper (I) metal ions due to the ions having a preferred tetrahedral geometry in coordination. Copper (I) ions are black spheres and nitrogen atoms are white spheres.[37]

Yet the geometrical preference of the metal ion is not the only factor which governs the formation of metallosupramolecular architectures. Ligands can also be designed and preprogramed with certain chemical information which can further determine the resulting structure. The ligand, L (Fig. 15 b.), contains two thiazole rings but still contains the same basic tetradentate N-donor domains as quaterpyridine (Fig. 15 a.). However, reaction of this ligand with a metal ion with an octahedral coordination geometry such as copper (II) does not lead to a mononuclear complex in a similar fashion to quaterpyridine. Instead it gives a dinuclear triple helicate species $[M_2L_3]^{4+}$. The reason for this is the change of the central two six-membered pyridine rings to two five-membered thiazole rings. Due to its now divergent nature, the bond angles of the ligand prevent the central dithiazole

domain acting as a bidentate unit, resulting in the ligand not being able to act as a tetradentate donor and hence resulting in the preferential formation of the dinuclear triple helicate over the mononuclear species (Fig. 15 c. and d.).[38]

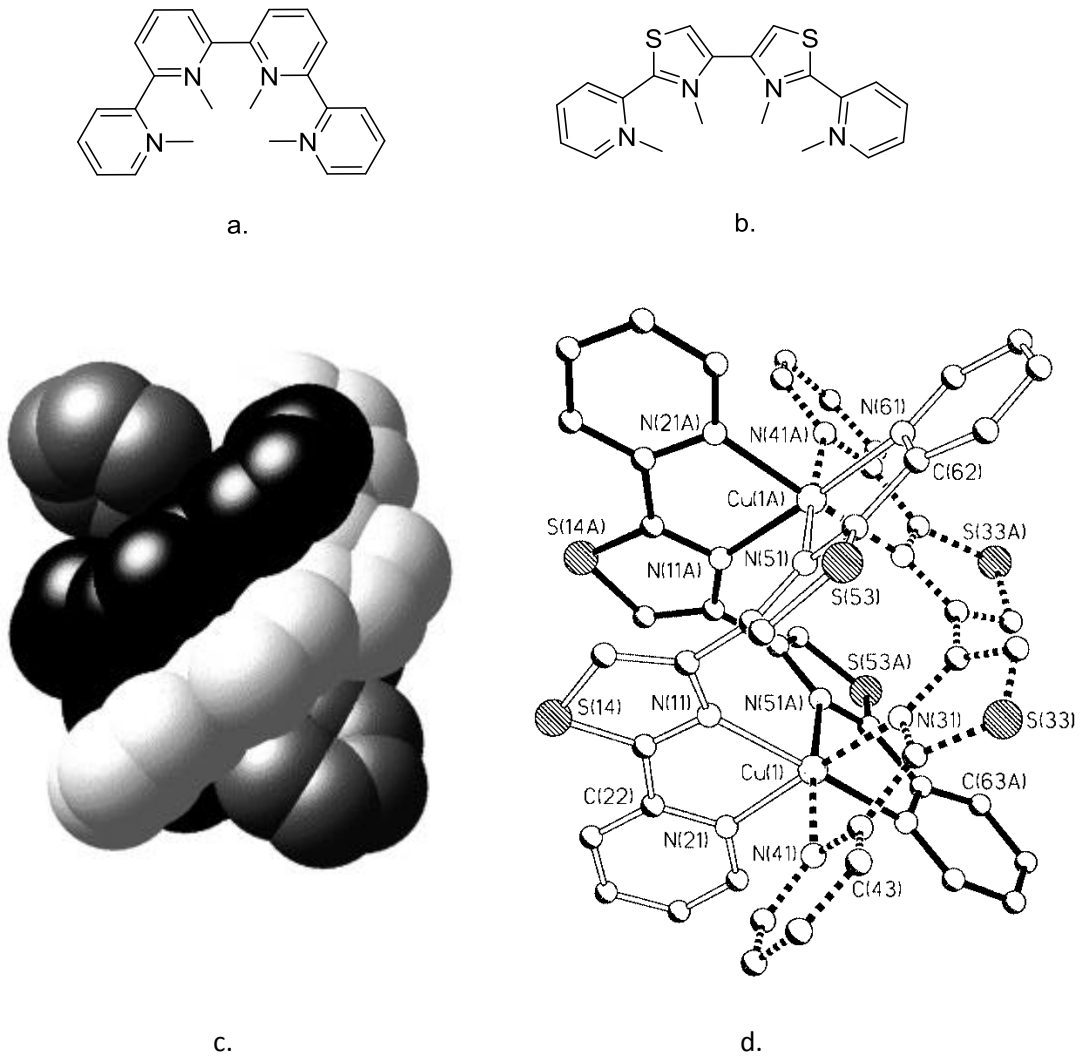

Fig. 15: Schematic representations of the ligands a. quaterpyridine (qtpy) and b. the dithiazole ligand, L. c. A spacefilling representation of d. the dinuclear triple helicate $[Cu_2(L)_3]^{4+}$.[38]

In all metallo-supramolecular assemblies the metal ions act almost like a 'supramolecular glue' and exhibit geometries that result in anywhere from two[39] to sixteen[40] interactions between the ligand and the metal ion. Generally metal ions in the d-block of the periodic table exhibit coordination numbers of four and six and the lanthanides and actinides of the f-block exhibit coordination numbers of eight to twelve. However there are examples of metal ions showing the capabilities of

having more than one fixed coordination number. Whilst lanthanides are known to adopt eight, nine and even up to twelve coordination numbers quite readily[41–43], various coordination numbers of silver (I) ions have been reported ranging from two to five[39,44–46] and the hotly debated topic of the coordination preferences of copper (II), whether four, five or six, still continues to this day.[47] This potential for adjustments in coordination number and geometry demonstrates the potential for a staggering variety across metallo-supramolecular chemistry through successful manipulation of these coordination capabilities.

1.9 Lehn does the twist

The work by Lehn *et al.* demonstrated that through complexation of different oligobipyridine ligands (Fig. 16 a. and b.) with copper (I) cations, separate dinuclear and trinuclear helicate assemblies could be formed (Fig. 16 c. and d.). However, the assembly of these complexes had occurred spontaneously by simply adding a solution of copper (I) perchlorate in acetonitrile to a solution of the respective ligand in chloroform. A major driving force behind this spontaneous assembly was the pre-programming of the ligand to ensure certain crucial properties were present.[48]

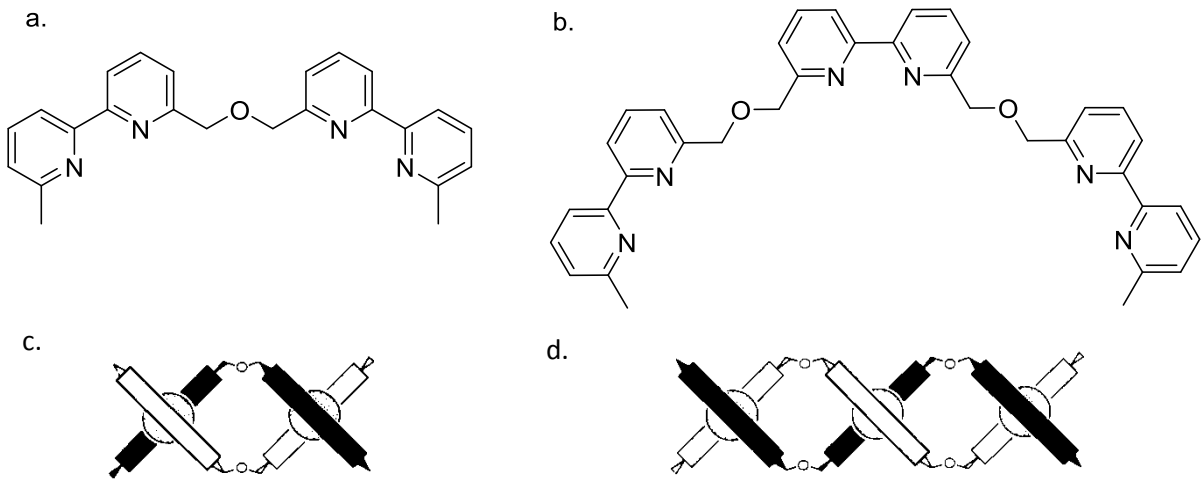

Fig. 16: Schematic representations of the ligands and assemblies formed by Lehn et al. a. The ligand that formed the dinuclear double helicate shown in c. upon addition of copper(I) ions. b. The ligand that formed the trinculear double helicate shown in d.[48]

In the double helicate assembly, the ligand had been pre-programmed to partition itself into two separate binding domains through the addition of a (-CH_2-O-CH_2-) spacer group in between the original quaterpyridine domain. The spacer group in question had not only been chosen due to its length being sufficient in dividing the binding domain into two (thus preventing the binding of a singular copper (I) ion in its preferred tetrahedral geometry from both bipyridine domains of the same ligand), but also as it was flexible enough to allow it to adopt a "strain-free coordination" to a separate copper (I) ion through the other, now separate, bipyridine domain. A separate ligand then completed the coordination desires of the copper (I) ions through its own partitioned binding domains. Manipulation of these properties was then extended to demonstrate the creation of another ligand that resulted in the spontaneous assembly of the trinuclear helicate variant.[48]

These assemblies were the first reported inorganic helicates and through their usage of the complementary binding requirements between the metal ions and the binding domains (much akin to the complementary hydrogen bonding seen between adenine, thymine, cytosine and guanine), bore a remarkable resemblance to the double helix of DNA.

Since these initial discoveries, the understanding of the forces that govern the self-assembly of specific types of supramolecular structures have been documented and the rules of formation of assemblies that were once mysteries, are now well understood.[26,27]

Therefore, further progression in supramolecular chemistry has been found by combining multiple interactions together to push the boundaries of what can be controlled and synthetically created.

1.10 Pushing the envelope: Combining self-assembly processes

Since the Nobel Prize-winning discoveries by Pederson, Cram and Lehn *et al.*,[8,12,20] the field of supramolecular chemistry has thrived. The further study and the consequent understanding of how to combine the forces and interactions that control the formation of supramolecular complexes has allowed for huge advances into how molecular structures and systems can be designed and synthesised.

One example of how non-covalent interactions and self-assembly processes can be combined and manipulated to control structural formation was shown by Rice *et al.* They designed a ligand that was capable of adopting a tetradentate or a bis-bidentate (two separate bidentate binding domains on the same ligand strand) coordination and also had a crown ether attached to the 'back' of the bipyridyl domain (Fig. 17).[49]

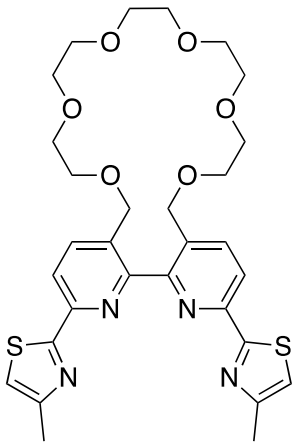

Fig. 17: Schematic representation of the ligand created by Rice et al. with the crown ether domain attached to the back of the central bipyridyl unit.[49]

Determination of the crystal structure when the ligand was reacted with mercury (II) perchlorate and sodium (I) perchlorate, showed a dinuclear double helicate with two ligands adopting bis-bidentate conformations and coordinating two mercury (II) ions in distorted tetrahedral geometries (Fig. 18 a.). The sodium (I) ions had been bound in the crown ether domains attached to the back of

each ligand yet, due to their size, were unable to coordinate all six oxygen atoms in the crown ether simultaneously. However, when the sodium (I) perchlorate was replaced with barium (II) perchlorate the structure changed to a mononuclear species where the mercury (II) ion was coordinated by the ligands tetradentate conformation instead. Similar to the sodium (I) ions in the dinuclear double helicate, the barium (II) ion was now bound within the crown ether of the ligand yet unlike the sodium (I) ion, it had coordinated all six oxygen atoms of the crown ether (Fig. 18 b.).[49]

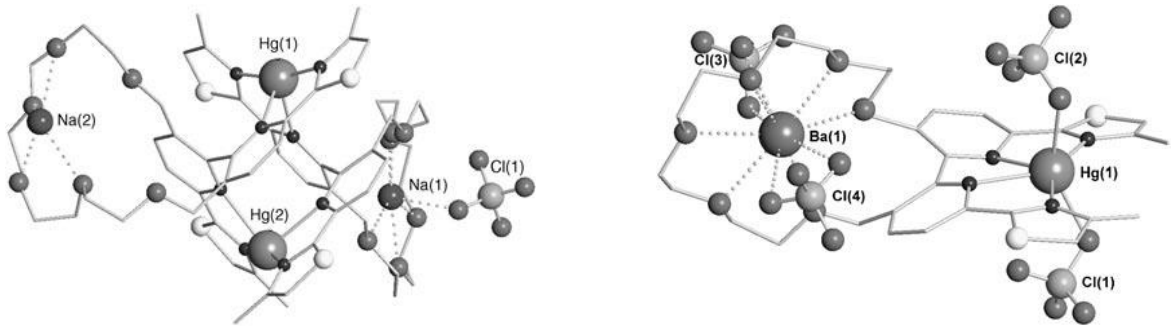

a. b.

Fig. 18: a. The X-ray crystal structure of the dinuclear double helicate species $[Hg_2(L)_2Na_2]^{6+}$ showing how the ligand has adopted a bis-bidentate conformation and that the sodium ions are only partially coordinating the crown ether domain of the ligand. b. The X-ray crystal structure of the mononuclear species $[Hg(L)Ba]^{4+}$ showing the ligand adopting its tetradentate conformation and the barium ion coordinating all six oxygen atoms of the crown ether.[49]

It was suggested that due to the barium (II) ion being able to coordinate the crown ether fully, its presence prevented the ligand from being able to twist and divide into its bis-bidentate conformation hence resulting in the mononuclear structure. Altering the metal ion bound in the crown ether of the ligand brought about a conformational change to the structure and hence indicated that it was an allosteric effect that was causing the difference in the dinuclear double helicate and the mononuclear species. NMR studies were carried out to confirm that the allosteric effect was the dominant force in changing the structure but evidence was found that changing the charge of the metal ion in the crown ether from singly charged to doubly charged, also gave rise to different species. Whilst allosteric effects have been shown to be a dominant force in controlling supramolecular structures on their own,[50] in this case it was concluded that both allosteric and

electrostatic effects were responsible for causing the changes in the type of supramolecular assembly formed.[49,51]

1.11 Mesocates: The helicates achiral cousin

In the dinuclear helicate assemblies previously discussed (and in dinuclear helicates in general) the metal centres possess the same chirality. Unless the chirality of the assembly is controlled, usually by the inclusion of a chiral centre in the ligand strand, this results in the formation of $[M_2L_2]^{n+}$ complexes of two configurations (e.g. $\Delta\Delta$ and $\Lambda\Lambda$).[52] Yet it is possible for the metal centres to adopt opposite chiralities (e.g. $\Delta\Lambda$) and in such situations a mesocate, the achiral analogue of the helicate, is formed.[53,54] Even though the first structure of a mesocate was reported some time ago,[55] in comparison to the helicate, mesocates are much fewer in number and the conditions required for their formation are much less understood.[56,57] One potential reason for this is that whilst the opposite chirality of the metal centres within the structure is what defines a mesocate, homochiral helicates exhibit a lower total energy and hence would be the thermodynamically preferred assembly.[58] However, through combining the forces that control the formation of supramolecular structures, the requirements for mesocate formation are becoming less elusive.[53,54]

1.12 Odd C's and Even S'

In helicates and mesocates, ligands generally adopt one of two conformations. In the case of helicates, the ligand strands adopt an 'S' shaped conformation where the ligand undergoes a twist and the binding domains face away from one another. However, with mesocates there is no helical twist in the ligand and as a result, the binding domains face in the same direction giving rise to a 'C' shaped ligand conformation. Albrecht reported how to control these conformations through development of an empirical 'odd-even rule'. By synthesising ligands with an odd or even number of

-CH_2- groups in the central space group, the conformation of the ligand, whether 'C' or 'S' respectively (Fig. 19), could be controlled and this resulted in mesocates and helicates being selectively formed.[59]

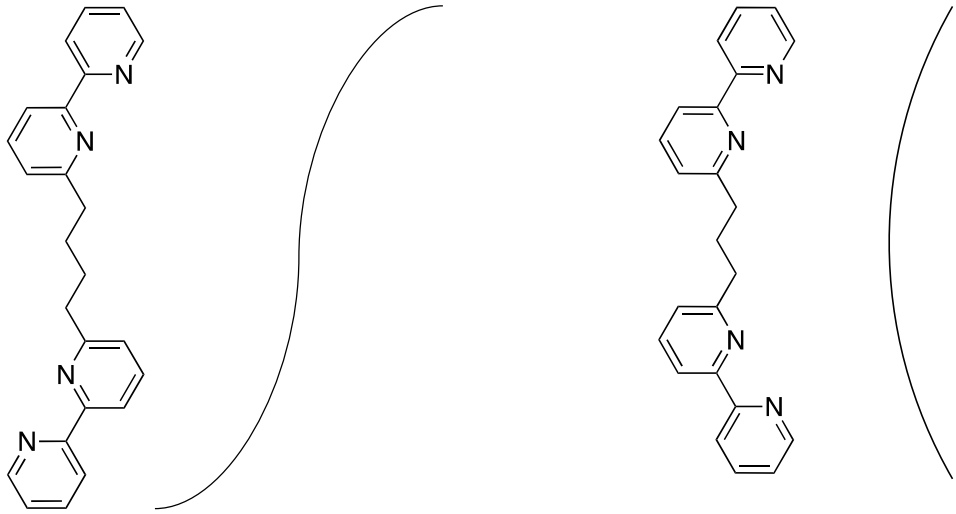

a. b.

Fig. 19: Schematic representations of generic bipyridine containing ligands displaying a. a ligand adopting the 'S' conformation associated with helicate formation as a result of an alkyl chain spacer with an even number of carbon atoms and b. a ligand adopting the 'C' conformation associated with mesocate formation as a result of an odd number of carbon atoms in the alkyl chain spacer.[59,60]

However, more recently Wu *et al.* demonstrated selective control over the formation of mesocates by combining metallo-supramolecular self-assembly alongside the effects of anions. They developed a ligand strand capable of forming both triple stranded dinuclear helicates and mesocates through reaction with copper (II), iron (II) and iron (III) metal ions. Due to the ligand design and the binding geometries of the metal ions, the shape of these assemblies had given rise to a cavity in the centre and the anions (whose presence was a consequence of the highly charged structures) had shown themselves to be able to bind within this cavity. It was noted that whilst the smaller anions of bromide (Br^-) and nitrate (NO_3^-) resulted in formation of the helicate structure, the larger anions such as tetrafluoroborate (BF_4^-), perchlorate (ClO_4^-) and sulphate (SO_4^{2-}) all templated the mesocate species. It was also noted that the shape of the anions may have played a part. The larger anions

that had resulted in the formation of the mesocates were all tetrahedral, unlike the bromide and nitrate anions associated with the helicate assemblies (Fig. 20).[60]

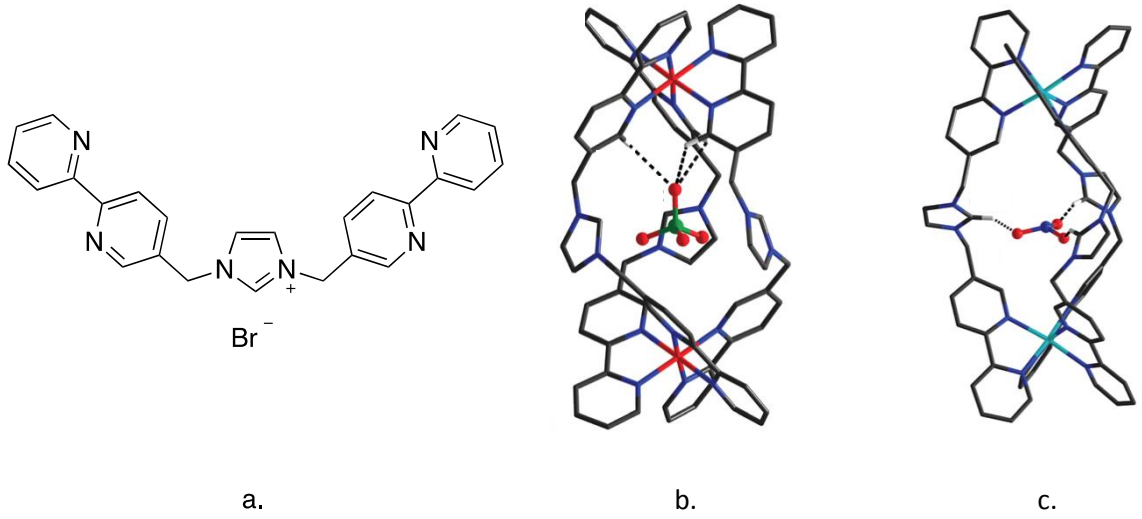

a. b. c.

Fig. 20: a. Schematic representation of the ligand produced by Wu et al. b. The triple stranded dinuclear mesocate species $[Fe_2L_3ClO_4]^{6+}$ showing the tetrahedral anion ClO_4^- bound in the central cavity. c. The triple stranded dinuclear helicate species $[Cu_2L_3NO_3]^{6+}$ showing the trigonal planar anion NO_3^- bound in the central cavity.[60]

Whilst Wu *et al.* had demonstrated selective control of mesocate or helicate formation through the use of anions, using the effects of anions in supramolecular self-assembly is not unique to this work and when combined alongside metallo-supramolecular self-assembly and other non-covalent forces, anions have been shown to have had huge effects on structural formation.

1.13 Anion effects: Negativity isn't necessarily a bad thing. . .

Combining anions (negatively charged ions or molecules) and their effects with the previously mentioned intermolecular forces that lead to the formation of 'super molecules', has led to even more potential for advancements in supramolecular self-assembly. The realisation of how important anionic species are across biology, the environment and the sciences as a whole, has led to research surrounding them expanding and naturally resulting in their effects on a molecular level being studied.[61]

Whilst Li *et al.* demonstrated a triple stranded anionic helicate that used a urea based ligand strand to bind phosphate (PO_4^{3-}) anions instead of the conventional metallo-coordinated helicate,[62] and Ward *et al.* used anion templation of a tetrafluoroborate (BF_4^-) ion to create tetrahedral cage complexes,[63] one recent and particularly striking example involving the effects of anions on a supramolecular structure was reported by Rice *et al*.[64]

They reported a trinuclear circular helicate held together through metallo-supramolecular interactions between a bis-bidentate ligand with two amine (R-NH) groups and copper (II) ions. This resulted in three, four coordinate copper (II) metal ion centres connecting the ligands and a fifth interaction was observed from each metal centre to an oxygen atom of a dihydrogen phosphate ($OPO_3H_2^-$) anion in the centre of the assembly. These anions were also H-bonded to the amine groups on the ligand strand as well as being hydrogen bound to one another through interactions between -OH···O-P- atoms of separate anions (Fig. 21).[64]

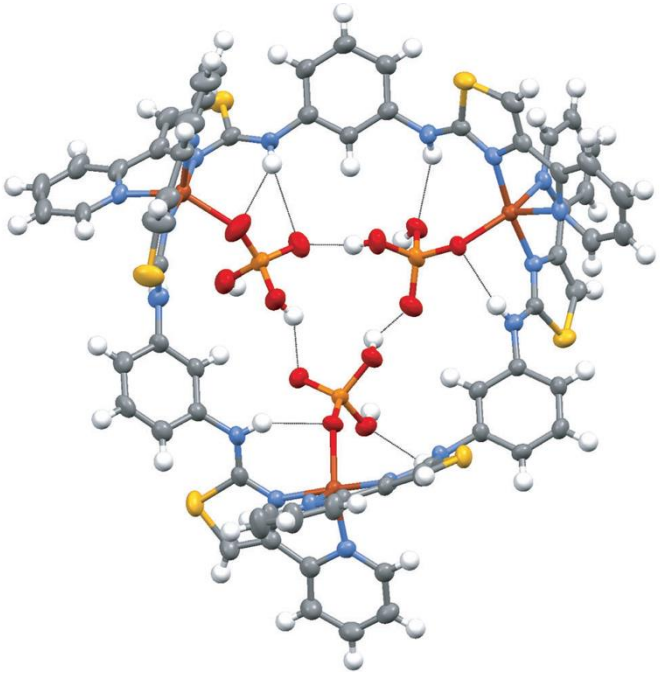

Fig. 21: X-ray crystal structure of the trinuclear circular helicate $[Cu_3L_3(OPO_3H_2)_3]^{3+}$ showing the dihydrogen phosphate anions in the core coordinating to the copper (II) ion metal centres, the amine groups of the ligand strand and other anions. The uncoordinated -OH groups of the dihydrogen atoms can also be seen pointing away from the core in the same direction.[64]

With the phosphate anions possessing two -OH groups each, each anion was able to hydrogen bond to another and leave one -OH group unbound, yet these unbound -OH groups all faced the same direction out of the core of the circular assembly. This was shown to be a result of the dihydrogen phosphate anions of one trinuclear circular assembly hydrogen bonding with another three dihydrogen phosphate anions from a separate trinuclear circular unit and ultimately resulting in the dimerisation of two trinuclear circular helicates (Fig. 22).[64]

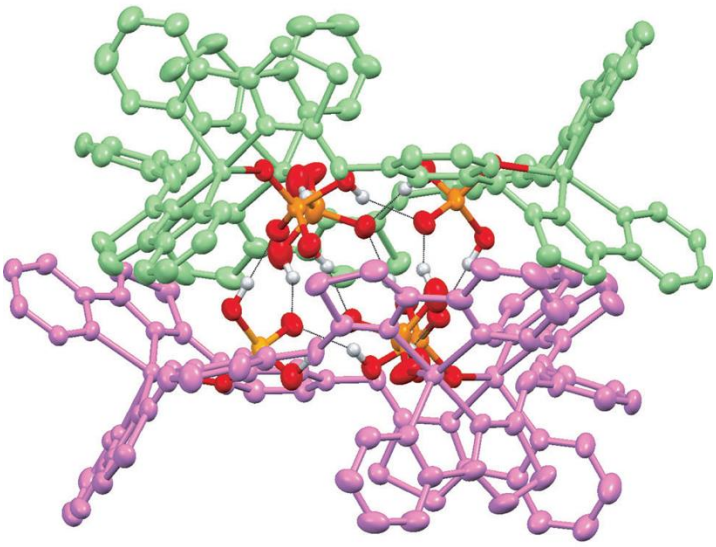

Fig. 22: X-ray crystal structure of the dimer of trinuclear helicates, dimerised through hydrogen bonding between dihydrogen phosphates in the core. The trinuclear circular helicate sub units are coloured pink and green for clarity.[64]

Further to this, it was shown that by stoichiometrically controlling the amount of dihydrogen phosphate present in the reaction (from one equivalent to half an equivalent), the supramolecular structure could be controlled from the dimer of trinuclear circular helicates to a more simple double helicate with a singular dihydrogen phosphate anion bridging the two metal centres. This also indicated that the circular nature of the trinuclear species was a direct result of the ligand strands templating around the dihydrogen phosphate anion core.[64]

1.14 Circular helicates: Everybody form a circle

Another impressive demonstration of how the effects of anions could be exploited to control supramolecular architecture formation was reported by Lehn *et al.* when they combined anionic effects to template the nuclearity of circular helicates. By changing the anion present from a sulphate (SO_4^-) to a chloride (Cl^-), the nuclearity of the self-assembled circular species changed from six to five as the ligands templated around the chloride anion.[65]

Circular helicates use much the same methodology of helicate assembly and contain the same binding arrangement of ligand strands, i.e. the ligand partitions into two binding domains each coordinating a different metal ion. However, unlike the helicates where all the metal ions are arranged in a linear fashion, they assemble in a circular arrangement giving rise to larger species of the formula $[M_nL_n]^{x+}$ where n = 3 to 10. The rules that govern the formation of these species are less understood compared to linear helicates and one of the major design implications is that the smaller, entropically favoured, linear helicates must be prevented from forming. This has been achieved mostly via utilising anion templation[65] and steric interactions.[66]

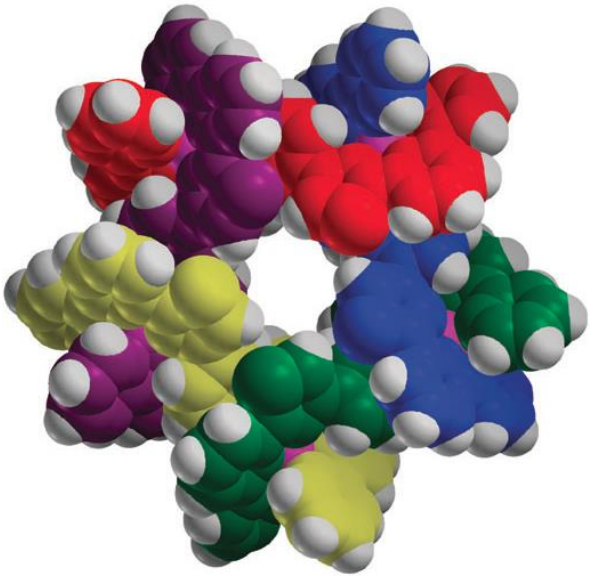

Fig. 23: An example of a circular helicate produced by Rice et al. This particular circular helicate was created through the manipulation of metal ionic radii, steric interactions and metallo-supramolecular coordination.[66]

Using this technique a number of polymetallic circular helicates have been reported as well as further preprogrammed ligands which form head-to-tail and heteroleptic circular helicates[67] and even circular mesocates.[68]

An impressive example of circular helicate formation, which is currently the highest nuclearity circular helicate reported and contains ten metal ion centres, was reported by Horng *et al.* This particularly large assembly was created by combining supramolecular forces such as steric interactions and ligand pre-programming. One of the issues with metallosupramolecular assembly is that the resultant species can have a large net positive charge and if this is sufficient in magnitude it can destabilise the desired assembly. As a result, the highest nuclearity circular helicate (that contains divalent metal ions and neutral ligands) is a pentanuclear assembly possessing a high net positive charge of ten (due to each of the five divalent zinc metal ions carrying a charge of 2+).[66] Even using divalent metal ions with coordinating counter anions[68] or simply using monovalent metal ions[69] only resulted in nuclearities of six being obtained.

Horng *et al.* circumvented this issue by using a dianionic ligand (Fig. 24) so that reaction with divalent transition metal ions produced a neutral assembly.

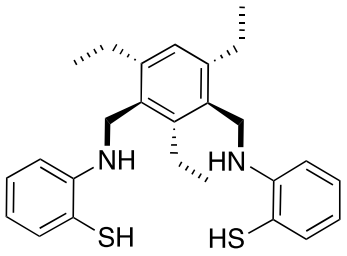

Fig. 24: Schematic representation of the ligand, H_2L, proposed by Horng et al, possessing a double negative charge and two bidentate domains, with the aim of forming neutral higher nuclearity helicates.[70]

With the ligand strand designed to compensate for any cationic charge exhibited by the metal ions, they reacted their ligand strand with zinc (II), cadmium (II) and mercury (II) and successfully obtained

crystal structures of the reactions with zinc (II) and mercury (II) metal ions. The X-ray crystal structure of the complex containing mercury (II) metal ions successfully yielded the neutrally charged double helicate $(HgL)_2$. However, the X-ray crystal structure of the reaction with zinc (II) metal ions successfully resulted in the neutral, decanuclear, circular helicate structure, $(ZnL)_{10}$ (Fig. 25).[70]

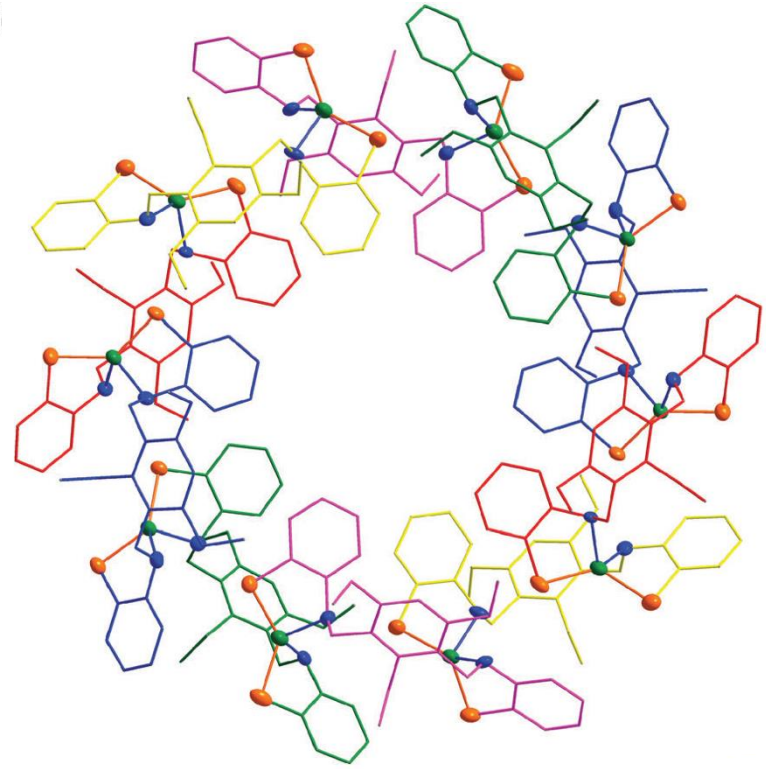

Fig. 25: The X-ray crystal structure of the neutrally charged decanuclear circular mesocate, $(ZnL)_{10}$, produced by Horng et al. Zinc (II) metal centres are represented as green spheres, sulphur atoms are orange spheres and nitrogen atoms are blue spheres. Ligand strands have been coloured pink, green, blue, red and yellow for clarity.[70]

Whilst changing the motif of the structure from a standard helicate to a circular helicate by changing the size of the metal ionic radii had previously been reported,[66] it was the successful formation of the neutrally charged decanuclear circular helicate that was the notable result. The zinc (II) metal centres had adopted four coordinate tetrahedral geometries and had coordinated through the sulfur and nitrogen atoms from different ligand strands. The ethyl branches on alternate carbons of the central aromatic spacer group, force the two bidentate domains on to the same side of the ligand

strand. This imposes a 'C' shaped ligand conformation (the ligand conformation generally associated with mesocate formation (Fig. 19)) and as a result, the zinc (II) metal centres all had alternate chiralties of Δ- and Λ-, causing the assembly to be a circular mesocate (Fig. 26).[70]

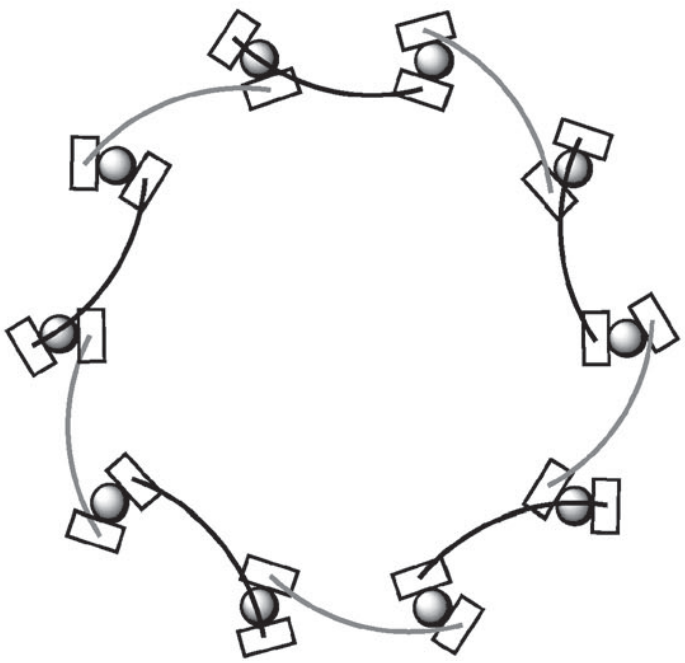

Fig. 26: Schematic representation of the decanuclear circular mesocate $(ZnL)_{10}$ by Horng et al. showing the 'C' shaped ligand conformation between metal ion centres resulting in the overall assembly being a circular mesocate.[70]

One further remarkable property of this work was how the fluorescence intensity of the circular mesocate behaved in the presence of anions. When the fluorescence intensity was measured in the presence of various anions including chloride (Cl^-), perchlorate (ClO_4^-), hydrogen sulphate (HSO_4^-) etc., there was no change. However, when the circular mesocate was in the presence of dihydrogen phosphate, ($H_2PO_4^-$) the fluorescence intensity was quenched considerably and ^1H NMR spectra of this final product indicated that the structure had completely disassembled itself into its constituent parts of ligand and zinc (II) metal ions.[70]

This work by Horng *et al.* was an impressive example of how the non-covalent forces that contribute to the formation of supramolecular structures, such as ligand pre-programming, the effects of

anions, steric interactions etc., can be combined together, to ultimately control the creation and destruction of the larger supramolecular molecule.[70]

1.15 Polymeric assemblies: To infinity and beyond the molecule

The creation of metallo-supramolecular polymers is a field within supramolecular chemistry which has seen a surge in development over recent years. With the uses of polymers being so diverse, efforts to develop self-assembled metallosupramolecular polymeric species through combinations of intermolecular and intramolecular interactions have seen major progress. Polymers in metallosupramolecular chemistry are a type of virtually infinite assembly summarised by the formula $[[M_1L_1]^{x+}]_n$. The formation of a metallosupramolecular polymer heavily relies on the ability of a ligand strand to bind two or more metal ion centres. Therefore, the most influential supramolecular forces for consideration are the coordination and geometric preferences of the metal ion centres to be bound. Further to this the resultant complex must also be able to facilitate polymer formation, whether this be through prevention of two ligands forming a closed complex with the same two metal ion centres or through the promotion of a polymeric species via an intermolecular force between molecular subunits.[71–73]

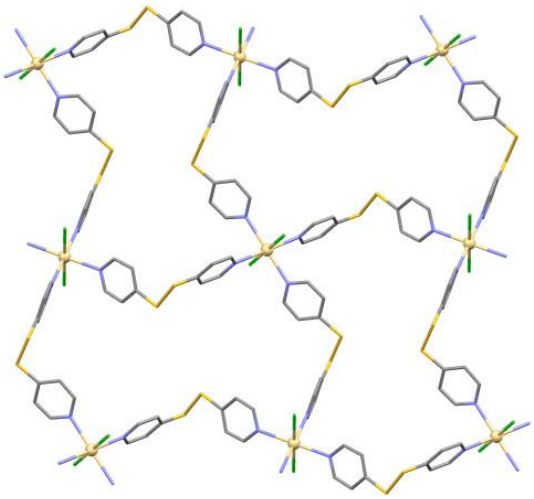

Fig. 27: A section of the X-ray crystal structure of the cadmium (II) containing polymer, $[CdCl_2(\mu\text{-dtdp})_2]_n$, reported by Seidel et al. showing just nine metal centres and twelve ligand strands of the polymeric structure.[73]

One example of how metallosupramolecular polymers can be created through a combination of intermolecular and intramolecular interactions was shown by Vazquez *et al.*[74]

They demonstrated an entire three dimensional network of dinuclear helicates held together through a combination of metal ion coordination and π-π stacking interactions. Their ligand strand was designed to coordinate a metal ion with a tetrahedral coordination geometry, yet it also contained six aromatic rings with four of them being aniline rings (Fig. 28). They reasoned that due to the aniline rings being electron-poor when coordinating to a metal ion, they would promote the aggregation of the network of helicates through π-π stacking interactions between the rings.[74]

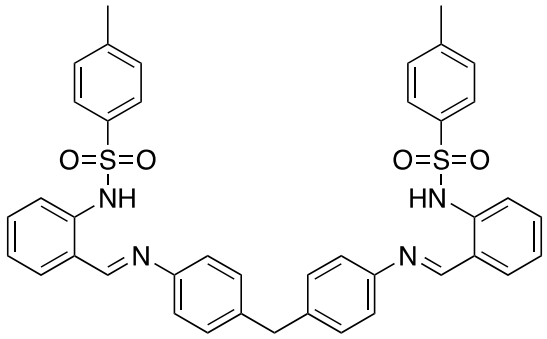

Fig. 28: Schematic representation of the tetradentate ligand strand proposed by Vazquez et al that had six aromatic rings including four aniline based rings.[74]

By using electrochemical oxidation[75–77] of a copper plate in an acetonitrile solution, they were able to coordinate their ligand with copper (I) metal ions and upon recrystallization and analysis by X-ray crystallography, it revealed the formation of a dinuclear double helicate species. Through combining the metal ion coordination interactions and their effect on the now electron-poor aromatic rings, the crystal structure also showed that each helicate connected itself to adjacent helicates through an offset alignment of π-π stacking interactions (Fig. 29). The assembled three-dimensional polymeric network of helicates was the first of its kind where the network was solely held together by π-π stacking interactions and further emphasised their influence on supramolecular structures.[74]

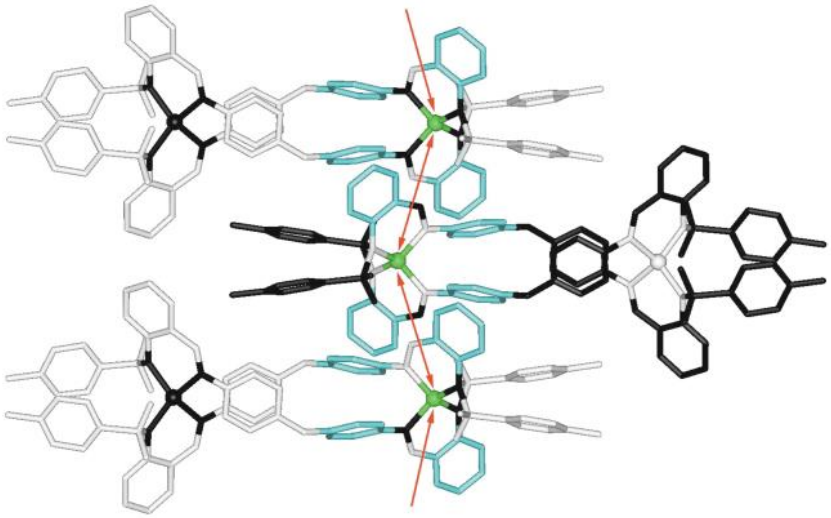

Fig. 29: A partial view of the unit cell of the three dimensional polymer of dinuclear double helicates formed through a combination of the coordination of metal ions and π-π stacking interactions. Aromatic rings exhibiting π-π stacking interactions are coloured blue. The red arrows indicate orthogonal sets of chains of copper (II) ions which are also potentially connected through π-π stacking interactions.[74]

1.16 Long Bond Silver

Another example of how intramolecular forces can be combined alongside intermolecular forces to promote the formation of metallosupramolecular self-assembled polymers, was demonstrated by Ward *et al*. In this work they reported a triple helix comprised of three infinite chains of double helicates. The basic unit was a bis-bidentate ligand which formed the simple dinuclear double helicate $[Ag_2L_2]^{2+}$ on reaction with silver (I) metal ions. However, this dinuclear double helicate was only a subunit of a much larger assembly as it interacted with a separate dinuclear double helicate via argentophilic interactions.[78]

Argentophilic interactions, or Ag···Ag interactions, are a type of intermolecular interaction which is observed between two adjacent silver metal ions and they are well recognised as being able to develop subunits into long one-dimensional polymeric chains, as well as into multi-dimensional polymeric assemblies.[79–84]

In this case the dinuclear double helicate, $[Ag_2L_2]^{2+}$, had formed Ag···Ag interactions between itself and another double helicate subunit, leading to the creation of a one-dimensional, infinite chain of

double helicates. The added combination of π-π stacking interactions between the terminal aromatic groups of the ligands, also helped stabilise the structure (Fig. 30).

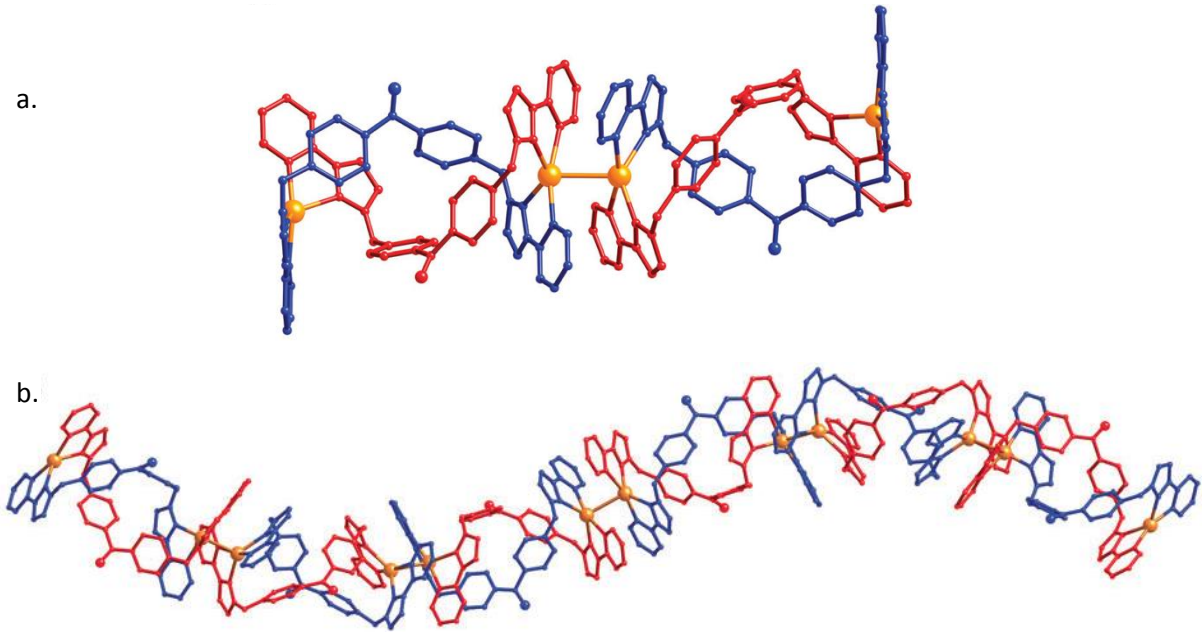

Fig. 30: The X-ray crystal structures showing a. two dinuclear double helicate subunits $[Ag_2L_2]^{2+}$ and b. a long chain of six dinuclear double helicates (resulting in one complete helical turn) connected together via argentophilic, or Ag···Ag, interactions.[78]

In addition to the Ag···Ag interactions, CH···π and π-π stacking interactions were also observed between the long chains of double helicates, culminating in three of these chains intertwining with each other and giving the final structure of an infinite triple helix of double helicates (Fig. 31). The helical motif of each long chain of double helicates helped influence the overall triple helical shape of the final assembly (Fig. 30 b.).[78]

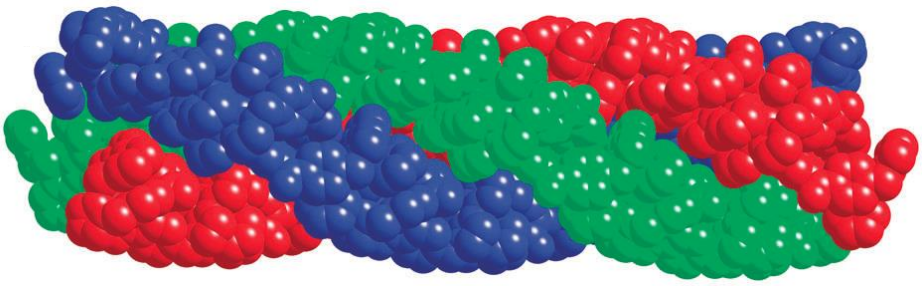

Fig. 31: The X-ray crystal structure of the triple helix of double helicates reported by Ward et al. with alternate long chains of double helicates coloured separately for clarity.[78]

1.17 Self-assembling the future

The initial discoveries and breakthroughs that sparked the interest and started the progress into supramolecular chemistry, were in their own way smaller subunits assembling a greater understanding to help further a larger field.

In such a relatively short period of time, the understanding of how the manipulation and combination of interactions that can control the assembly of larger and more functional supramolecular species has dramatically increased and led to some truly impressive super molecules being realised.

From visually spectacular creations such as the 'Star of David' catenane,[85] functional assemblies such as metal organic frameworks (or MOFs) capable of storing clean energy,[86] metallo-supramolecular cages that can bind chemical warfare agent simulants,[87] and even to the development of molecular machinery,[88] the field of supramolecular chemistry has shown its potential to continually advance and flourish.

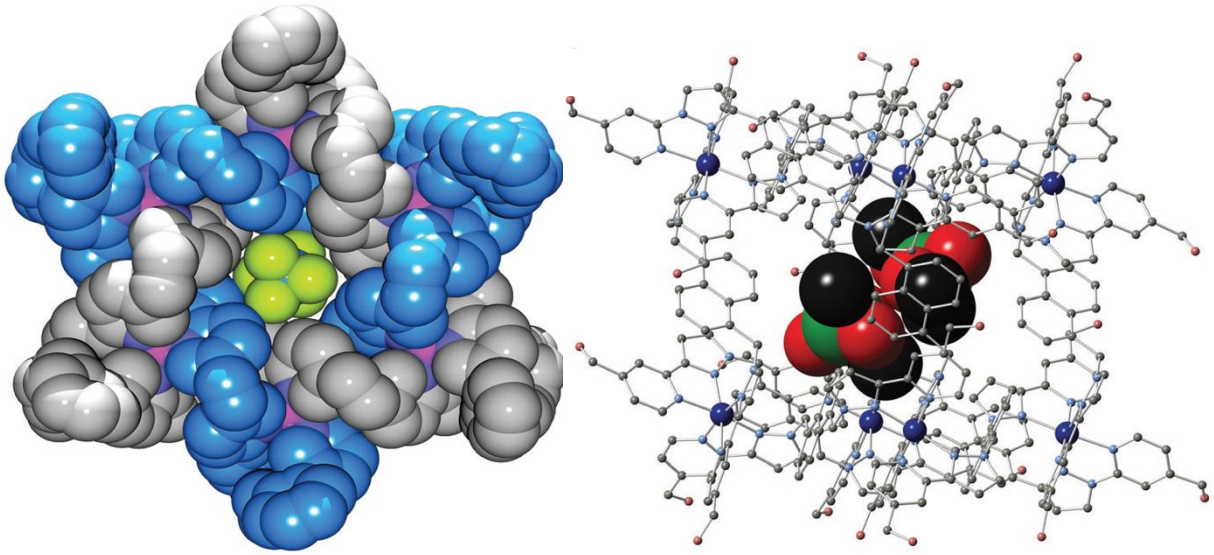

a. b.

Fig. 32: The X-ray crystal structures of a. the impressive 'Star of David' catenane super molecule produced by Leigh et al., consisting of two interlocked trinuclear circular helicates with a hexafluorophosphate anion (PF_6^-) occupying the central cavity and b. the self-assembled supramolecular cage reported by Ward et al. showing the successful binding of the chemical warfare agent simulant DMMP (dimethyl methylphosphonate) in its central cavity through hydrogen bonding.[85,87]

2 Chapter 2: Synthesis and coordination chemistry of a ditopic hexadentate ligand strand

Described in this chapter is the synthesis and coordination chemistry of a hexadentate ditopic ligand strand **L^1** (Fig. 33). **L^1** consists of two pyridyl (py) and two pyrimidine (pyr) groups in a py-pyr-pyr-py coordination motif. Due to free rotation around the single bond connecting the two pyrimidine units, **L^1** is able to adopt two different ditopic conformations *i.e.* a bis-tridentate conformation and a tetradentate-bidentate conformation. Upon reaction of **L^1** with copper (II) metal ions, the dinuclear complex $[Cu_2(\mathbf{L^1})(ClO_4)_2(MeCN)_4]^{2+}$ is formed. However, adjusting the metal to ligand stoichiometry gives rise to the dinuclear complex $[Cu_2(\mathbf{L^1})_3]^{4+}$. Reacting **L^1** with cadmium (II) and europium (III) metal ions results in the formation of the complexes $[Cd(\mathbf{L^1})_2]^{2+}$ and $[Eu(\mathbf{L^1})_2(CF_3SO_3)]^{2+}$ respectively. However, reacting **L^1** with europium (III) and silver (I) metal ions results in the creation of the tetranuclear dimetallic assembly $[Eu_2Ag_2(\mathbf{L^1})_3(CF_3SO_3)_8]$. Reaction of **L^1** with rhenium (I) pentacarbonyl chloride ($ReCl(CO)_5$) results in the *ter*-**L^1**$ReCl(CO)_3$ complex in which the rhenium (I) metal centre coordinates to the terminal pyridyl-pyrimidine bidentate domain of the ligand. However, using lanthanum (III) trifluoromethanesulfonate to template the ligand strand allows for the creation of the *cent*-**L^1**$ReCl(CO)_3$ complex. In this complex, the rhenium (I) metal ion coordinates to the central bipyrimidine domain, leaving the remaining tetradentate site uncoordinated and suitable for the binding of transition metal ions.

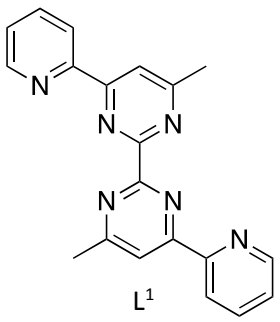

L^1

*Fig. 33: Schematic representation of the ditopic and potentially hexadentate ligand strand **L^1**.*

2.1 Synthesis of L^1

Unless otherwise stated, all solvents and materials were purchased from either Sigma Aldrich, Acros Organics or Fisher Scientific and were used without further purification. ^1H and/or ^{13}C NMR data was recorded on either a Bruker AV (III) 400 MHz NMR spectrometer or a Bruker Advance 500 MHz NMR spectrometer. Mass spectra were obtained on an Agilent 6210 TOF MS with electrospray ionisation operating in positive ion mode or a Bruker Micro TOF-q LC mass spectrometer with electrospray ionisation operating in positive ion mode. Single crystal studies were recorded on a Bruker D8 Venture with Dual IμS Microfocus Sources using Mo or Cu radiation at 150 (2) K.

2.1.1 Synthesis of **1**

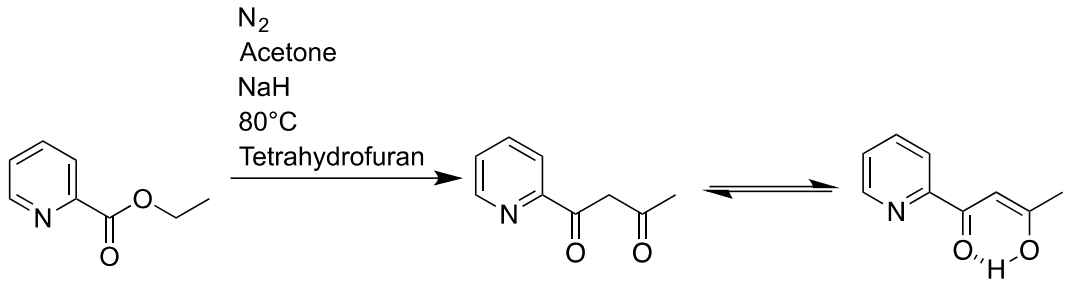

1

Under an atmosphere of N_2, anhydrous acetone (3 mL) and ethyl picolinate (6.38 g, 0.042 mol) were slowly added to a solution of anhydrous THF (50 mL) and NaH (60% dispersion in mineral oil, 2.0 g, 0.083 mol) and the reaction set to heat at 80 °C for 12 hours with stirring. After cooling and quenching any remaining NaH with MeOH, the reaction was evaporated to dryness, water (10 mL) was added, which was extracted into DCM (30 mL) and the organic phase discarded. The pH was decreased by the addition of acetic acid to the aqueous layer to produce a white suspension which was extracted into DCM, dried over $MgSO_4$ and evaporated to dryness to yield **1** as a dark brown liquid (6.1 g, 0.037 mol, 88.6 %) which was of sufficient purity to be used in the subsequent reaction. ^1H NMR (400 MHz, ($CDCl_3$) δ: 15.7 (s, 1H, -OH, due to the enol isomer), 8.68 (dq, *J* = 4.72, 0.8, 1H, py), 8.1 (d, *J* = 7.84, 1H, py),

7.86 (td, *J* = 7.68, 1.72, 1H, py), 7.43 (ddd, *J* = 7.6, 4.76, 1.2 *Hz*, 1H, py), 6.84 (s, 1H, -CH), 2.26 (s, 3H, $-CH_3$). ^{13}C NMR (400 MHz, ($CDCl_3$) δ: 195, 181, 152, 149, 137, 126, 122, 97, 26. *HRMS (m/z): $[M+H]^+$ for $C_9H_9O_2N$ calculated 164.0706, measured 164.0699.*

2.1.2 Synthesis of 2

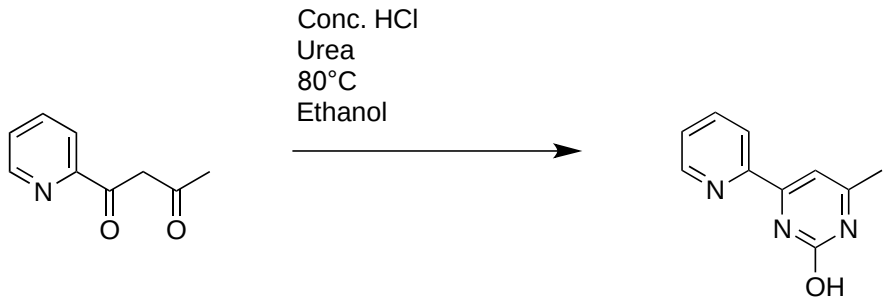

1 **2**

To a solution of **1** (5 g, 0.031 mol), urea (2.76 g, 0.046 mol) and EtOH (40 mL), was added conc. HCl until the solution was ~ pH 1 and then set to reflux for 12 hours after which time the reaction was cooled and the EtOH was removed by rotary evaporation. To the resulting brown solid, aqueous $NaHCO_3$ was added (20 mL) and this was then repeatedly extracted with DCM (40 mL) containing a small amount of MeOH (~ 3 %) as the compound is only sparingly soluble in this solvent. The combined organic phases were dried over $MgSO_4$ and evaporated to dryness to give a brown solid. This was then suspended in DCM (20 mL), filtered and washed with a further portion of DCM (10 mL) giving **2** as a white solid (3.08 g, 16.5 mmol, 54 %). ^1H NMR (400 MHz, $(CD_3)_2SO$) δ: 12.0 (s, 1H, -OH), 8.72 (dd, *J* = 4.68, 0.64, 1H, py), 8.31 (d, *J* = 7.92, 1H, py), 7.99 (td, *J* = 7.72, 1.76, 1H, py), 7.57 (ddd, *J* = 7.52, 4.72, 1.08 Hz, 1H, py), 7.22 (s, 1H, pyr), 2.31 (s, 3H, $-CH_3$). ^{13}C NMR was not obtained due to the poor solubility of this compound. *HRMS (m/z): $[M+H]^+$ for $C_{10}H_9N_3O$ calculated 188.0818, measured 188.0814.*

2.1.3 Synthesis of **3**

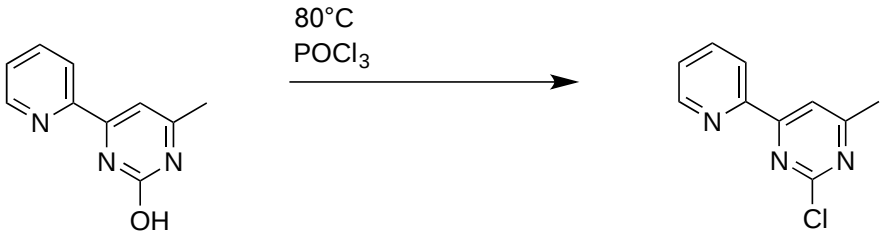

2 **3**

A solution of $POCl_3$ (30 mL) and **2** (3.1 g, 0.017 mol) was heated at 80 °C with stirring for 16 hours giving a dark brown solution. This was then evaporated to dryness, neutralised with aqueous $NaHCO_3$ (30 mL), extracted into DCM (40 mL) and dried over $MgSO_4$. Purification was achieved by column chromatography (SiO_2, 3 % MeOH in DCM) to yield a white solid **3** (1.1 g, 5.35 mmol, 32.4%). ^{1}H NMR (400 MHz, ($CDCl_3$) δ: 8.73 (dq, *J* = 4.76, 0.88, 1H, py), 8.50 (dt, *J* = 7.92, 0.96, 1H, py), 8.21 (s, 1H, pyr), 7.89 (td, *J* = 7.72, 1.76, 1H, py), 7.45 (ddd, *J* = 7.56, 4.76, 1.16 Hz, 1H, py), 2.64 (s, 3H, -CH_3). ^{13}C NMR (100 MHz, ($CDCl_3$) δ: 171, 165, 161, 153, 150, 137, 126, 122, 115, 24. *HRMS (m/z): $[M+H]^+$ for $C_{10}H_8N_3{}^{35}Cl$ calculated 206.048, measured 206.0477.*

2.1.4 Synthesis of **4**

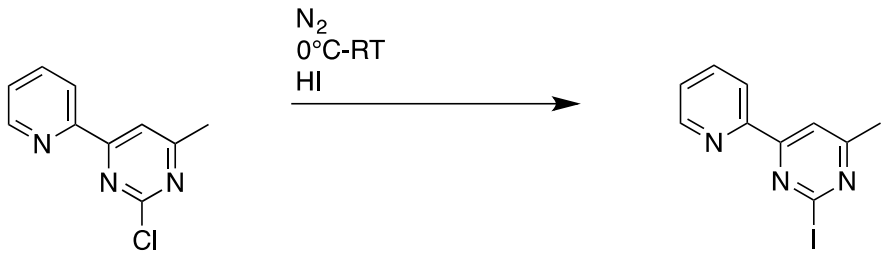

3 **4**

Under an atmosphere of N_2 at 0 °C, HI acid (10 mL) was added to **3** (1.1 g, 5.35 mmol) and this was allowed to warm to room temperature and left to stir for 48hrs. Aqueous $NaHCO_3$ (30 mL) was added to neutralise the reaction and sodium metabisulfite was added before extracting into DCM, drying with $MgSO_4$ and evaporating to dryness to yield **4** (1.1 g, 3.70 mmol, 69 %) as a white solid. Purification was achieved by column chromatography (SiO_2, 3 % MeOH in DCM) ^{1}H NMR (500 MHz, ($CDCl_3$) δ: 8.69 (dq, *J* = 4.75, 0.9, 1H, py), 8.45 (dt, *J* = 7.9, 0.95, 1H, py), 8.21 (s, 1H, pyr), 7.86 (td, *J* = 7.75, 1.8, 1H, py), 7.42 (ddd, *J*= 7.55, 4.75, 1.15 Hz, 1H, py), 2.64 (s, 3H, -CH_3). ^{13}C NMR (125 MHz, ($CDCl_3$) δ: 171, 164, 152, 149, 137, 129, 126, 122, 116, 24. *HRMS (m/z): $[M+H]^+$ for $C_{10}H_8N_3I$ calculated 297.9836, measured 297.9834.*

2.1.5 Synthesis of L^1

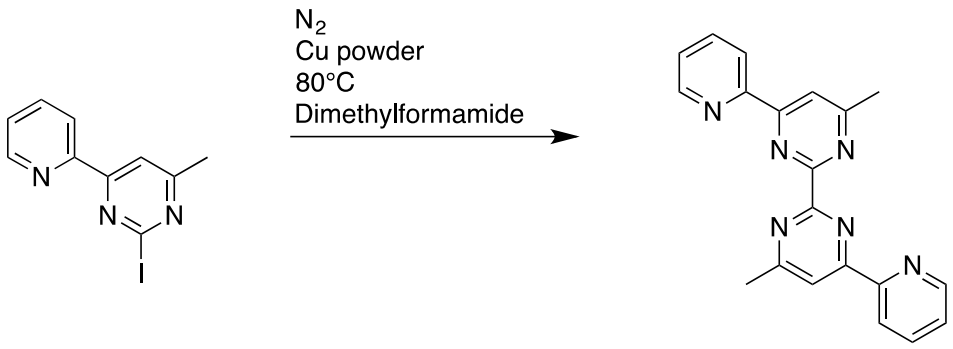

4 **L^1**

To a two necked 50 mL round bottomed flask was added freshly activated copper bronze[89] (3.0 g, 0.047 mol) and the iodo compound **4** (1.7 g, 5.72 mmol) and the flask purged with N_2 for 1 hour. To this was then added anhydrous DMF (20 mL) and the reaction heated with stirring at 80°C for 48 hours. The DMF was removed by rotary evaporation and to the resulting solid ammonia (0.88 spg, 50 mL) was added and the reaction stirred for 24 hours during which time the solution developed an intense blue colour. This was extracted into DCM (3 x 40 mL), dried over $MgSO_4$ and evaporated to dryness. Purification was carried out by column chromatography (Al_2O_3, 1 % MeOH DCM) to yield **L^1** (190 mg, 0.56 mmol, 19.5 %, see Results and Discussion) as an off white solid. ^{1}H NMR (400 MHz, ($CDCl_3$) δ: 8.78-8.76 (m, 2H, overlapping, py, py), 8.4 (s, 1H, pyr), 7.93 (td, *J* = 7.84, 1.6, 1H, py), 7.46 (ddd, *J* = 7.56, 4.72, 1.2 Hz, 1H), 2.84 (s, 3H, -CH_3). ^{13}C NMR (100 MHz, ($CDCl_3$) δ: 169, 163.5, 163.1, 154, 149, 137, 126, 123, 117, 25. *HRMS (m/z): $[M+H]^+$ for $C_{20}H_{16}N_6$ calculated 341.1509, measured 341.1510.*

2.1.6 Synthesis of *ter*-**L**^{1}ReCl(CO)$_3$

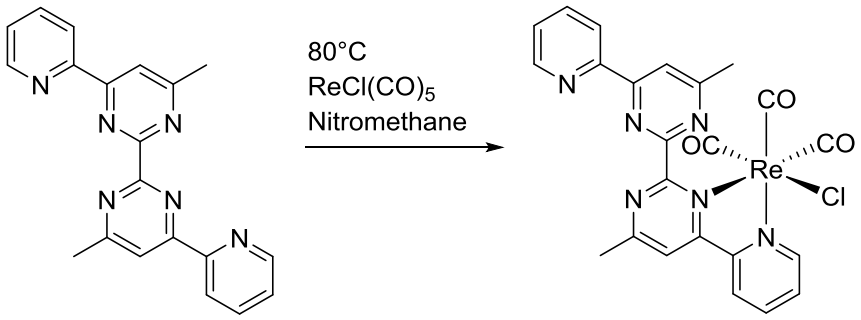

L^{1} *ter*-**L**^{1}ReCl(CO)$_3$

A solution of **L**^{1} (23 mg, 0.07 mmol) and $Re(CO)_5Cl$ (24.52 mg, 0.07 mmol) in $MeNO_2$ was heated at 80°C for 4 hours. The $MeNO_2$ was removed by rotary evaporation and water (10 mL) added. The product was then extracted into DCM (2 x 30 mL), dried with $MgSO_4$ and evaporated. Purification was achieved by column chromatography (Al_2O_3, 1% MeOH in DCM) to yield *ter*-**L**^{1}ReCl(CO)$_3$ as an orange powder (17 mg, 0.026 mmol, 38 %). Crystals suitable for solid state analysis by X-ray diffraction were obtained from layering a solution of the product (5 mg, 0.008 mmol) in dichloromethane (2 mL) with hexane (10 mL). ^{1}H NMR (400 MHz, (CD_3NO_2) δ: 9.15 (dd, *J* = 5.4, 0.72 1H, py), 8.77 (dt, *J* = 3.96, 0.76, 1H, py), 8.69 (d, *J* = 8.28, 1H, py), 8.55 (d, *J* = 7.92, 1H, py), 8.51 (s, 1H, pyr), 8.50 (s, 1H, pyr), 8.37 (td, *J* = 7.92, 1.48, 1H, py), 7.95 (td, *J* = 7.72, 1.72, 1H, py), 7.81 (ddd, *J* = 7.60, 5.48, 1.12 Hz, 1H, py), 7.54 (ddd, *J* = 7.56, 4.76, 1.12 Hz, 1H, py), 2.87 (s, 3H, -CH_3), 2.77 ppm (s, 3H, -CH_3). *HRMS (m/z): [M+H]$^{+}$ for $C_{23}H_{16}N_6O_3ClRe$ calculated 647.0603, measured 647.0568.*

2.1.7 Synthesis of *cent*-$\mathbf{L^1}ReCl(CO)_3$

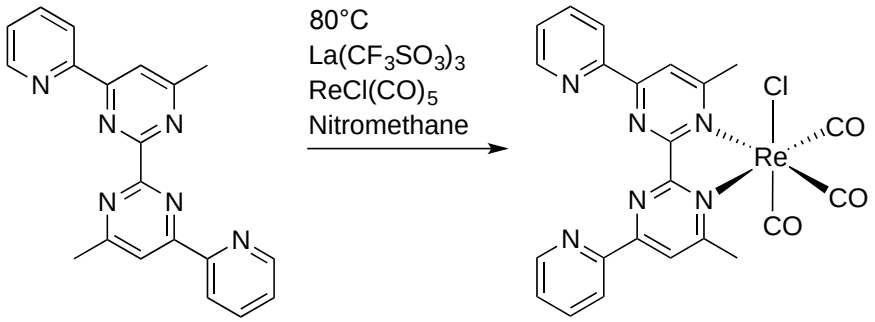

$\mathbf{L^1}$ *cent*-$\mathbf{L^1}ReCl(CO)_3$

A solution of $\mathbf{L^1}$ (31.0 mg, 0.09 mmol) and $La(CF_3SO_3)_3$ (53.4 mg, 0.09 mmol) in $MeNO_2$ was heated at 80°C for 1 hour before adding $Re(CO)_5Cl$ (33.0 mg, 0.09 mmol) and the heating continued for a further 3 hours. The $MeNO_2$ was removed by rotary evaporation, a solution of Na_4EDTA (347.0 mg, 1.0 mmol) in water (20 mL) was added and the crude product was isolated by extracting into DCM (2 x 30 mL) followed by drying over $MgSO_4$ and evaporation. Purification was achieved by column chromatography (Al_2O_3, 1 % MeOH in DCM) to yield *cent*-$\mathbf{L^1}ReCl(CO)_3$ as an orange powder (25 mg, 0.039 mmol, 43 %). Crystals suitable for solid state analysis by X-ray diffraction were obtained from layering a solution of the product (5 mg, 0.008 mmol) in dichloromethane (2 mL) with hexane (10 mL). ^1H NMR (400 MHz, (CD_3NO_2) δ: 9.35 (d, *J* = 4.44, 1H), 8.72-8.69 (m, overlapping, 2H, pyr, py), 8.40 (td, *J* = 7.88, 1.60, 1H, py), 7.99 (td, *J* = 5.24, 0.68 Hz, 1H, py), 3.32 ppm (s, 3H, $-CH_3$). *HRMS (m/z): $[M+H]^+$ for $C_{23}H_{16}N_6O_3ClRe$ calculated 647.0603, measured 647.0601.*

2.1.8 Synthesis of $[Cu_2(\mathbf{L^1})(ClO_4)_2(MeCN)_4]^{2+}$

To a suspension of $\mathbf{L^1}$ (5.00 mg, 0.015 mmol) in MeCN (2 mL), $Cu(ClO_4)_2$ (11.99 mg, 0.032 mmol) was added and the reaction briefly heated and sonicated until all the ligand dissolved to give a light blue solution. Chloroform was allowed to slowly diffuse into the solution and after a few days, blue crystals had formed (5 mg, 32 %). ESI-MS *m/z* = 848 corresponding to $\{[Cu_2(\mathbf{L^1})(ClO_4)_2(MeCN)_4](ClO_4)\}^+$.

2.1.9 Synthesis of $[Cu_2(\mathbf{L^1})_3]^{4+}$

To a suspension of $\mathbf{L^1}$ (5.00 mg, 0.015 mmol) in MeCN (2 mL), $Cu(CF_3SO_3)_2$ (3.55 mg, 0.010 mmol) was added and the reaction briefly heated and sonicated until all the ligand dissolved to give a light blue solution. Diisopropyl ether was allowed to slowly diffuse into the solution and after a few days, blue crystals had formed (3 mg, 17 %). ESI-MS *m/z* = 1594 corresponding to $\{[Cu_2(\mathbf{L^1})_3](CF_3SO_3)_3\}^+$.

2.1.10 Synthesis of $[Cd(\mathbf{L^1})_2]^{2+}$

To a suspension of $\mathbf{L^1}$ (5.00 mg, 0.015 mmol) in MeCN (2 mL), $Cd(ClO_4)_2$ (6.78 mg, 0.008 mmol) was added and the reaction briefly heated and sonicated until all the ligand dissolved to give a light blue solution. Chloroform was allowed to slowly diffuse into the solution and after a few days, small colourless crystals had formed (4 mg, 63 %). ESI-MS *m/z* = 941 corresponding to $\{[Cd(\mathbf{L^1})_2](CF_3SO_3)\}^+$.

2.1.11 Synthesis of $[Eu(\mathbf{L^1})_2]^{3+}$

To a suspension of $\mathbf{L^1}$ (5.00 mg, 0.015 mmol) in MeCN (2 mL), $Eu(CF_3SO_3)_3$ (4.41 mg, 0.008 mmol) was added and the reaction briefly heated and sonicated until all the ligand dissolved to give a clear yellow solution. This solution was layered with diethyl ether and after a few days, yellow crystals had formed (5 mg, 75 %). ESI-MS *m/z* = 1130 corresponding to $\{[Eu(\mathbf{L^1})_2](CF_3SO_3)_2\}^+$.

2.1.12 Synthesis of $[Eu_2Ag_2(\mathbf{L^1})_3(CF_3SO_3)_8]$

To a suspension of $\mathbf{L^1}$ (5.00 mg, 0.015 mmol) in MeCN (2 mL), $Eu(CF_3SO_3)_3$ (5.87 mg, 0.010 mmol) and $Ag(CF_3SO_3)$ (2.52 mg, 0.010 mmol) was added and the reaction briefly heated and sonicated until all the ligand dissolved to give a clear pale yellow solution. This solution was layered with diethyl ether and after a few days, yellow crystals had formed (5 mg, 56 %). ESI-MS *m/z* = 2583 corresponding to $\{[Eu_2Ag_2(L^1)_3(CF_3SO_3)_7]\}^+$.

2.1.13 Synthesis of *ter*-$\mathbf{L^1}Re(CO)_3(H_2O).(CF_3SO_3)$

To a suspension of *ter*-$\mathbf{L^1}ReCl(CO)_3$ (10.00 mg, 0.016 mmol) in MeCN (5 mL), $Zn(CF_3SO_3)_2$ (6.19 mg, 0.017 mmol) was added and the reaction heated and sonicated. The MeCN was removed by rotary evaporation, a solution of Na_4EDTA (347 mg, 1.0 mmol) in water (10 mL) was added and this was extracted into DCM (2 x 15 mL), dried with $MgSO_4$ and evaporated. The resulting powder was dissolved in DCM (2 mL) and this solution was layered with hexane (8 mL). After a few days, yellow crystals had formed (2 mg, 16 %). ESI-MS *m/z* = 611 corresponding to $\{[\mathbf{L^1}ReCO_3]\}^+$.

2.1.14 Synthesis of *cent*-$\mathbf{L^1}ReCl(CO)_3.[CuCl_4]^{2-}$:

To a suspension of *cent*-$\mathbf{L^1}ReCl(CO)_3$ (5.00 mg, 0.008 mmol) in MeCN (2 mL), $Cu(ClO_4)_2$ (3.15 mg, 0.009 mmol) was added and the reaction was briefly heated and sonicated until an orange solution was obtained. Chloroform was allowed to slowly diffuse into the solution and after two weeks, small orange crystals had formed (3 mg, 44 %).

2.2 Results and Discussion

The potentially hexadentate ditopic ligand **L[1]** had been designed so that it would be able to adopt two separate modes of conformation depending on the preferred coordination number of the metal ions present. Due to an inbuilt flexibility between the pyrimidine units, **L[1]** was able to adopt a bis-tridentate binding conformation and also a tetradentate-bidentate binding conformation depending upon the preferred coordination desires of any potential metal ions (Fig. 34). With these two binding motifs available to the ligand, it would be able to complex a wide variety of metal ion centres with differing coordination numbers and binding geometries.

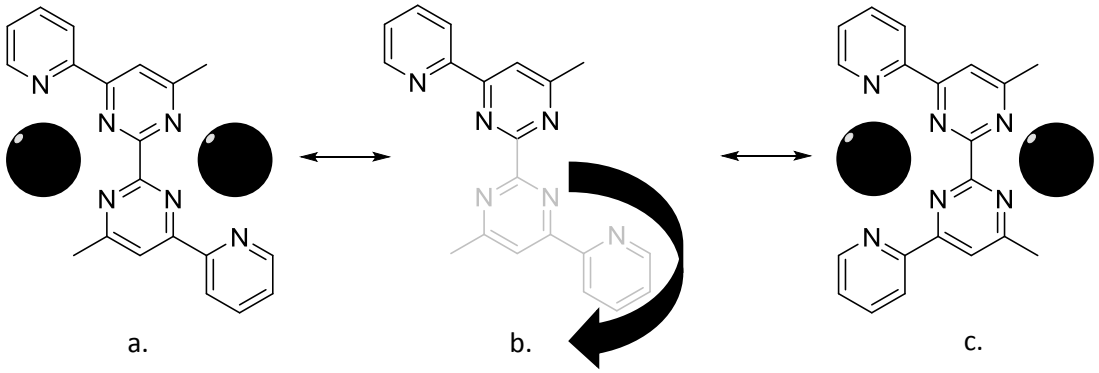

*Fig. 34: Schematic representations of the ligand **L[1]** and its two possible modes of conformation. a. The bis-tridentate conformation, b. a diagram to illustrate the flexible rotation between the two py-pyr domains and c. the tetradentate-bidentate conformation. The black spheres represent metal ions bound in the binding domains.*

L[1] was synthesised in five steps from ethyl picolinate. The first step involved reaction of ethyl picolinate with acetone and NaH to give the dione (**1**). The NMR of this product contained an –OH signal (15.7 ppm) which was attributed to the enol isomer of compound **1**. Reaction with urea gave the pyrimidinol compound which was chlorinated by $POCl_3$. However, the chloro compound **3** was unreactive and had to be converted to the iodo by reaction with HI. Ullmann coupling with copper bronze gave the final product **L[1]**. However, the Ullmann coupling was found to be highly sensitive to the purity of both the iodo-starting material and the freshly activated copper bronze powder, as well as being highly sensitive to the presence of oxygen. Successful synthesis gave variable yields but by

ensuring that the iodo-compound was purified by column chromatography and that the copper had been scrupulously activated[89], acceptable yields (15 – 20 %) were generated.

Suspension of **L¹** in acetonitrile (MeCN) and reaction with two equivalents of copper (II) perchlorate gave a clear blue solution which, after slow diffusion of ether, produced crystals suitable for X-ray analysis. Analysis in the solid state showed the formation of the dinuclear complex $[Cu_2(\mathbf{L^1})(ClO_4)_2(MeCN)_4]^{2+}$ (Fig. 35).

a.

b.

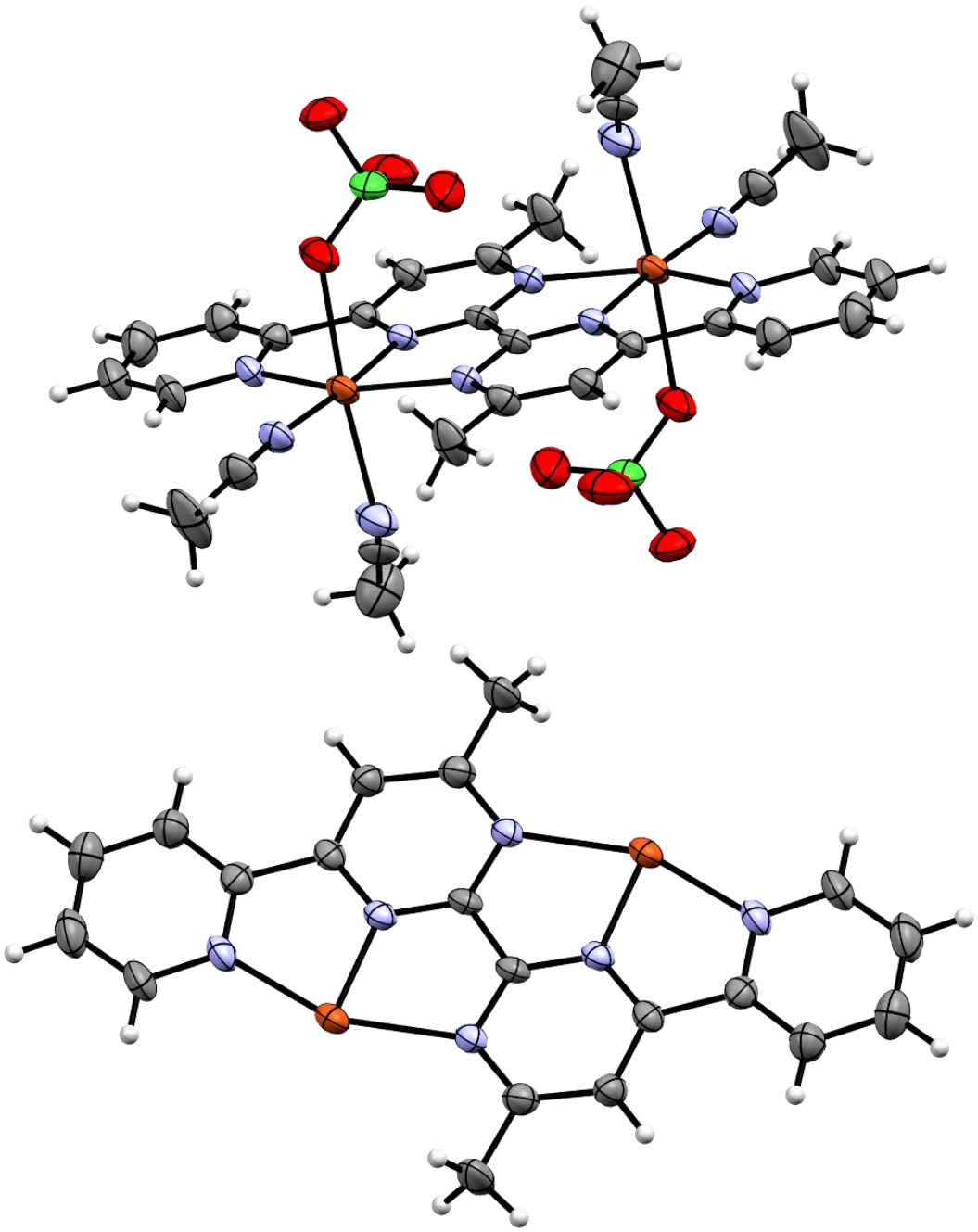

Fig. 35: a. The X-ray crystal structure of the dinuclear complex $[Cu_2(\mathbf{L^1})(ClO_4)_2(MeCN)_4]^{2+}$ and b. a partial view of the X-ray crystal structure with perchlorate anions and acetonitrile molecules removed to better show the bis-tridentate conformation of the ligand strand. Thermal ellipsoids are shown at 50% probability

In this structure the ligand had adopted its bis-tridentate conformation and partitioned itself into two pyridyl-pyrimidine-pyrimidine domains with each coordinating a separate copper (II) metal ion. The copper (II) ion adopts an octahedral coordination geometry comprising three nitrogen atoms from the ligand, two acetonitrile solvent molecules and a perchlorate counter anion. The Cu-N bond lengths range from 1.935 (5) Å to 2.306 (6) Å with the longest bond length arising from the Cu-O bond between the metal centre and the perchlorate anion at 2.415 (4) Å. The distance between the two copper (II) metal centres was measured at 5.531 Å.

Reaction of three equivalents of **L^1** with two equivalents of copper (II) trifluoromethanesulfonate in nitromethane gave a clear blue solution and slow diffusion of diisopropyl ether formed blue crystals suitable for X-ray analysis. Analysis in the solid state revealed the dinuclear complex $[Cu_2(\mathbf{L^1})_3]^{4+}$ (Fig. 36).

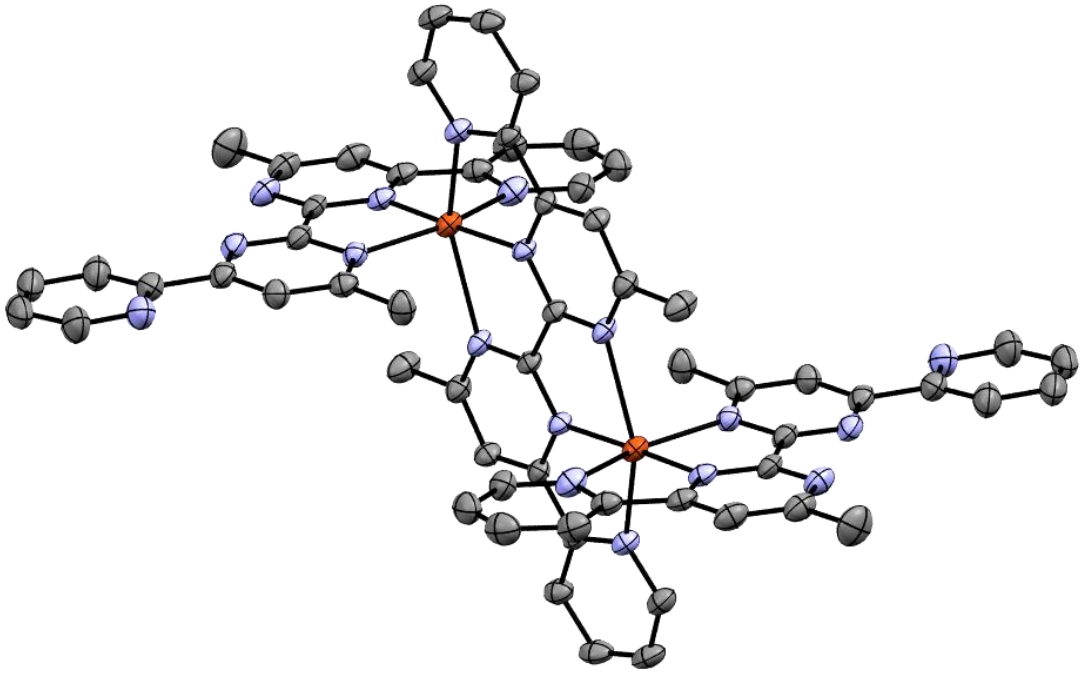

Fig. 36: The X-ray crystal structure of the complex $[Cu_2(\mathbf{L^1})_3]^{4+}$. Hydrogen atoms have been omitted for clarity and thermal ellipsoids are shown at 50% probability.

The X-ray crystal structure showed the complex had been formed through coordination of two copper (II) metal centres by three **L^1** ligand strands. The ligands had adopted their bis-tridentate

conformation and as a result had created two six coordinate binding domains suitable for the octahedral geometries of the copper (II) metal ions. Whilst the 'central' ligand in the complex had provided two pyridyl-pyrimidine-pyrimidine binding domains (as observed previously in Fig. 35), the two 'outer' ligands in the complex only contributed one tridentate binding domain and the other potential binding domains remained uncoordinated (Fig. 37).

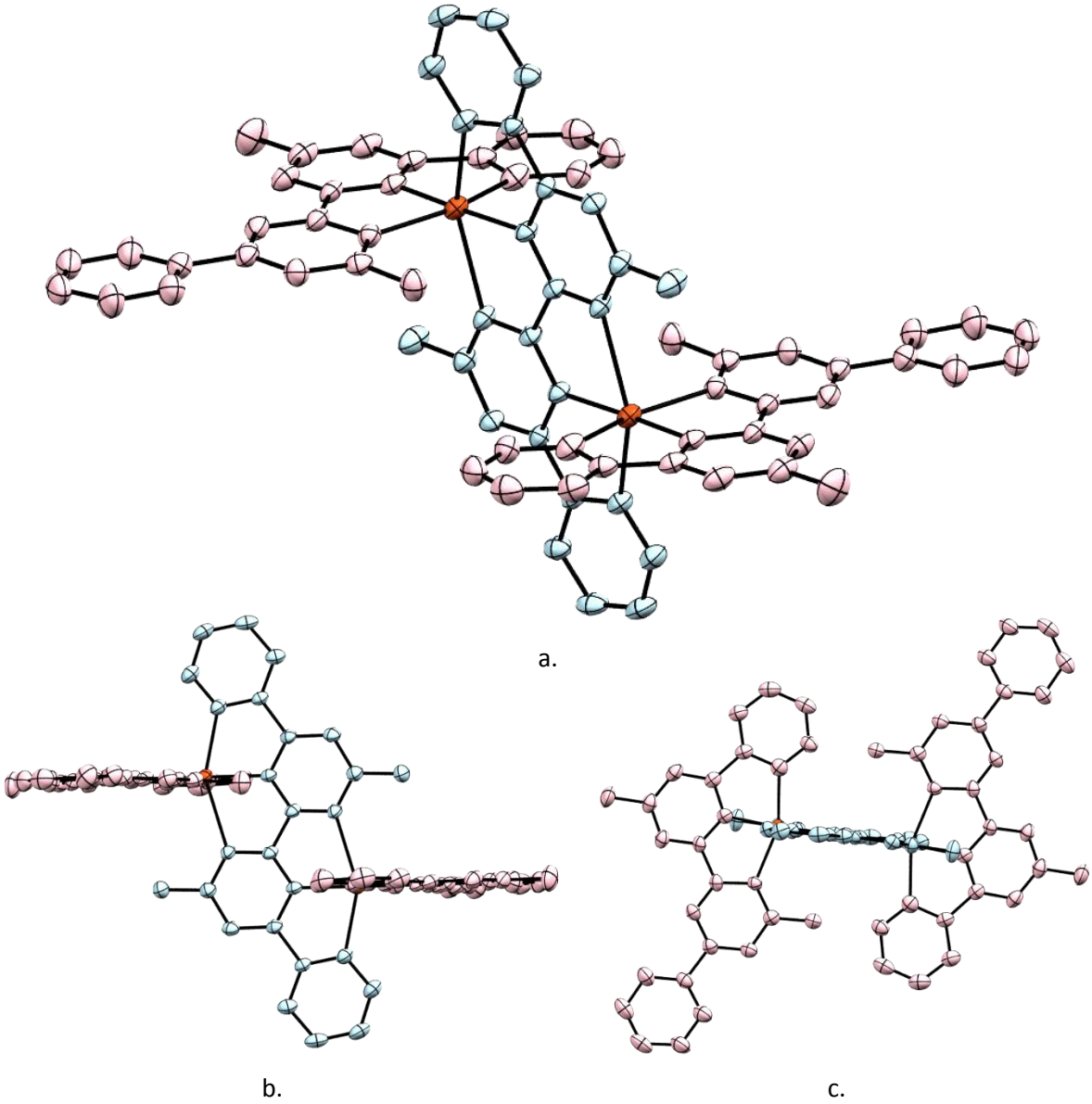

Fig. 37: Alternate views of the X-ray crystal structure of $[Cu_2(\mathbf{L^1})_3]^{4+}$ with the 'central' and 'outer' ligand strands coloured blue and pink respectively. Hydrogen atoms have been removed for clarity and thermal ellipsoids are shown at 50% probability.

The Cu-N bond lengths from coordinated domains, range from 1.927 (3) Å to 2.444 (3) Å with the longest bond length observed between the nitrogen atom of the pyrimidine unit of the 'central' ligand and the copper (II) metal centre. The distance between the two metal centres in this complex was 5.894 Å which is longer than what was observed in the previously reported $[Cu_2(\mathbf{L^1})(ClO_4)_2(MeCN)_4]^{2+}$ complex (Fig. 35).

Reaction of two equivalents of $\mathbf{L^1}$ with one equivalent of cadmium (II) perchlorate in acetonitrile gave a clear, light yellow solution and when this solution was subjected to slow diffusion of chloroform, crystals suitable for X-ray analysis were obtained. Analysis in the solid state gave the mononuclear complex $[Cd(\mathbf{L^1})_2]^{2+}$ (Fig. 38).

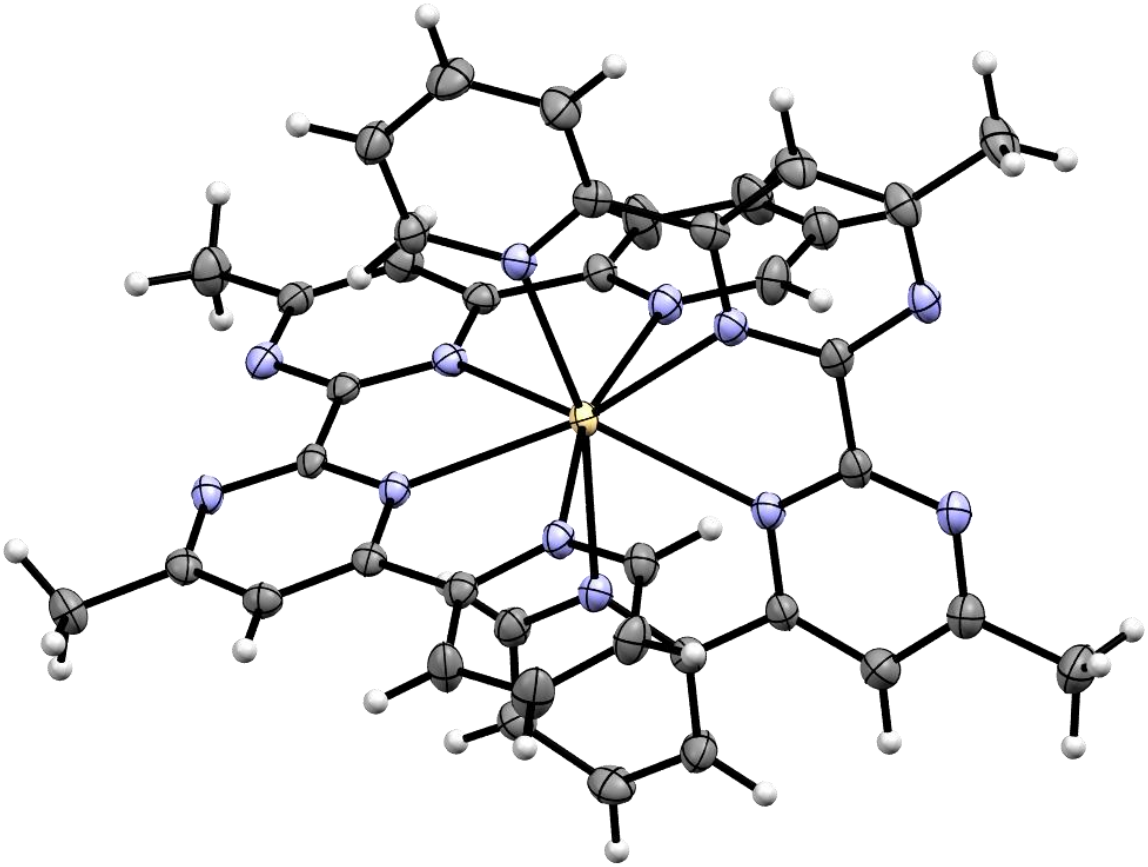

Fig. 38: The X-ray crystal structure of the mononuclear complex $[Cd(\mathbf{L^1})_2]^{2+}$ showing how the cadmium (II) metal centre is coordinated by two tetradentate binding domains with the bidentate domain at the 'back' of the ligand strand remaining uncoordinated. Thermal ellipsoids are shown at 50% probability.

To allow it to successfully coordinate the cadmium (II) metal centre, $\mathbf{L^1}$ had adopted an alternate conformation to what had been observed in the previous two complexes containing copper (II) metal ions. The cadmium (II) metal ion exhibits a preference for a coordination number of eight and so the ligand strand adopts a tetradentate-bidentate binding conformation. Due to the stoichiometry of the reaction, two ligands provided an octadentate binding domain consisting of two pyridyl-pyrimidine-pyrimidine-pyridyl tetradentate domains which were suitable for the metal centre to occupy. Whilst the two tetradentate domains had bound the cadmium (II) metal ion, the bidentate domain at the 'back' of the ligand (formed by the nitrogen atoms of the 'outer' pyrimidine-pyrimidine sites) remained uncoordinated. This molecular structure had demonstrated that the ligand strand was able to adopt its tetradentate-bidentate binding conformation providing the coordination preferences of a potential metal ion guest encouraged it to do so (Fig. 39).

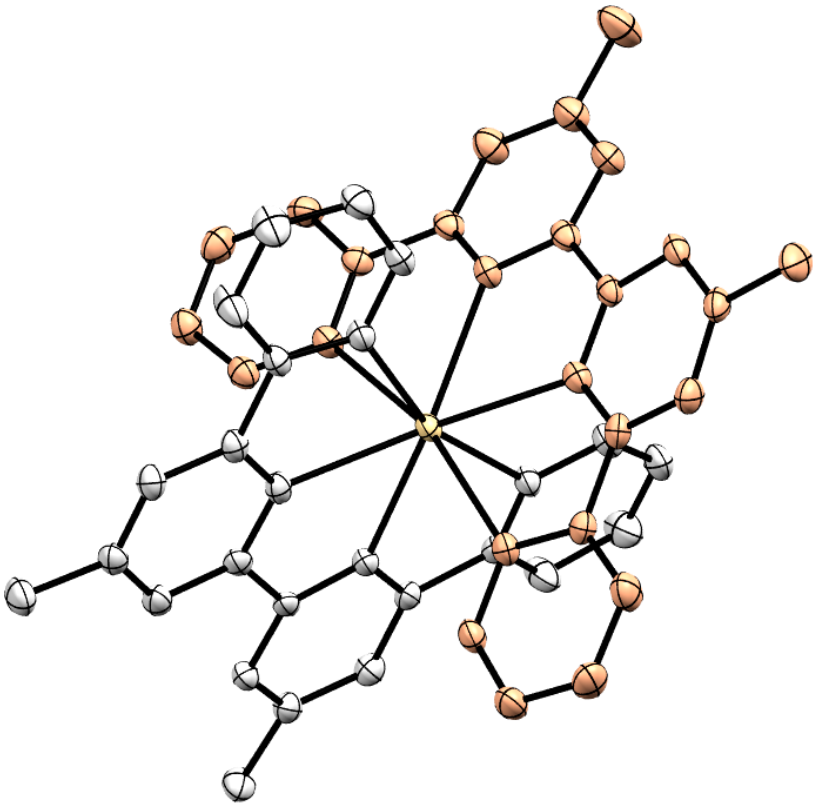

Fig. 39: The X-ray crystal structure of the eight coordinate $[Cd(\mathbf{L^1})_2]^{2+}$ complex. Alternate ligand strands have been coloured orange and silver for clarity of the tetradentate-bidentate binding conformation the ligand has adopted. Hydrogen atoms have also been removed for clarity and thermal ellipsoids are shown at 50% probability.

Cd-N bond lengths from the coordinated nitrogen atoms of the pyridyl-pyrimidine-pyrimidine-pyridyl domains ranged from 2.468 (2) Å to 2.526 (3) Å.

Reaction of **L^1** with europium (III) trifluoromethanesulfonate in acetonitrile gave a clear yellow solution, which after layering with diethyl ether gave small yellow crystals of X-ray quality. Analysis of these crystals by X-ray diffraction revealed the mononuclear complex $[Eu(\mathbf{L^1})_2(CF_3SO_3)]^{2+}$ (Fig. 40).

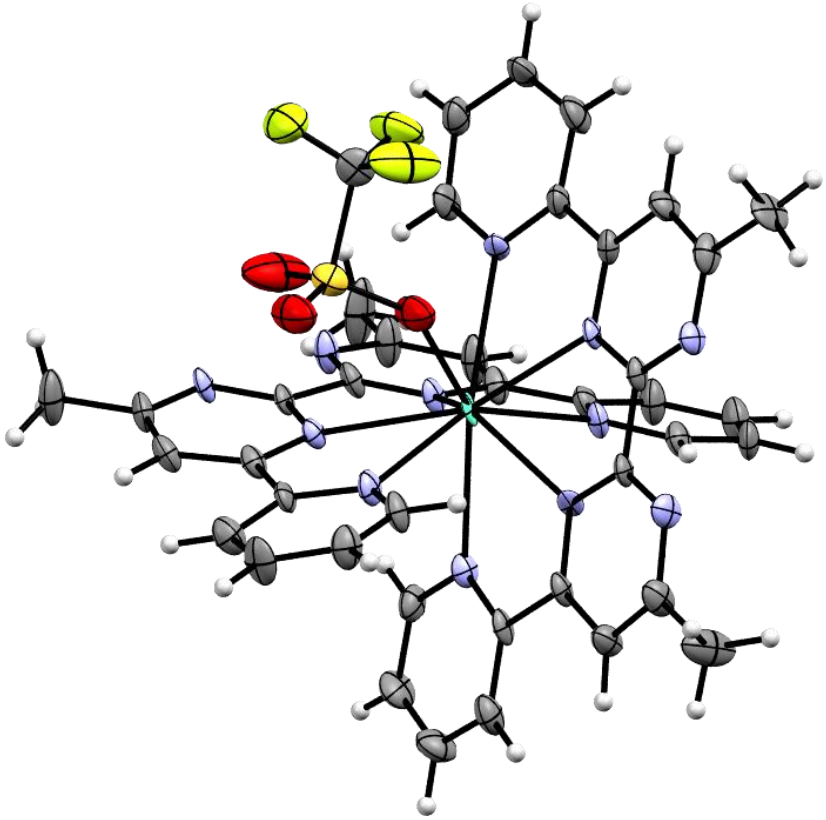

Fig. 40: The X-ray crystal structure of the nine coordinate $[Eu(\mathbf{L^1})_2(CF_3SO_3)]^{2+}$ complex with the uncoordinated bi-pyrimidine domain at the 'back' of the ligand strands. Thermal ellipsoids shown at 50% probability.

The molecular structure revealed that, in the same manner as the reaction with cadmium (II) perchlorate, the ligand had partitioned into tetradentate-bidentate domains. The pyridyl-pyrimidine-pyrimidine-pyridyl tetradentate unit coordinated the europium (III) metal ion, whilst the 'outer' pyrimidine nitrogen atoms remained uncoordinated. However, unlike the cadmium (II) metal ion in the $[Cd(\mathbf{L^1})_2]^{2+}$ complex, the europium (III) ion was nine coordinate arising from the coordination of two tetradentate ligands and an additional trifluoromethanesulfonate counter ion. Bond lengths

from the coordinated nitrogen atoms of the pyridyl-pyrimidine-pyrimidine-pyridyl domains to the europium (III) metal ion ranged from 2.507 (6) Å to 2.633 (6) Å with the bond length between the coordinating oxygen from the trifluoromethanesulfonate counter ion measuring 2.400 (7) Å. This mononuclear species was also found to exist in solution as an ion at *m/z* 1131 corresponding to $[Eu(\mathbf{L^1})_2(CF_3SO_3)_2]^+$ in the ESI-MS.

In both the $[Cd(\mathbf{L^1})_2]^{2+}$ and the $[Eu(\mathbf{L^1})_2(CF_3SO_3)]^{2+}$ complexes, the ligand strands adopted the tetradentate-bidentate conformation and had coordinated the metal centres through the tetradentate binding domain. The major difference between the two complexes was the difference in coordination of the metal centres. The cadmium (II) metal ion was eight coordinate and the europium (III) metal ion was nine coordinate as it was coordinated by a trifluoromethanesulfonate counter ion as well as the nitrogen atoms of the pyridyl-pyrimidine-pyrimidine-pyridyl domains (Fig. 41).

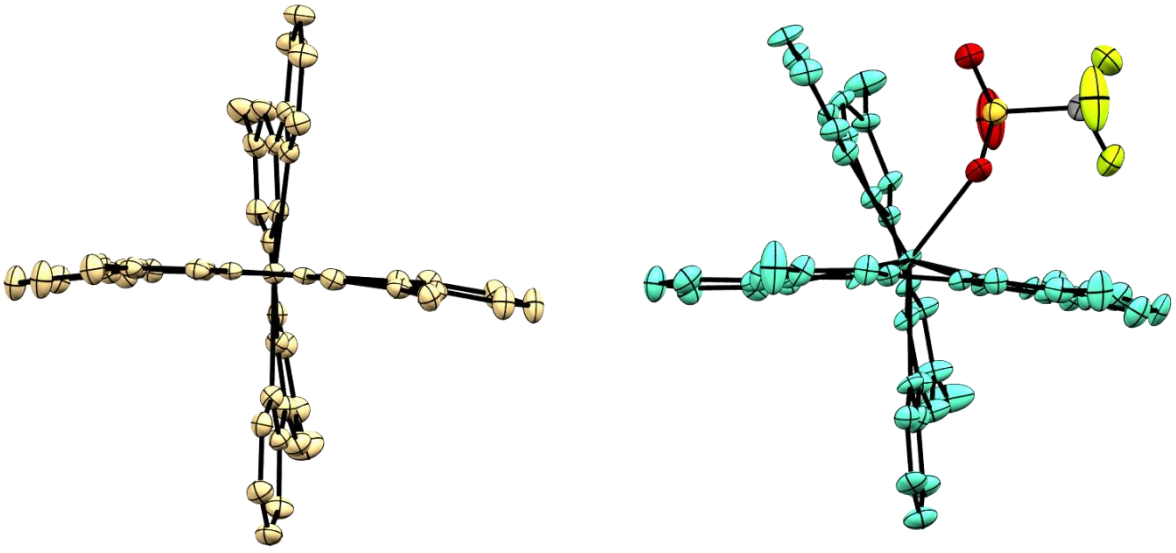

a. b.

Fig. 41: The X-ray crystal structures of a. $[Cd(\mathbf{L^1})_2]^{2+}$ (yellow) and b. $[Eu(\mathbf{L^1})_2(CF_3SO_3)]^{2+}$ (blue) illustrating how the presence of the coordinated trifluoromethanesulfonate anion alters the geometry of the ligand strands in the final complex.

It was observed that access to the bidentate domain on the back of **L**[1] becomes available when the ligand strand has been coordinated to a europium (III) metal ion (Fig. 40). Hence an attempt was made to create a chain of complexes by introducing a four coordinate metal ion that could potentially connect complexes together by coordinating the bidentate domains from separate complexes.

Reaction of three equivalents of the **L**[1] ligand strand with two equivalents of europium (III) trifluoromethanesulfonate and two equivalents of silver (I) trifluoromethanesulfonate in acetonitrile gives a clear yellow solution. Layering this solution with diethyl ether resulted in small yellow crystals being obtained which were of sufficient X-ray quality to reveal the molecular structure of the complex (Fig. 42).

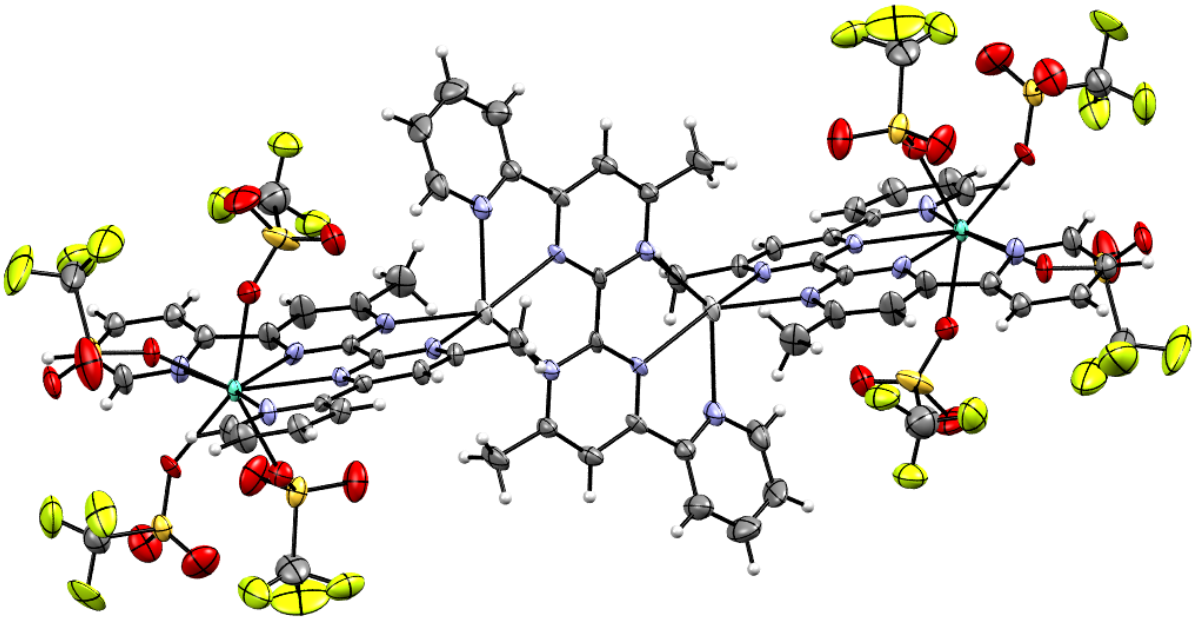

*Fig. 42: The X-ray crystal structure of the tetranuclear complex [Eu_2Ag_2(**L**[1])$_3$(CF_3SO_3)$_8$]. Different **L**[1] ligand strands adopt both the bis-tridentate and tetradentate-bidentate conformations within the same structure to accommodate both the eight coordinate europium (III) and the five coordinate silver (I) metal ions in the complex. Thermal ellipsoids are shown at 50% probability.*

The crystal structure revealed a tetranuclear dimetallic complex [Eu_2Ag_2(**L**[1])$_3$(CF_3SO_3)$_8$] formed by coordination of four metal centres (two europium (III) and two silver (I) metal ions) by three **L**[1] ligand strands.

The europium (III) metal ions were both eight coordinate and the silver (I) metal ions were both five coordinate in the complex. As seen previously, the europium (III) metal centres were coordinated by the nitrogen atoms from the pyridyl-pyrimidine-pyrimidine-pyridyl tetradentate domain of $\mathbf{L^1}$. However, the remaining coordination sites of the europium (III) metal centres were occupied by four trifluoromethanesulfonate counter ions giving each centre a final coordination number of eight. With the ligand strands adopting the tetradentate-bidentate binding motif so as to necessitate the coordination of the europium (III) metal ions, the bidentate domain at the 'back' of the ligand was now accessible for coordination of another metal centre (Fig. 43).

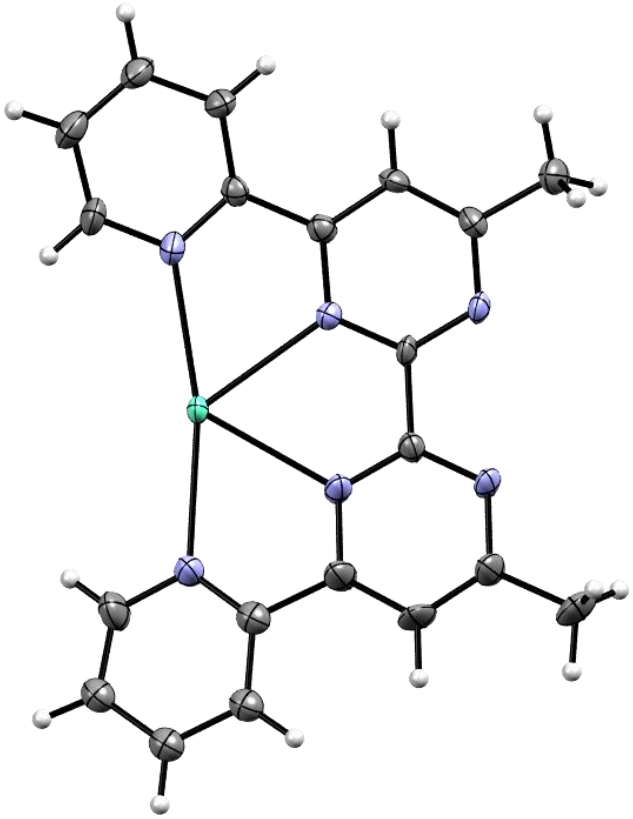

Fig. 43: A partial view of the X-ray crystal structure of $[Eu_2Ag_2(\mathbf{L^1})_3(CF_3SO_3)_8]$ showing one $\mathbf{L^1}$ ligand strand coordinating one europium (III) metal centre in the pyridyl-pyrimidine-pyrimidine-pyridyl domain of the tetradentate-bidentate binding conformation. Thermal ellipsoids are shown at 50% probability.

The silver (I) metal ions in the complex had coordinated to the bidentate domain at the 'back' of the tetradentate-bidentate binding motif and also through the nitrogen atoms of the pyridyl-pyrimidine-pyrimidine domain of a separate $\mathbf{L^1}$ ligand strand. This separate strand had partitioned into two

terdentate domains and as a result, gave five coordinate silver (I) metal ions. This central ligand strand also acted as a bridge in connecting the tetradentate-bidentate ligand strands together through coordination of the silver (I) metal ions (Fig. 44).

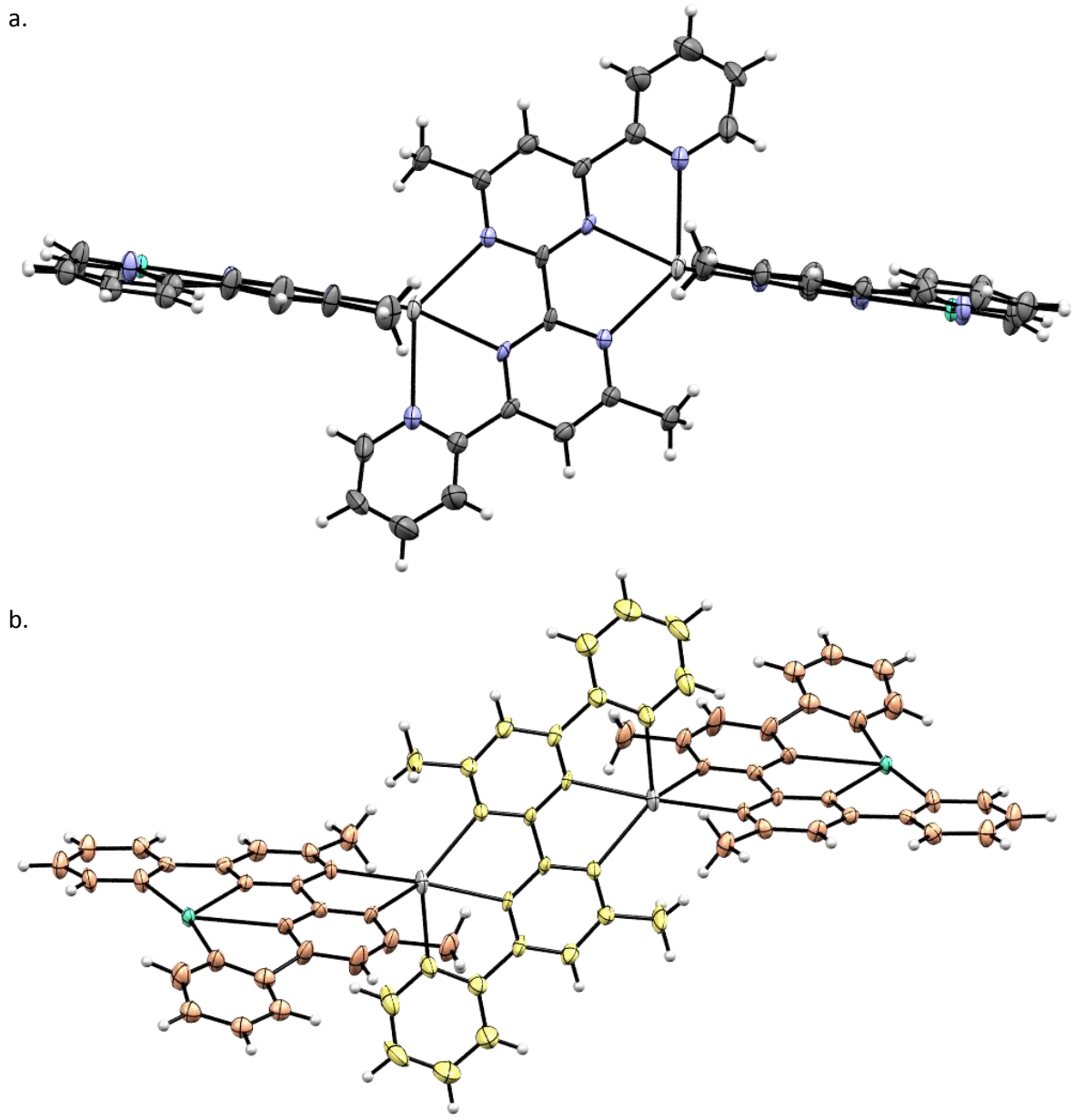

Fig. 44: Partial views of the X-ray crystal structure of $[Eu_2Ag_2(\mathbf{L^1})_3(CF_3SO_3)_8]$ showing only the ligand strands and coordinated metal ions. a. demonstrates how the central ligand strand in the complex has adopted the bis-tridentate conformation and has coordinated a silver (I) metal ion in each tridentate domain. b. illustrates how the central ligand strand (yellow) acts as a bridge, connecting both 'ends' of the overall complex together through coordination of the silver (I) metal ions. The silver (I) metal ions coordinate the bidentate domain of the terminal ligand strands (orange) that are coordinating the europium (III) metal ions in the tetradentate domain. Thermal ellipsoids are shown at 50% probability and trifluoromethanesulfonate anions have been omitted for clarity.

So far it has been demonstrated that the ligand **L[1]** due to its polydentate nature, is able to partition into different binding domains dependent upon what metal ion it is coordinated to. As a result of this work, it was decided that the coordination chemistry of **L[1]** with a kinetically inert metal ion such as rhenium (I) would be investigated. We also aimed to investigate if metal ions could template the reaction and hence control which binding domain of the ligand strand this 3rd row d-block metal ion would coordinate to.

Thus reaction of the ligand **L[1]** with one equivalent of rhenium (I) pentacarbonyl chloride ($ReCl(CO)_5$) in CD_3NO_2 and monitoring by ^1H NMR spectroscopy showed the formation of one major product (Fig. 45). An ion at *m/z* 647 in the ESI-MS corresponding to $[\mathbf{L^1}ReClCO_3]^+$ confirmed that the ligand had reacted with $ReCl(CO)_5$. However, the ^1H NMR spectrum gave ten aromatic signals of equal intensity indicating that upon reaction with rhenium (I) metal ions, the ligand is unsymmetrical (Fig. 45 b.).

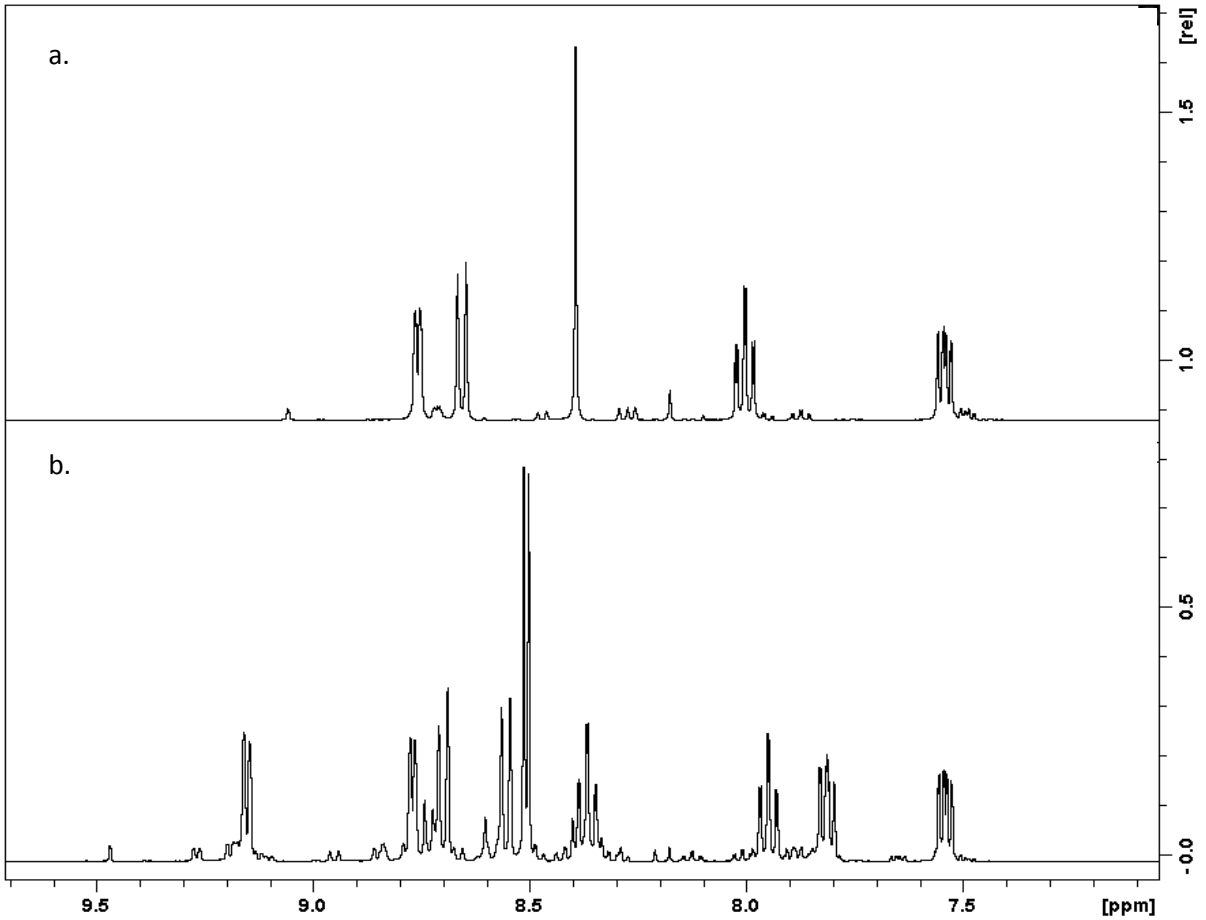

*Fig. 45: The aromatic regions of ^1H NMR spectra in CD_3NO_2 of a. **L[1]** and b. **L[1]** after reaction with $ReCl(CO)_5$. The increase in the number of environments in the aromatic region from a. to b. indicates that the ligand is no longer symmetrical.*

The only mode of binding that would result in an unsymmetrical ligand is coordination of the terminal pyridyl-pyrimidine domain giving a bound rhenium (I) metal ion at the end of the ligand strand. This mode of coordination was confirmed by X-ray crystallography as crystals of the *ter*-**L**^{1}ReCl(CO)$_3$ product suitable for analysis, were obtained from layering a solution of the product in dichloromethane with hexane. In the solid-state the coordination of the rhenium (I) metal ion is fulfilled by the diimine unit from the pyridyl-pyrimidine domain as well as three carbonyl groups and a chloride. Bond lengths to the rhenium (I) metal centre were 2.158 (7) Å from the nitrogen atom of the pyridyl domain and 2.200 (8) Å from the nitrogen atom of the pyrimidine domain. The remaining coordination sites play no role in any coordination and lie orthogonal to the coordinated end of the ligand (Fig. 46).

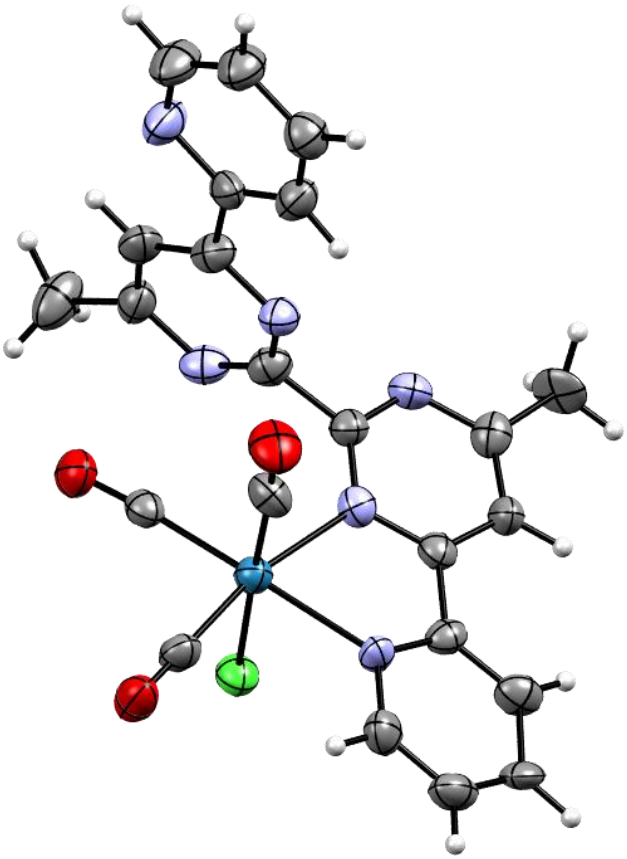

*Fig. 46: The X-ray crystal structure of the ter-**L**^{1}ReCl(CO)$_3$ product showing the rhenium (I) metal ion coordinated at the terminal pyridyl-pyrimidine domain. Thermal ellipsoids are shown at 50% probability.*

However, formation of the complex in which the rhenium (I) ion is coordinated to the 'outer' bidentate pyrimidine nitrogen atoms would be of interest as this mode of coordination would result in a species containing rhenium (I) with an uncoordinated tetradentate domain; making it ideal for the coordination of metal ions. Whilst reaction of **L^1** with $ReCl(CO)_5$ gives none of this desired species, reaction of **L^1** with a lanthanide metal ion involves coordination of the tetradentate domain and leaves the 'outer' bipyrimidine uncoordinated. This was previously described in this chapter when **L^1** was reacted with europium (III) trifluoromethanesulfonate to give the mononuclear complex $[Eu(\mathbf{L^1})_2]^{3+}$. Analysis by X-ray crystallography showed that the ligand partitions into tetradentate-bidentate domains (Fig. 47).

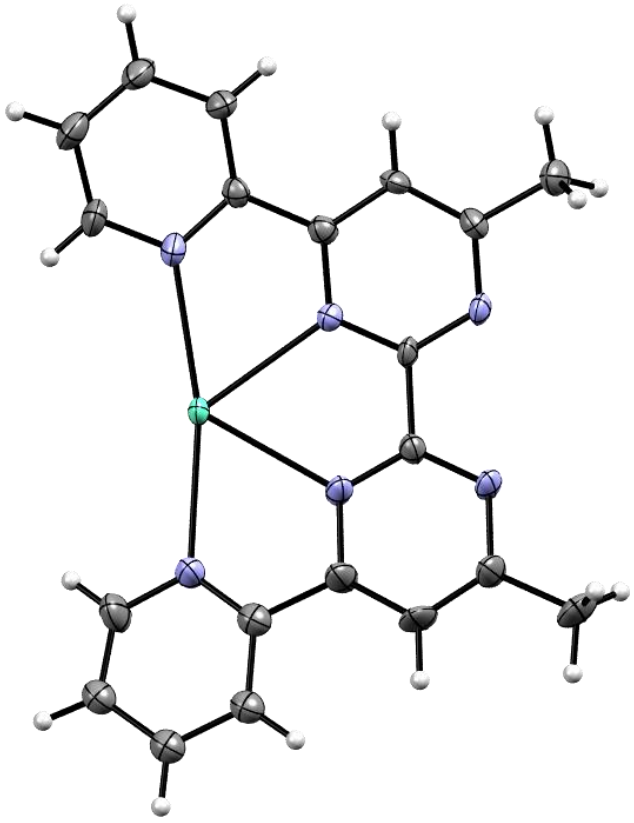

Fig. 47: A partial view of the X-ray crystal structure of the $[Eu(\mathbf{L^1})_2(CF_3SO_3)]^{2+}$ complex showing the europium (III) metal ion coordinating the pyridyl-pyrimidine-pyrimidine-pyridyl tetradentate domain. The 'outer' bipyrimidine domain is accessible for the coordination of another metal ion whilst the ligand is in this tetradentate-bidentate binding motif. Thermal ellipsoids are shown at 50% probability.

Whilst in this mode of coordination, access to the central bidentate domain and the potential coordination of rhenium (I) to this site is now possible. Consequently reacting the ligand **L^1** with one

equivalent of lanthanum (III) trifluoromethanesulfonate, one equivalent of rhenium (I) pentacarbonyl chloride and monitoring its progress by ^{1}H NMR, resulted in the presence of one major product. This product contained only five aromatic protons all of equal intensity, indicating that the ligand had remained symmetrical. However, a shift in the positioning of the signals in the spectrum suggested that the rhenium (I) metal ion had reacted with the ligand (Fig. 48).

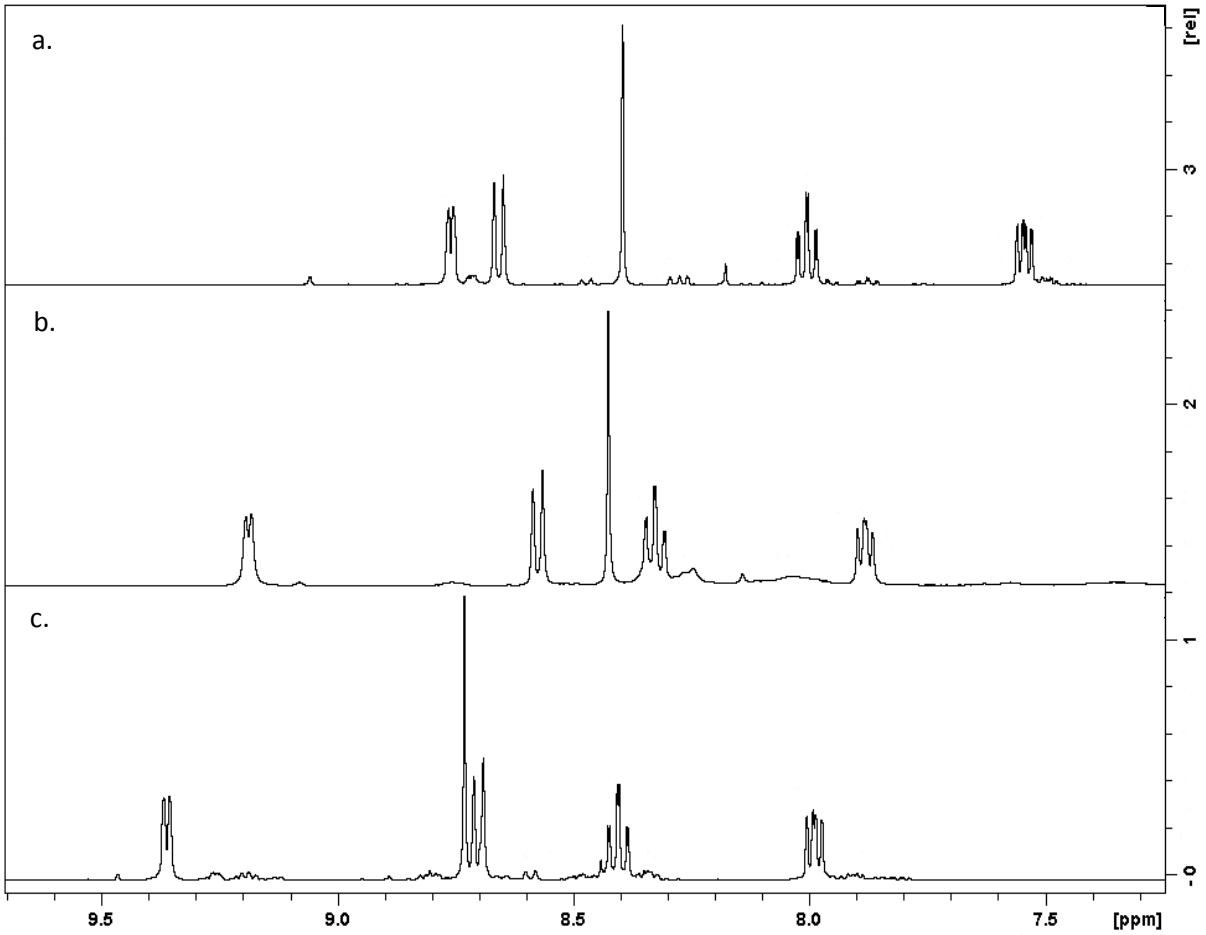

*Fig. 48: The aromatic regions of ^{1}H NMR spectra in CD_3NO_2 of a. **L^{1}**, b. **L^{1}** upon reaction with $La(CF_3SO_3)$ and c. **L^{1}** upon reaction with $ReCl(CO)_5$ after using $La(CF_3SO_3)_3$ as a template. It can be seen that all spectra contain five signals in the aromatic regions indicating symmetrical conformations of **L^{1}**. Yet due to the shifting of the signals, it can be determined that each species is different.*

Further confirmation that **L^{1}** had reacted with the rhenium (I) pentacarbonyl chloride was found in the ESI-MS through observation of an ion at *m/z* 647 corresponding to a **L^{1}**$ReCl(CO)_3$ species. Small orange crystals of this new material were grown by layering a solution of the material in

dichloromethane with hexane and analysis of these by X-ray diffraction gave the molecular structure of the complex as *cent*-**L**^{1}ReCl(CO)$_3$ (Fig. 49).

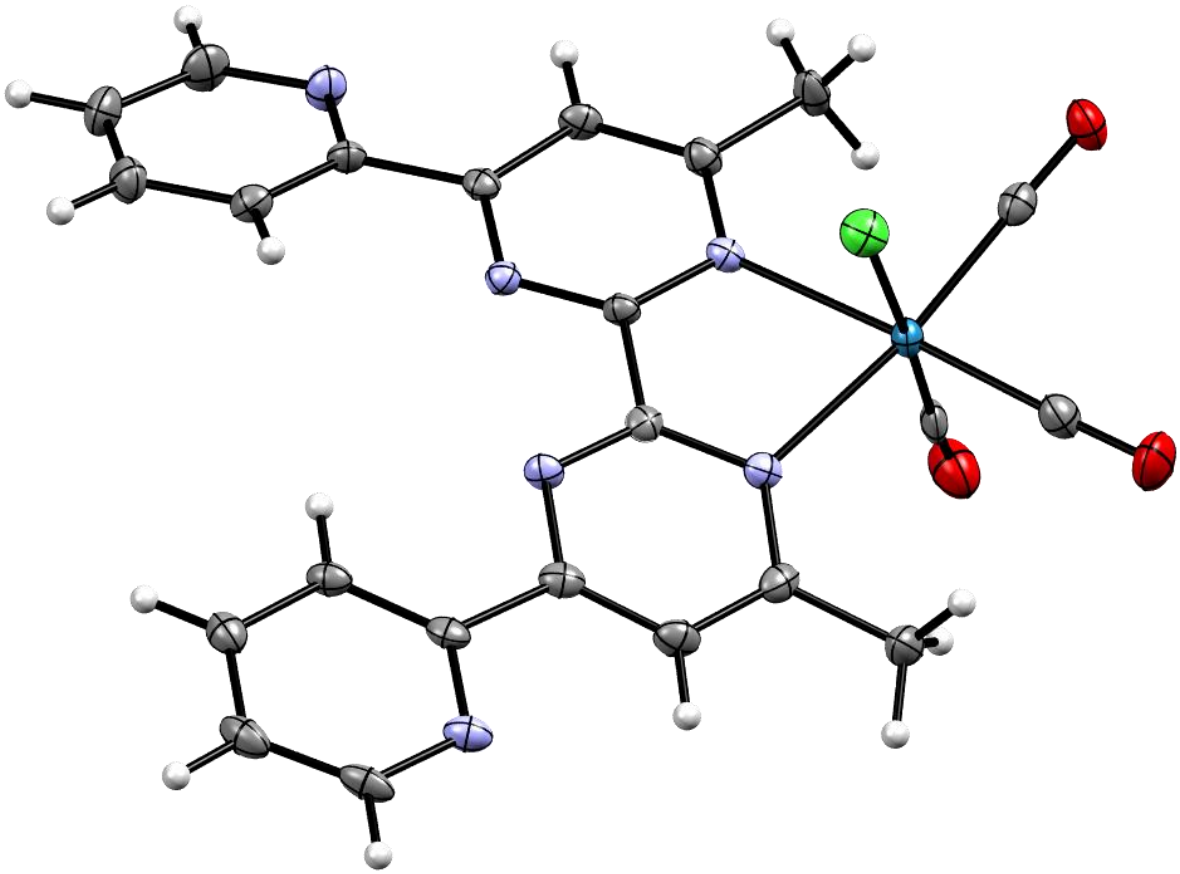

*Fig. 49: X-ray crystal structure of the cent-**L**^{1}ReCl(CO)$_3$ complex showing the rhenium (I) metal ion coordinated by the nitrogen atoms of the central pyrimidine-pyrimidine domain. It can be seen that the tetradentate pyridyl-pyrimidine-pyrimidine-pyridyl domain remains uncoordinated. Thermal ellipsoids are shown at 50% probability.*

In the crystal structure the rhenium (I) metal ion is six coordinate through the central 'outer' pyrimidine nitrogen atoms, three carbonyl groups and a chloride ion. Bond lengths to the rhenium (I) metal centre are 2.213 (3) Å and 2.214 (3) Å from the nitrogen atoms of the central pyrimidine domains, 2.464 (11) Å from the chloride ion and are ave. 1.923 Å for the coordinated carbon atoms of the carbonyl groups. The remaining uncoordinated tetradentate pyridyl-pyrimidine-pyrimidine-pyridyl domain adopts a planar confirmation on the other side of the rhenium (I) metal centre and this uncoordinated domain would be ideally suited for the binding of transition metal ions.

Due to both the *ter*-**L**^{1}ReCl(CO)$_3$ and *cent*-**L**^{1}ReCl(CO)$_3$ species containing a number of nitrogen donor atoms, these Re(I)-containing complexes may be suitable for the coordination of different transition metal ions.

Upon reaction of one equivalent of *ter*-**L**^{1}ReCl(CO)$_3$ with zinc (II) trifluoromethanesulfonate in CD_3CN, a virtual instant colour change from orange to pale yellow was observed. In the H^1 NMR, ten different aromatic proton environments were observed as would be expected but the chemical shift of these signals was substantially different to the starting material (e.g. *ter*-**L**^{1}ReCl(CO)$_3$) (Fig. 50).

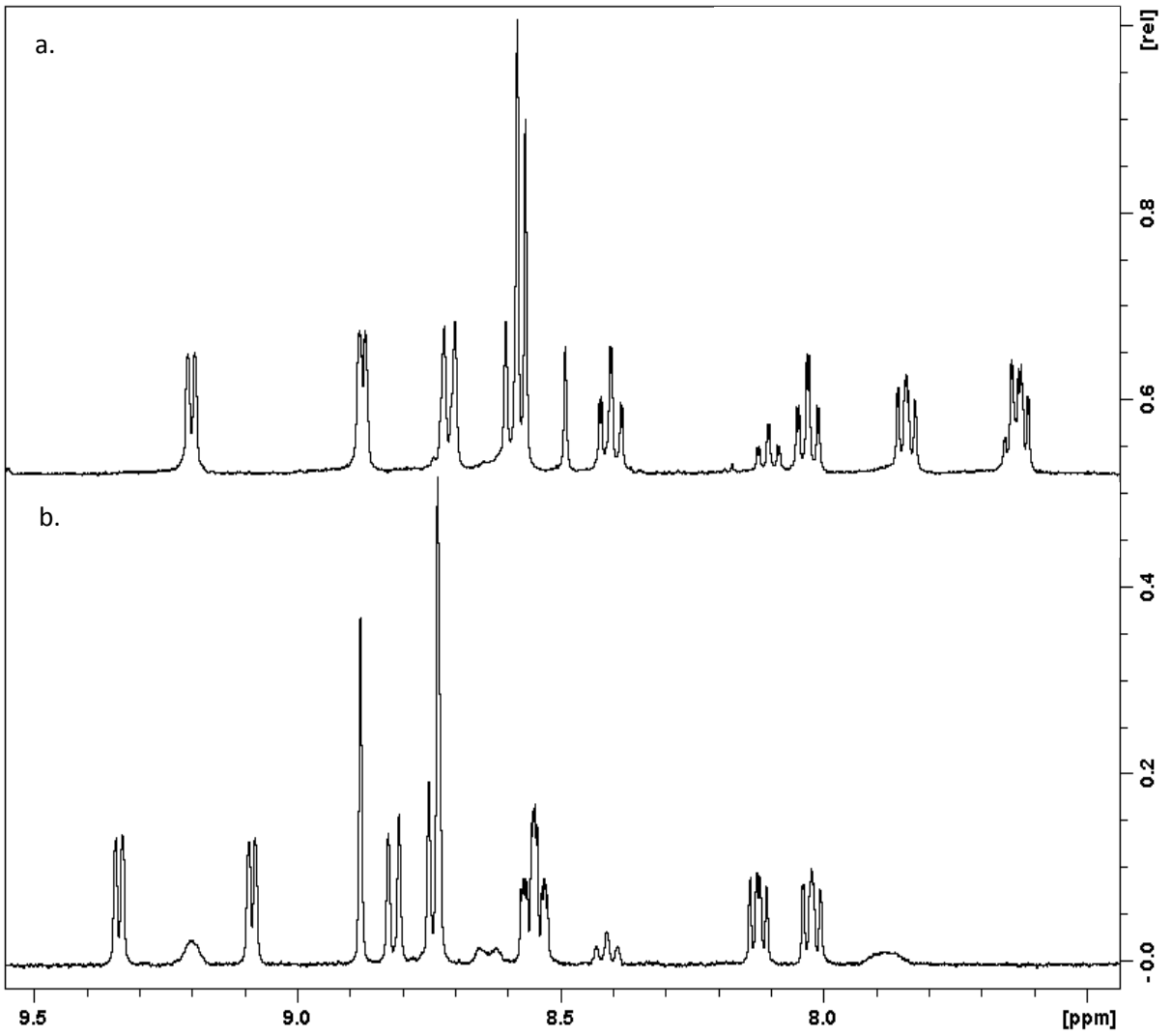

*Fig. 50: The aromatic regions of ^{1}H NMR spectra in CD_3CN of a. ter-**L**^{1}ReCl(CO)$_3$ and b. ter-**L**^{1}ReCl(CO)$_3$ upon reaction with zinc (II) trifluoromethanesulfonate. As to be expected ten aromatic signals are observed in both aromatic regions however a clear shift is observed as a result of the reaction with the zinc (II) trifluoromethanesulfonate ions.*

Crystals of this new material (after removal of any zinc (II) metal ions) were grown and analysis by X-ray diffraction showed that the ligand had remained unsymmetrical with the rhenium (I) ion bound to the pyridyl-pyrimidine domain at the terminal end of the ligand. However, the molecular structure showed the chloride was no longer bound to the rhenium (I) centre and that it had been replaced with a coordinated molecule of H_2O and an uncoordinated trifluoromethanesulfonate counter ion (Fig. 51).

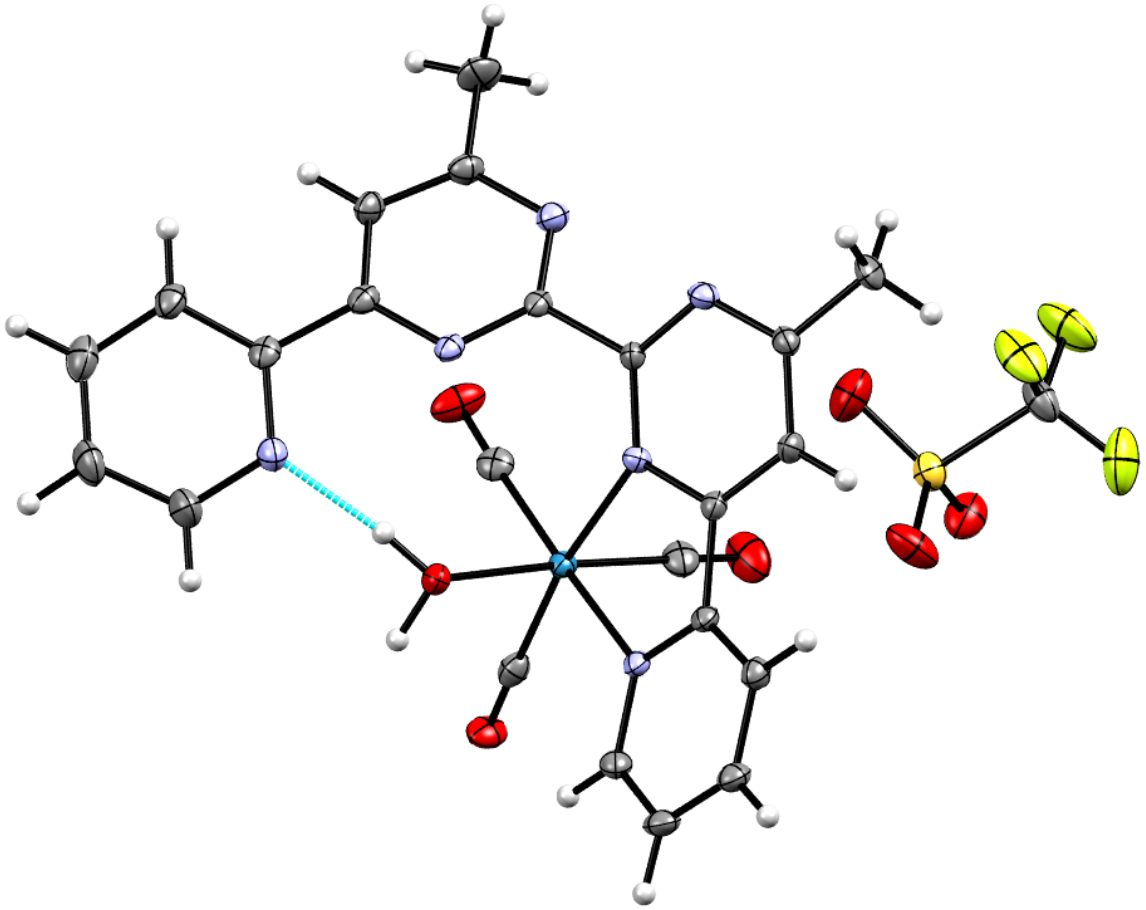

*Fig. 51: The X-ray crystal structure of ter-**L**^{1}Re(CO)$_3$(H$_2$O).(CF$_3$SO$_3$) showing the abstracted chloride having been replaced by an H$_2$O molecule. Hydrogen bonding is also observed between a hydrogen atom of the water molecule and the nitrogen atom of the uncoordinated pyridyl domain (dashed blue line) at the opposite end of the ligand strand to the coordinated rhenium (I) metal centre. Thermal ellipsoids are shown at 50% probability.*

Measured bond lengths to the rhenium (I) ion were ave. 1.91 Å for the carbon atoms of the three carbonyl groups, 2.172 (4) Å and 2.222 (3) Å for the nitrogen atoms of the pyridyl and the pyrimidine respectively and 2.172 (3) Å for the newly coordinated oxygen atom of the H_2O molecule. Formation

of this species was further confirmed by ESI-MS which gave an ion at *m/z* 611 corresponding to $[\mathbf{L^1}ReCO_3]^+$. The removal of the chloride anion from *ter*-$\mathbf{L^1}ReCl(CO)_3$ by zinc (II) metal ions is quite unexpected as usually abstraction of the halide from a ReCl-diimine system requires more forcing conditions such as the addition of silver (I) trifluoromethanesulfonate with heating and prolonged reaction times. The ease of removal of the chloride anion in this instance can be attributed to the nitrogen atoms present in the remainder of the uncoordinated ligand. Thus with the rhenium (I) ion coordinated at the terminal pyridyl-pyrimidine domain, the ligand can coordinate zinc (II) metal ions in the other terminal bidentate pyridyl-pyrimidine domain. In doing so, the zinc (II) ion is brought into a closer proximity to the rhenium (I) metal centre and consequently facilitates the abstraction of the chloride anion. Interestingly, the only other example of zinc (II) mediated abstraction of chloride in rhenium (I) diimine systems comprises a rhenium (I) terpyridine system where the terpyridine only coordinates via two nitrogen atoms with one of the terminal nitrogen atoms being hypodentate. It is possible that, in an analogous fashion to our system, this uncoordinated nitrogen atom coordinates the zinc (II) ion facilitating the halide abstraction.[90]

Reaction of *cent*-$\mathbf{L^1}ReCl(CO)_3$ with zinc (II) trifluoromethanesulfonate shows none of the colour changes observed with the terminal isomer, but the ^1H NMR does show a change in the chemical shift indicative of coordination of the tetradentate unit. Further confirmation of the coordination was given by reaction of *cent*-$\mathbf{L^1}ReCl(CO)_3$ with copper (II) perchlorate which showed an ion in the ESI-MS at *m/z* 808 corresponding to $\{[\mathbf{L^1}ReCl(CO)_3Cu(ClO_4)]\}^+$ although this is also accompanied with some aggregation in the ESI-MS giving oligomers e.g. $\{[(\mathbf{L^1}ReCl(CO)_3Cu)_2(ClO_4)_3]\}^+$. Hence in this case, the divalent metal cations are simply coordinated by the nitrogen atoms of the tetradentate pyridyl-pyrimidine-pyrimidine-pyridyl domain and no halide abstraction is observed as this tetradentate domain is remote from the rhenium (I) metal centre.

Extensive attempts were made to grow X-ray quality crystals of *cent*-$\mathbf{L^1}ReCl(CO)_3$ with a transition metal ion coordinated in the tetradentate domain and even though various solvent systems and

transition metals were used, crystals could not be obtained. However, reaction of *cent*-**L**^{1}ReCl(CO)$_3$ with copper (II) perchlorate in nitromethane with slow diffusion of chloroform resulted in a small amount of crystalline material and analysis by X-ray diffraction revealed the molecular structure of *cent*-**L**^{1}ReCl(CO)$_3$.[CuCl$_4$] (Fig. 52). In the solid-state, **L**^{1} was present with the 'outer' bidentate bipyrimidine unit coordinated by the ReCl(CO)$_3$ fragment. However, also present within the structure is a [CuCl$_4$]$^{2-}$ anion which forms hydrogen bonds to the two, now protonated, pyridyl nitrogen atoms. The probable formation of this product is due to slight decomposition of the chloroform solvent, which is well known to form HCl impurities. This would lead to the protonation of the ligand (observed at the terminal pyridyl domains) and any remaining Cl$^-$ being bound to the copper (II) ion to create the [CuCl$_4$]$^{2-}$ counter ion. However, it does provide further evidence that the chloride isn't abstracted from the rhenium (I) metal centre when metal ions are added to *cent*-**L**^{1}ReCl(CO)$_3$.

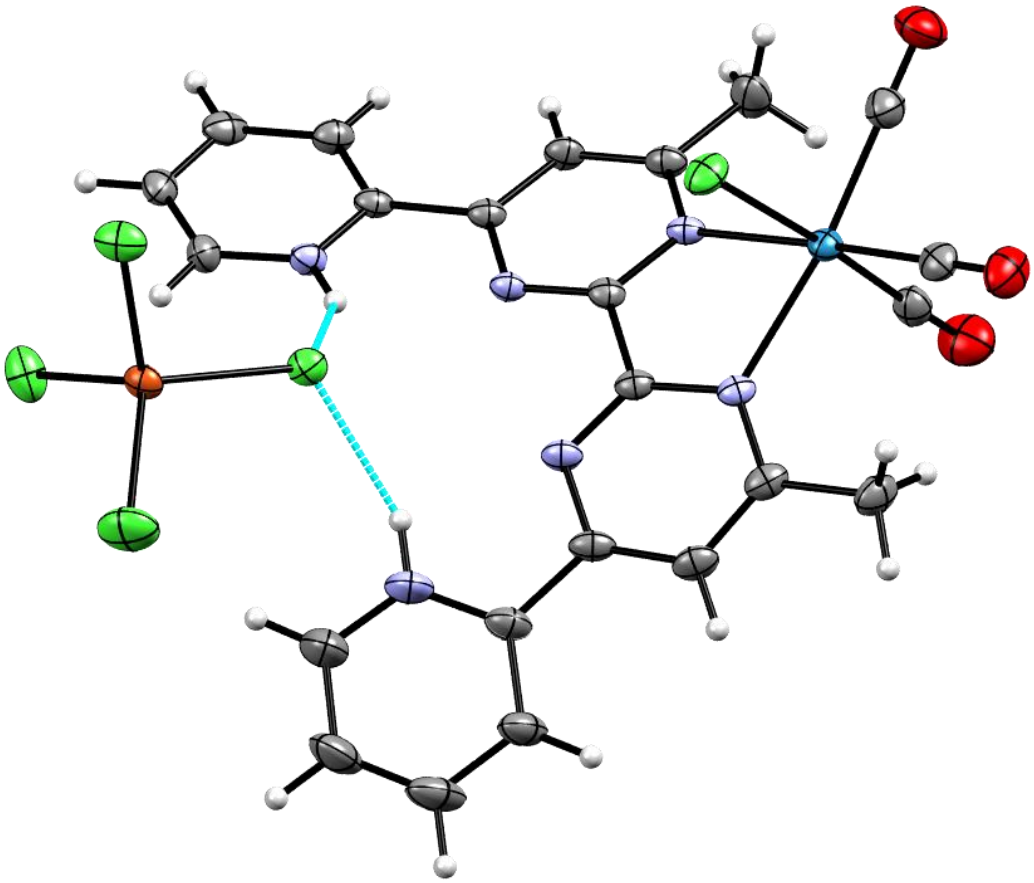

*Fig. 52: The X-ray crystal structure of the protonated cent-**L**^{1}ReCl(CO)$_3$ species with the [Cu(Cl)$_4$]$^{2-}$ anion hydrogen bonding to the protonated pyridine units (dashed blue lines). Thermal ellipsoids are shown at 50% probability.*

Analysis of the photophysical properties of *cent*-**L**^{1}ReCl(CO)$_3$ shows that the emission spectra is modulated upon addition of different *d*-block metal ions. The emission spectrum of *cent*-**L**^{1}ReCl(CO)$_3$ shows two components with the lower energy likely to have significant ^{3}MLCT character, whilst the shorter wavelength is ligand centred (Fig. 53).

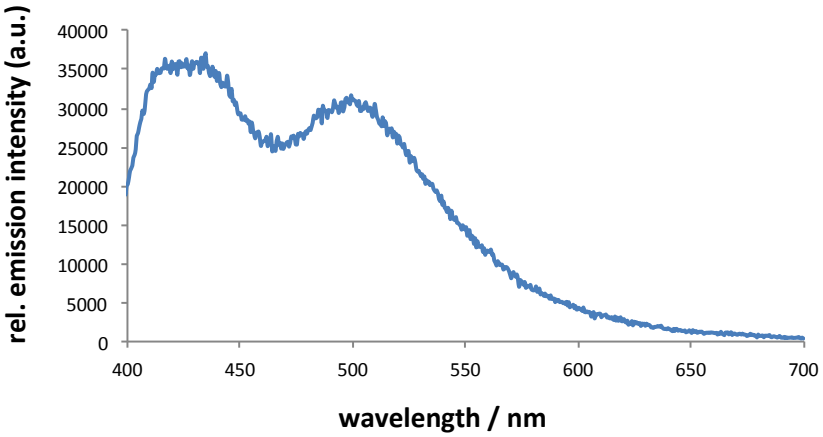

*Fig. 53: The emission spectrum of cent-**L**^{1}ReCl(CO)$_3$ in acetonitrile at 370 nm showing two components. The lower energy indicating significant ^{3}MLCT character and the shorter wavelength being ligand centred.*

Addition of the metal ions zinc (II), copper (II) and mercury (II) (all as the perchlorate salts) showed that all the ions resulted in an increase of emission. As would be expected the mercury (II) emission is substantially less than zinc (II) and this can be attributed to the heavy atom mediated intersystem crossing to ligand-centred triplet states which are sensitive to quenching via triplet oxygen. Additionally, copper (II) also causes an increase in the metal centred emission but to a lesser degree than zinc (II) which is possibly a consequence of energy loss by charge and energy transfer to this paramagnetic metal ion (Fig. 54).

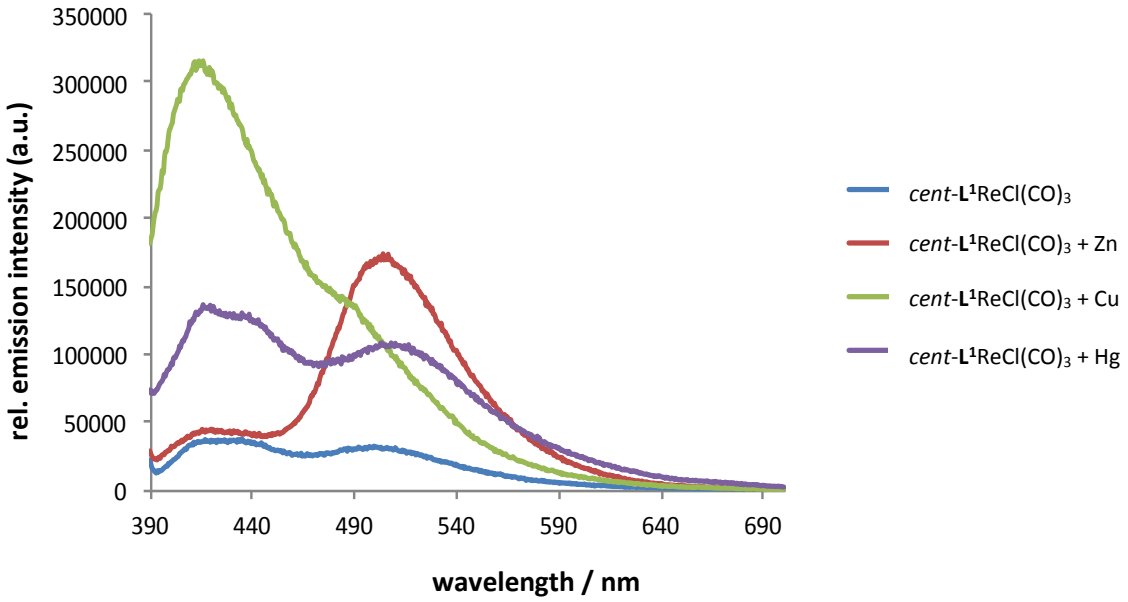

*Fig. 54: The emission spectra of cent-**L**^{1}ReCl(CO)$_3$ upon addition of Zn (II), Cu (II) and Hg (II). It can be seen that the emission spectra modulate depending upon the metal ion present.*

It is important to note that the emission profile is atypical of rhenium (I) complexes and these are just preliminary results. Further work is currently ongoing so that the actual nature of the emission is fully understood. Regardless, it does show that the emission profile of *cent*-**L**^{1}ReCl(CO)$_3$ is modulated upon addition of different metal ions.

2.3 Conclusions

The work reported in this chapter has demonstrated the manipulation and control of the ligand strand, **L^1**, through utilisation of the coordination preferences of various metal ions. As **L^1** contains an inbuilt flexibility to freely rotate around the central bond between the pyrimidine domains, it is able to adopt a bis-tridentate and a tetradentate-bidentate binding motif. Although the ligand isn't preprogramed, it was demonstrated that the binding motif of the ligand strand could be controlled through reaction with metal ions with different coordination preferences.

Reaction of **L^1** with copper (II) metal ions in different metal to ligand stoichiometric ratios of 2 : 1 and 2 : 3 gave the complexes $[Cu_2(L^1)(ClO_4)_2(MeCN)_4]^{2+}$ and $[Cu_2(L^1)_3]^{4+}$ respectively. The ligand strand **L^1** adopted the bis-tridentate binding motif in both complexes so as to satisfy the preferred coordination of six for the copper (II) metal centres.

Separate reactions of **L^1** with cadmium (II) and **L^1** with europium (III) metal ions (in metal to ligand stoichiometric ratios of 1 : 2 in both cases) gave the complexes $[Cd(\mathbf{L^1})_2]^{2+}$ and $[Eu(\mathbf{L^1})_2(CF_3SO_3)]^{2+}$, respectively. In these complexes, **L^1** had adopted the tetradentate-bidentate binding motif so that it was able to satisfy the preferred coordination desires of eight for the cadmium (II) metal centre and nine for the europium (III) metal centre. In both complexes, the bidentate domain consisting of the nitrogen atoms of the 'outer' pyrimidine remained uncoordinated.

The tetranuclear dimetallic complex $[Eu_2Ag_2(\mathbf{L^1})_3(CF_3SO_3)_8]$ arose from reaction of **L^1** with europium (III) and silver (I) metal ions in a metal to ligand stoichiometric ratio of 2 : 2 : 3. Two of the three ligand strands in this complex had adopted the tetradentate-bidentate binding conformation so as to coordinate the europium (III) metal ions. The silver (I) metal ions were coordinated through the 'outer' pyrimidine domain and the remaining ligand in the complex had adopted the bis-tridentate binding conformation to complete the coordination preferences of both silver (I) metal ions and act as a bridge between the ligands adopting the tetradentate-bidentate motif. Four trifluoromethanesulfonate counter ions completed the eight coordination of each europium (III) metal ion.

Reaction of **L[1]** with rhenium (I) pentacarbonyl chloride results in the formation of the *ter*-**L[1]**$ReCl(CO)_3$ complex. In the complex, the $ReCl(CO)_3$ fragment coordinated to the terminal pyridyl-pyrimidine domain of the **L[1]** ligand strand with the remaining N-donor atoms uncoordinated.

However, reaction of **L[1]** with europium (III) trifluoromethanesulfonate results in the ligand partitioning itself into its tetradentate-bidentate binding conformation with the lanthanide ion coordinating the tetradentate domain and leaving the bidentate domain uncoordinated. Reacting **L[1]** with rhenium (I) pentacarbonyl chloride in the presence of lanthanum (III) trifluoromethanesulfonate templates the ligand strand and results in the formation of the *cent*-**L[1]**$ReCl(CO)_3$ complex. In this complex, the $ReCl(CO)_3$ fragment is coordinated to the central bipyrimidine domain with the pyridyl-pyrimidine-pyrimidine-pyridyl tetradentate domain remaining uncoordinated and resulting in an ideal binding domain for different transition metal ions.

Reaction of *ter*-**L[1]**$ReCl(CO)_3$ with zinc (II) trifluoromethanesulfonate resulted in the complex ter-**L[1]**$Re(CO)_3(H_2O).(CF_3SO_3)$. Unusually, the chloride anion had been abstracted from the rhenium (I) metal centre and replaced with a coordinated water molecule and a triflate counter anion. Whilst more forcing conditions are usually required for the abstraction of a halide from a rhenium (I) metal centre, it was the proximity of the chloride anion to the zinc (II) ion coordinated at the other periphery of the ligand strand that facilitated this abstraction.

Reaction of *cent*-**L[1]**$ReCl(CO)_3$ with copper (II) perchlorate in nitromethane with slow diffusion of chloroform resulted in the formation of the complex $[H_2$-*cent*-**L[1]**$ReCl(CO)_3]^{2+}$ species accompanied by a $[Cu(Cl)_4]^{2-}$ anion. The $[Cu(Cl)_4]^{2-}$ anion was hydrogen bonded between the protonated terminal pyridyl domains. Formation of this product is believed to be a result of the decomposition of the chloroform into HCl impurities, resulting in protonation of the pyridyl domains and the formation of the $[Cu(Cl)_4]^{2-}$ anion.

Photophysical analysis of the *cent*-**L[1]**$ReCl(CO)_3$ species showed two components with the lower energy likely to have ^{3}MLCT character and the shorter wavelength being ligand centred. Addition of

metal ions (zinc (II), copper (II) and mercury (II)) led to modulation in the emission spectra. However, further analysis is required to fully understand the emission profile and the observed modulation.

3 Chapter 3: Formation of Tetra- and Pentanuclear Circular Helicates

Described in this chapter is the synthesis and coordination chemistry of three polydentate ligands, **L²**, **L³** and **L⁴** (Fig. 55). The ligand **L²** possesses two bipyridyl-thiazole binding domains on the 1,3-positions of the central cresol spacing group resulting in a potentially hexadentate ligand strand. Reaction of **L²** with zinc (II) trifluoromethanesulfonate results in the formation of the tetranuclear circular helicate species $[Zn_4(\mathbf{L^2})_4]^{8+}$.[1] The hexadentate ligand **L³** is similar to **L²** as it also contains two bipyridyl-thiazole domains on the 1,3- positions of the central aromatic spacing group but the –OH group on the central spacer has been replaced by an –OMe group. Reaction of **L³** with zinc (II) trifluoromethanesulfonate results in the formation of the pentanuclear circular helicate species $[Zn_5(\mathbf{L^3})_5]^{10+}$. The potentially pentadentate ligand strand **L⁴** also contains a central anisole spacing group however it is an unsymmetrical ligand as it possesses a bipyridyl-thiazole binding domain on one side of the space group and a pyridyl-thiazole binding domain on the other side. Reaction of **L⁴** with copper (II) perchlorate gives a pentanuclear circular helicate assembly, $[Cu_5(\mathbf{L^4})_5]^{10+}$, but due to the unsymmetrical nature of the ligand strand, a head-to-tail binding conformation is achieved.

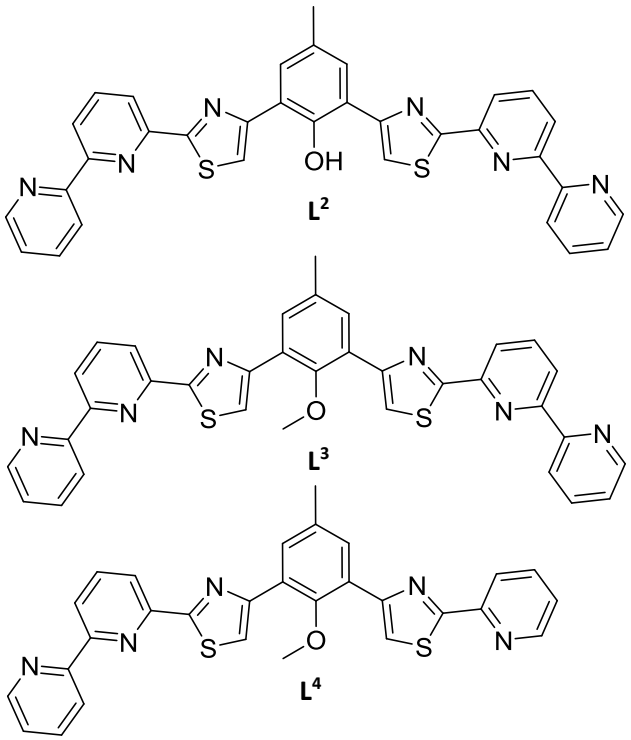

*Fig. 55: The three ligand strands **L²**, **L³** and **L⁴** to be reported and discussed in this chapter.*

3.1 Synthesis of L^2, L^3 and L^4

Unless otherwise stated, all solvents and materials were purchased from Sigma Aldrich, Acros Organics or Fisher Scientific and were used without further purification. The 1,3-di(α-bromoacetyl)cresol (**1**) was prepared by a previously reported method by bromination of 1,3-di(acetyl)cresol.[91] ^{1}H and/or ^{13}C NMR data was recorded on either a Bruker AV (III) 400MHz NMR spectrometer or a Bruker Advance 500 MHz NMR spectrometer. Mass spectra were obtained on either an Agilent 6210 TOF MS with electrospray ionisation, operating in positive ion mode or a Bruker Micro TOF-q LC mass spectrometer with electrospray ionisation, operating in positive ion mode. Single crystal studies were recorded on a Bruker D8 Venture with Dual IμS Microfocus Sources using either Mo or Cu radiation at 150 (2) K.

3.1.1 Synthesis of **5**

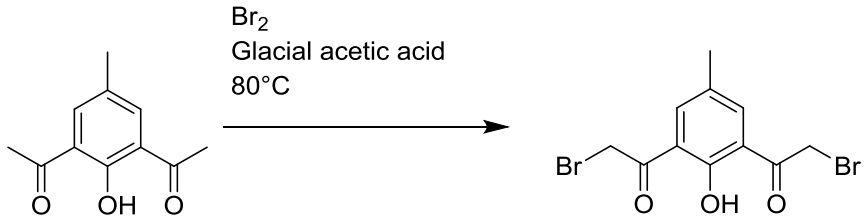

5

1,3-Diacetyl cresol (500 mg, 2.6 mmol) was dissolved in glacial acetic acid (20 mL) and set to stir at 80 ˚C. To this was added a solution of Br_2 (833 mg, 0.267 mL, 5.2 mmol) in acetic acid (1 mL) over a period of 2 hours. Progress of the reaction was monitored *via* TLC (SiO_2, 1 % hexane in DCM) and once the starting material had been consumed, the solution was evaporated to dryness. Purification was achieved by column chromatography (SiO_2, 1 % hexane in DCM) and gave the di-bromo containing product **5** as a yellow solid (350 mg, 1.0 mmol, 38 %). ^{1}H NMR (400 MHz, $CDCl_3$) δ: 12.8 (s, H, -OH); 7.9 (s, 2H, Ar); 4.6 (s, 4H, -CH_2); 2.4 (s, 3H, -CH_3) ppm.

3.1.2 Synthesis of L^2

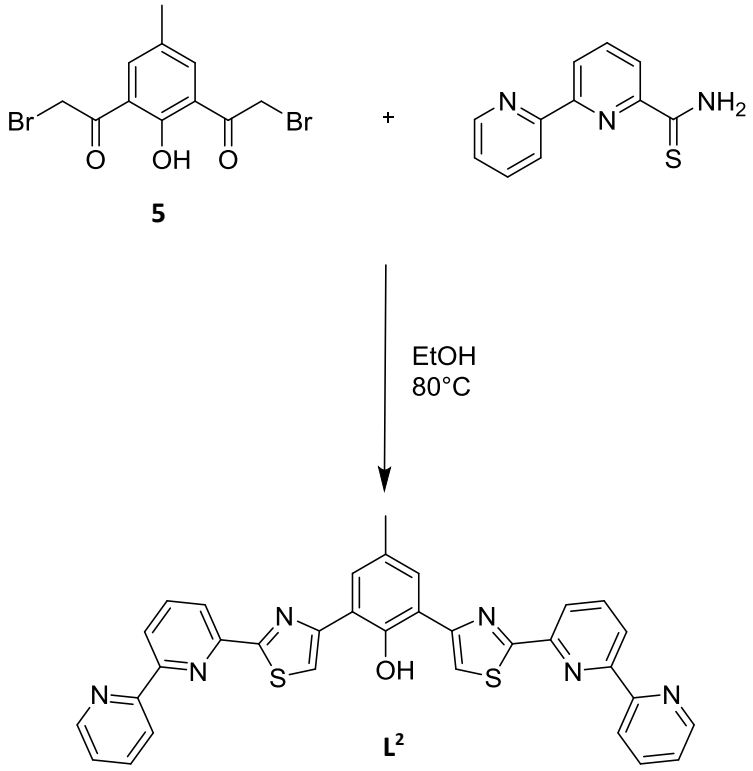

To a two-necked round bottom flask containing 2,2-bipyridyl-6-carbothioamide (100 mg, 0.47 mmol) and ethanol (25 mL) the dibromo species (**5**) (81.4 mg, 0.24 mmol) was added and the reaction heated to 80 ˚C. After 12 hours a precipitate had formed which was isolated by vacuum filtration and washed with ethanol (1 x 5 mL) and diethyl ether (2 x 5 mL) to give the hydrobromide salt of the product as a yellow solid. This solid was then suspended in concentrated aqueous ammonia (0.88 sp. gr., 10 mL) for 12 hours after which time the yellow solid was isolated by vacuum filtration and washed with water (2 x 2 mL), ethanol (2 x 2 mL) and diethyl ether (2 x 2 mL) giving the free-base ligand **L^2** as a yellow powder (74 mg, 0.13 mmol, 53 %). ^{1}H NMR (500 MHz, $(CD_3)_2SO$) δ: 12.3 (s, 1H, -OH); 8.77 (d, *J*= 4.35, 2H, py); 8.53 (d, *J*= 1.4, 2H, py); 8.52 (d, *J*= 1.45, 2H, py); 8.50 (s, 2H, tz); 8.34 (d, *J*= 7.25, 2H, py); 8.20 (t, *J*= 7.90, 2H, py); 8.07 (td, J= 7.85, 1.90, 2H, py); 8.02 (s, 2H, ph); 7.53 (td, J= 5.70, 0.85, 2H, py); 2.46 (s, 3H, -CH_3) ppm. *HRMS (m/z): $[M+H]^+$ for $C_{33}H_{22}N_6OS_2$ calculated 583.1369, measured 583.1393.*

3.1.3 Synthesis of **L³**

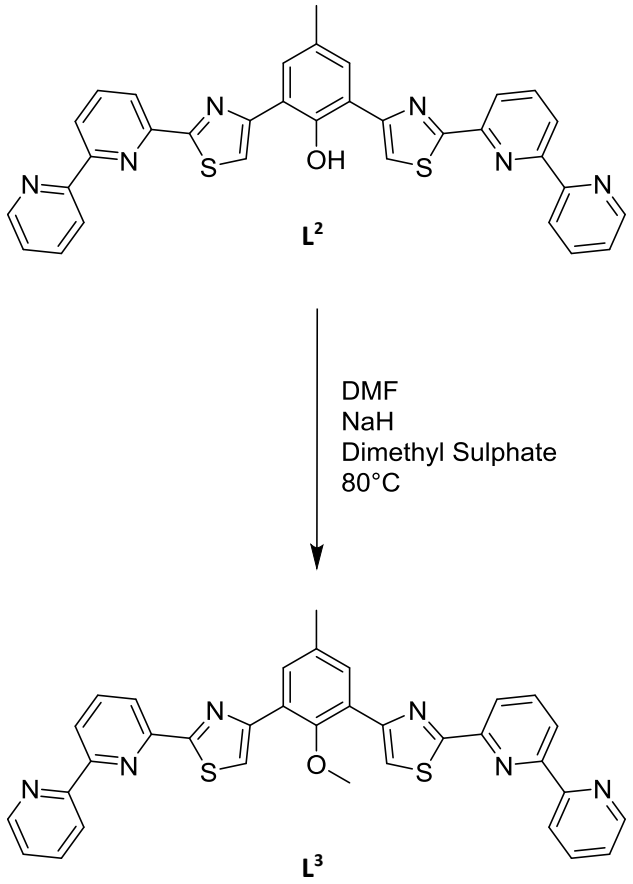

A two necked round bottom flask containing **L²** (120 mg, 0.21 mmol) and sodium hydride (60% dispersion in mineral oil, 100 mg, 2.5 mmol) was placed under an atmosphere of N_2 and left to purge for 30 minutes. To this, anhydrous DMF (20 mL) was added and left to stir at 80 °C for 1 hour and after adding dimethyl sulphate (0.5 mL, 5.0 mmol), heating was continued for a further 12 hours. After this time the reaction was allowed to cool and methanol was added whilst under N_2 (to remove any unreacted NaH) and the reaction was evaporated to dryness. Purification *via* column chromatography (Al_2O_3, 1 % MeOH DCM) gave the final product **L³** as a pale brown powder (71 mg, 0.12 mmol, 56%). ^{1}H NMR (400 MHz, $CDCl_3$) δ: 8.65 (d, *J*= 4.32, 2H, py), 8.55 (d, *J*= 7.92, 2H, py), 8.43 (d, *J*= 7.8, 2H, py), 8.31 (d, *J*= 7.68, 2H, py), 8.08 (s, 2H, tz), 8.00 (s, 2H, Ar), 7.91 (t, *J*= 7.8, 2H, py), 7.84 (t, *J*= 6.56, 2H, py), 7.30 (dd, *J*= 6.36, 4.92 Hz, 2H, py), 3.59 (s, 3H, -OC*H₃*), 2.30 (s, 3H, CH_3) ppm. *HRMS (m/z): $[M+H]^+$ for $C_{34}H_{24}N_6OS_2$ calculated 597.1526, measured 597.1507.*

3.1.4 Synthesis of **6**

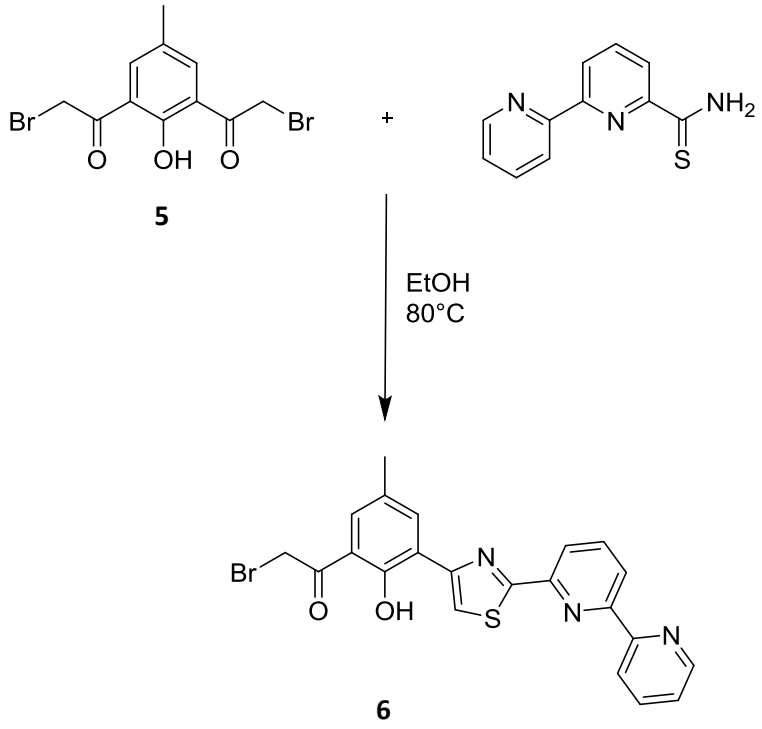

Ethanol (20 mL) was added to a round bottom flask charged with 1,3-di(α-bromoacetyl)cresol (**5**) (200 mg, 0.571 mmol) and was set to heat at 80 °C. Once at this temperature, the 2,2-bipyridyl-6-carbothioamide (111 mg, 0.516 mmol) was added over the course of 2 hours and this was then left to heat. After ~ 4 hours, a yellow solid had developed in solution which was isolated by vacuum filtration, washed with ethanol (2 x 2 mL) and diethyl ether (2 x 2 mL) to yield **6** as a yellow powder (180 mg, 0.386 mmol, 67.6 %). ^{1}H NMR (400 MHz, $CDCl_3$) δ: 12.80 (s, 1H, -OH); 8.73 (d, *J*= 4.56, 1H, py); 8.62 (d, *J*= 7.92, 1H, py); 8.53 (d, *J*= 7.88, 1H, py); 8.38 (d, *J*= 1.32, 1H, Ph); 8.32 (d, *J*= 7.72, 1H, py); 8.22 (s, 1H, tz); 8.00 (t, *J* = 7.8, 1H, py); 7.92 (dt, J = 7.84, 1.56, 1H, py); 7.61 (d, *J*= 1.32, 1H, Ph); 7.38 (dd, *J* = 7.28, 4.88 Hz, 1H, py); 4.64 (s, 2H, -CH_2Br); 2.46 (s, 3H, -CH_3) ppm.

3.1.5 Synthesis of **7**

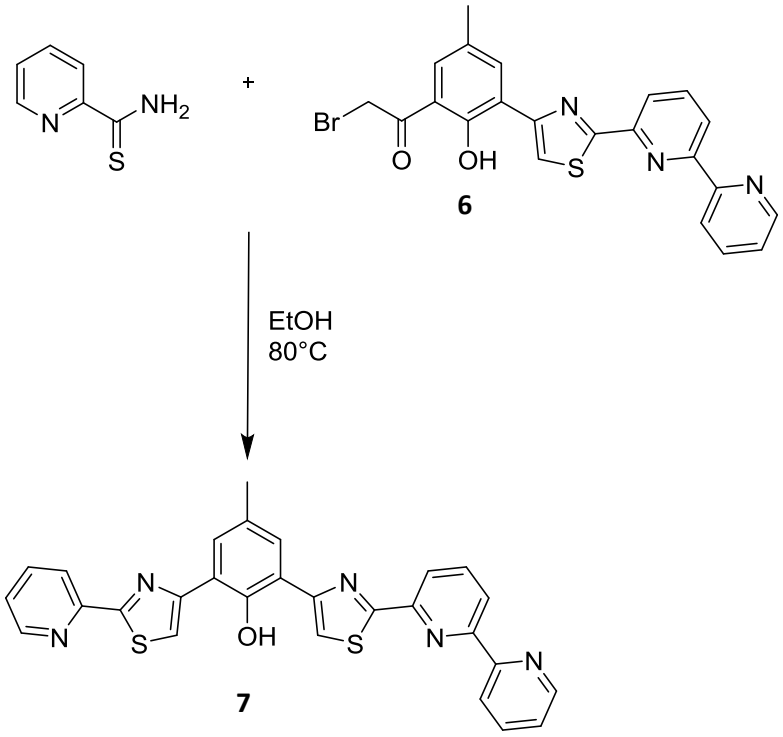

A round bottom flask charged with **6** (180 mg, 0.386 mmol) and pyridine thioamide (59 mg, 0.425 mmol) and ethanol (20 mL) was added. The solution was set to heat at 80 °C and after ~ 12 hours, a yellow solid had developed. The solid was isolated by vacuum filtration and washed with ethanol (2 x 2 mL) and diethyl ether (5 mL) to yield **7** as a yellow solid (140 mg, 0.277 mmol, 72 %). ^{1}H NMR (400 MHz, $(CD_3)_2SO$) δ: 12.5 (s, 1H, -OH); 8.77 (d, *J*= 4.48, 1H, py); 8.71 (d, *J*= 4.44, 1H, py); 8.55 (s, 1H, tz); 8.52 (m, 2H, overlap); 8.49 (s, 1H, tz); 8.35 (d, *J* = 7.64, 1H, py); 8.28 (d, *J* = 7.88, 1H, py); 8.21 (t, *J* = 7.84, 1H, py); 8.10 (m, 2H, overlap); 8.04 (d, *J* = 2.0, 1H, Ph); 8.0 (d, *J* = 2.0, 1H, Ph); 7.57 (m, 2H, overlap); 2.43 (s, 3H, $-CH_3$) ppm. *HRMS (m/z): $[M+H]^+$ for $C_{28}H_{19}N_5OS_2$ calculated 506.1104, measured 506.1089.*

3.1.6 Synthesis of **L⁴**

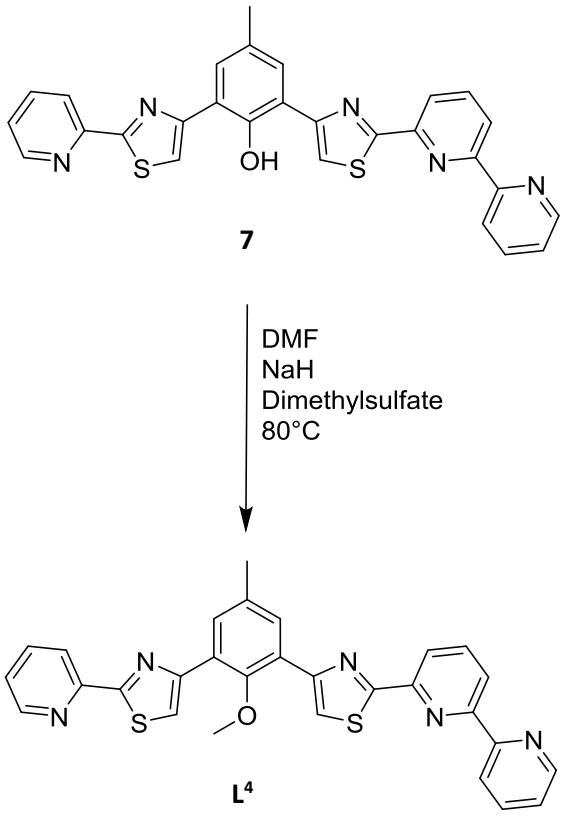

A two necked round bottom flask containing **7** (120 mg, 0.21 mmol) and sodium hydride (60 % dispersion in mineral oil, 100 mg, 2.5 mmol) was placed under an atmosphere of N_2 and left to purge for 30 minutes. To this, anhydrous DMF (20 mL) was added and the reaction left to stir at 80 °C for 1 hour after this time dimethyl sulphate (0.5 mL, 5.0 mmol), was heating continued for a further 12 hours. After this time the reaction was allowed to cool and methanol was added whilst under N_2 (to remove any unreacted NaH) and the reaction was evaporated to dryness. Purification *via* column chromatography (Al_2O_3, 1 % MeOH DCM) gave the final product **L⁴** as a pale brown powder (55 mg, 0.09 mmol, 43%). ^{1}H NMR (400 MHz, $CDCl_3$) δ: 8.73 (d, *J*= 4.68, 1H, py); 8.67 (d, *J*= 4.76, 1H, py); 8.64 (d, *J* = 7.92, 1H, py); 8.51 (d, *J* = 7.8, 1H, py); 8.39 (m, 2H, overlap, py); 8.16 (s, 1H, tz); 8.15 (s, 1H, tz); 8.07 (m, 2H, overlap, Ph); 8.00 (t, *J* = 7.8, 1H, py); 7.92 (dt, *J* = 7.76, 1.48, 1H, py); 7.87 (dt, *J* = 7.76, 1.40, 1H, py); 7.37 (m, 2H, overlap, py); 3.66 (s, 3H, -OCH_3); 2.53 (s, 3H, -CH_3) ppm. *HRMS (m/z): [M+H]⁺ for $C_{28}H_{19}N_5OS_2$ calculated 520.1260, measured 520.1250.*

3.1.7 Synthesis of $(Zn_4(\mathbf{L^2})_4)^{8+}$

To a suspension of $\mathbf{L^2}$ (5.00 mg, 0.086 mmol) in MeCN (2 mL), $Zn(CF_3SO_3)_2$ (3.44 mg, 0.095 mmol) was added and the reaction briefly heated and sonicated until all the ligand dissolved to give a pale yellow solution. Diethyl ether was allowed to slowly diffuse into the solution and after a few days, yellow crystals had formed (6 mg, 73 %).

3.1.8 Synthesis of $(Zn_5(\mathbf{L^3})_5)^{10+}$

To a suspension of $\mathbf{L^3}$ (5.00 mg, 0.084 mmol) in MeCN (2 mL), $Zn(ClO_4)_2$ (3.43 mg, 0.092 mmol) was added and the reaction briefly heated and sonicated until all the ligand dissolved to give a clear and colourless solution. Diisopropyl ether was allowed to slowly diffuse into the solution and after a few days, small colourless crystals had formed (4 mg, 56 %).

3.1.9 Synthesis of $(Cu_5(\mathbf{L^4})_5)^{10+}$

To a suspension of $\mathbf{L^4}$ (5.00 mg, 0.090 mmol) in MeCN (2 mL), $Cu(ClO_4)_2$ (4.03 mg, 0.095 mmol) was added and the reaction briefly heated and sonicated until all the ligand dissolved to give a clear green solution. Diisopropyl ether was allowed to slowly diffuse into the solution and after a few days, small green crystals had formed (4 mg, 67 %).

3.2 Results and discussion

The ligand **L²** was prepared by reaction of 2,2'-bipyridine-6-thioamide with 2,6-di(2-bromoethanone)cresol which can be functionalised at the oxygen atom by deprotonation and reaction of dimethyl sulfate to give **L³**. The unsymmetrical **L⁴** was prepared by reaction of one equivalent of 2,2'-bipyridine-6-thioamide with 2,6-di(2-bromoethanone)cresol and the intermediate product was then reacted with one equivalent of pyridine-2-thioamide. The –OH group of the resulting product was then functionalised by deprotonation and reaction of dimethyl sulfate to give **L⁴**.

Suspension of **L²** in acetonitrile and reaction with zinc (II) trifluoromethanesulfonate gave a clear yellow solution which after slow diffusion of diisopropyl ether gave crystals suitable for X-ray analysis. Analysis in the solid state shows that the tetranuclear circular helicate species $[Zn_4(\mathbf{L^2})_4]^{8+}$ is formed (Fig. 56).

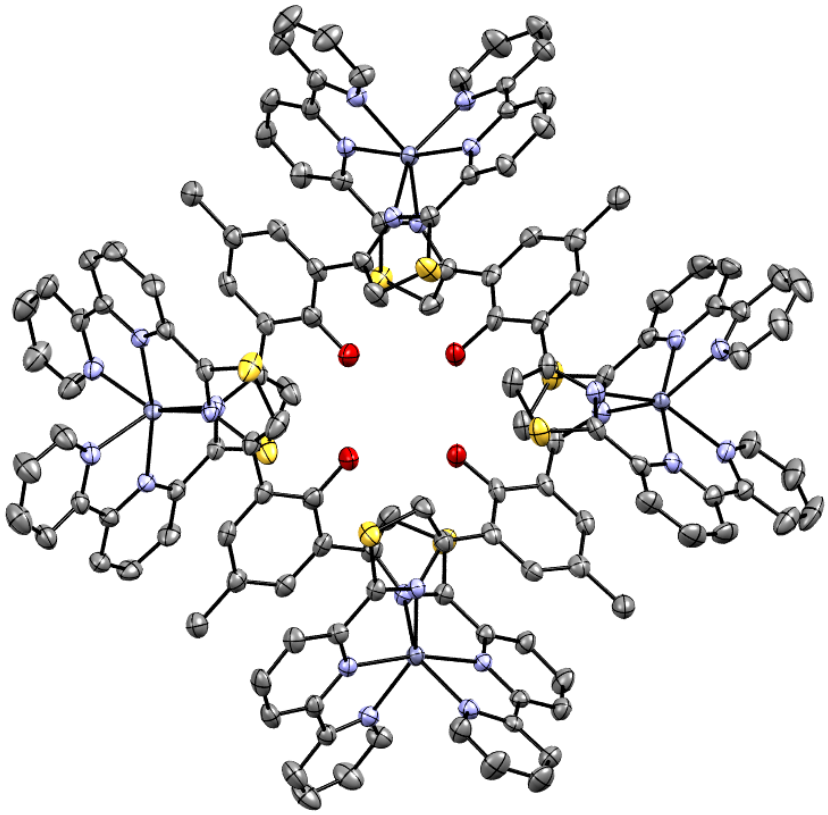

*Fig. 56: The X-ray crystal structure of the tetranuclear circular helicate $[Zn_4(\mathbf{L^2})_4]^{8+}$ formed from reaction of **L²** with zinc (II) trifluoromethanesulfonate. Hydrogen atoms have been omitted for clarity and thermal ellipsoids are shown at 50% probability.*

In this structure the ligand strand **L²** partitions into two bipyridyl-thiazole domains and coordinates a different zinc (II) metal centre via each domain (Fig. 57). All four zinc (II) metal centres in the assembly are coordinated by two different ligand strands and as a result are six coordinate. Bond lengths from the nitrogen atoms of the bipyridyl-thiazole domains to the metal centres are ave. 2.157 Å. It is also observed that the hydrogen atom of the cresol group of the **L²** ligand strand exhibits hydrogen bonding to an oxygen atom on an adjacent ligand strand and that this proceeds with a directionality around the core of the assembly (Fig. 57 b.).

a.

b.

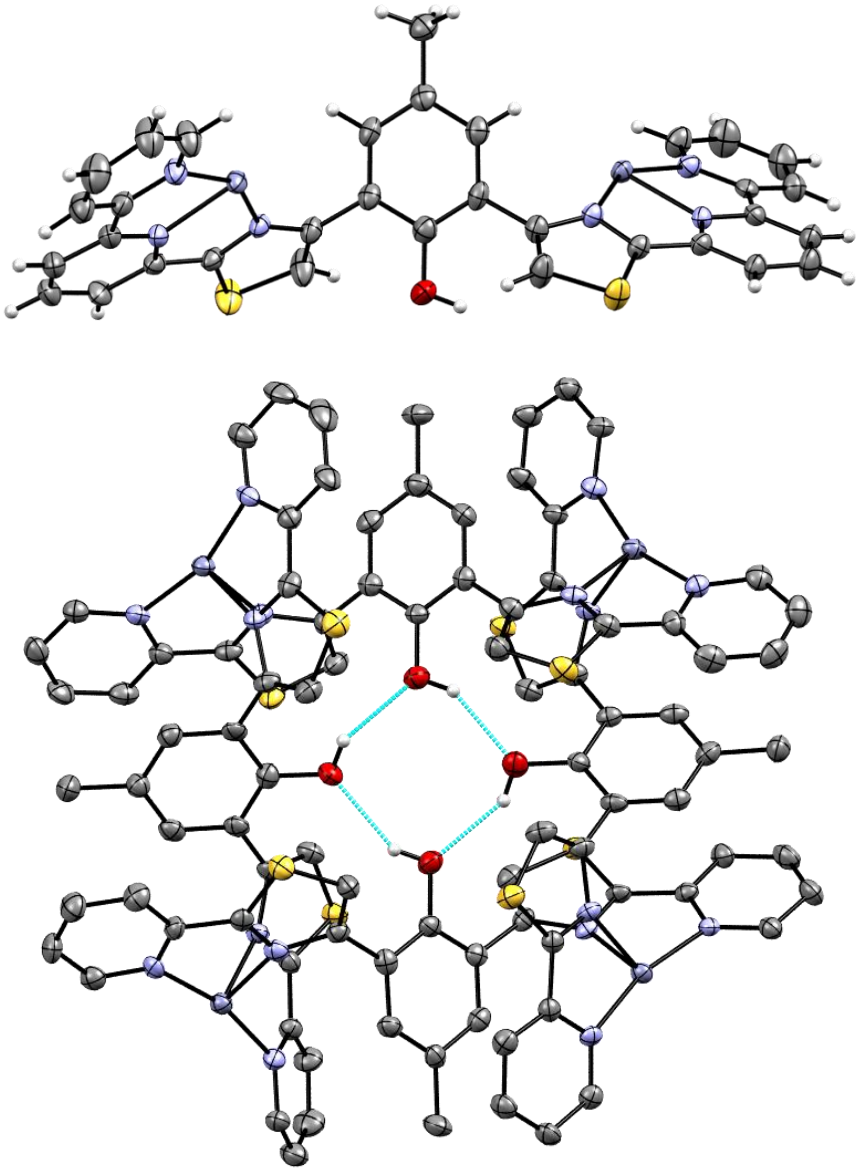

Fig. 57: Partial views of the X-ray crystal structure of the tetranuclear circular helicate $[Zn_4(\mathbf{L^2})_4]^{8+}$. a. shows the partitioning of the ligand strand into its bipyridyl-thiazole domains with a zinc (II) metal ion coordinated in each and b. the hydrogen bonding observed between the hydrogen atom of a cresol unit and the oxygen atom of an adjacent ligand strand (dashed blue lines). Thermal ellipsoids are shown at 50% probability and in b. the terminal pyridyl rings of each ligand strand and hydrogen atoms have been omitted for clarity.

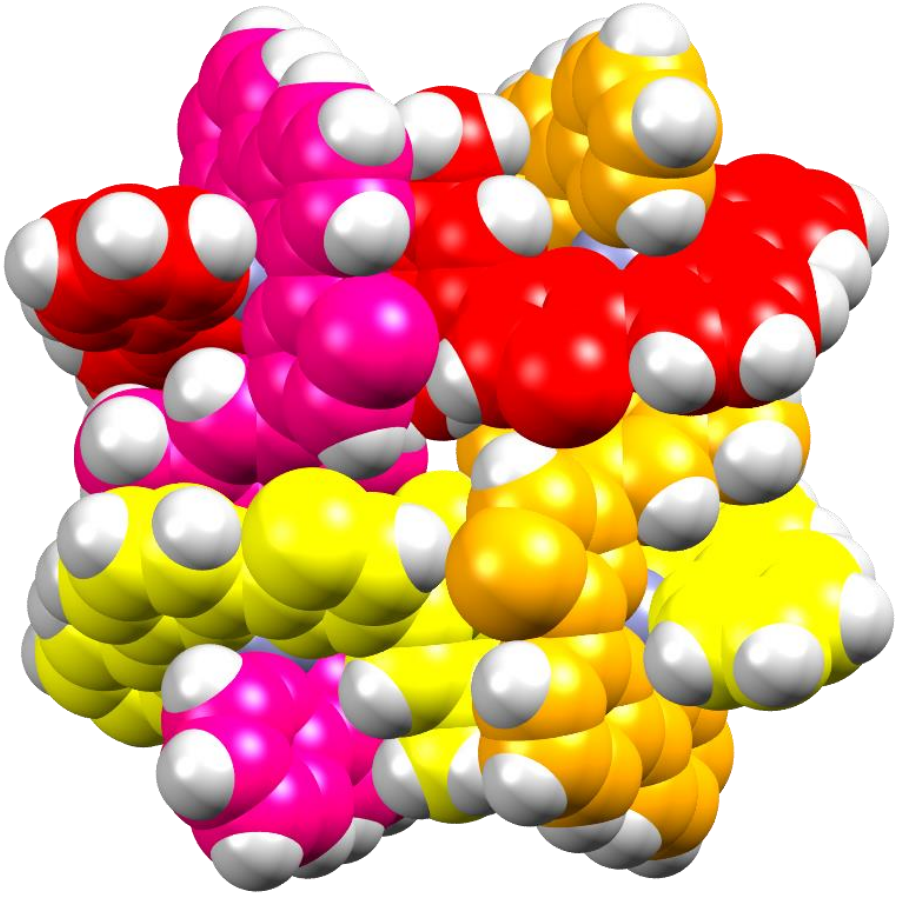

Fig. 58: An alternate view of the X-ray crystal structure of the tetranuclear circular helicate $[Zn_4(\mathbf{L^2})_4]^{8+}$ shown in spacefilling format. $\mathbf{L^2}$ ligand strands have been coloured red, orange, yellow and pink to better show the helical wrapping of the ligand strands throughout the structure. Hydrogen atoms are coloured white.

Suspension of **L^3** in acetonitrile and reaction with zinc (II) perchlorate gave a clear colourless solution which after slow diffusion of diisopropyl ether gave crystals suitable for X-ray analysis. Analysis in the solid state shows that the pentanuclear circular helicate species $[Zn_5(\mathbf{L^3})_5]^{10+}$ is formed (Fig. 59).

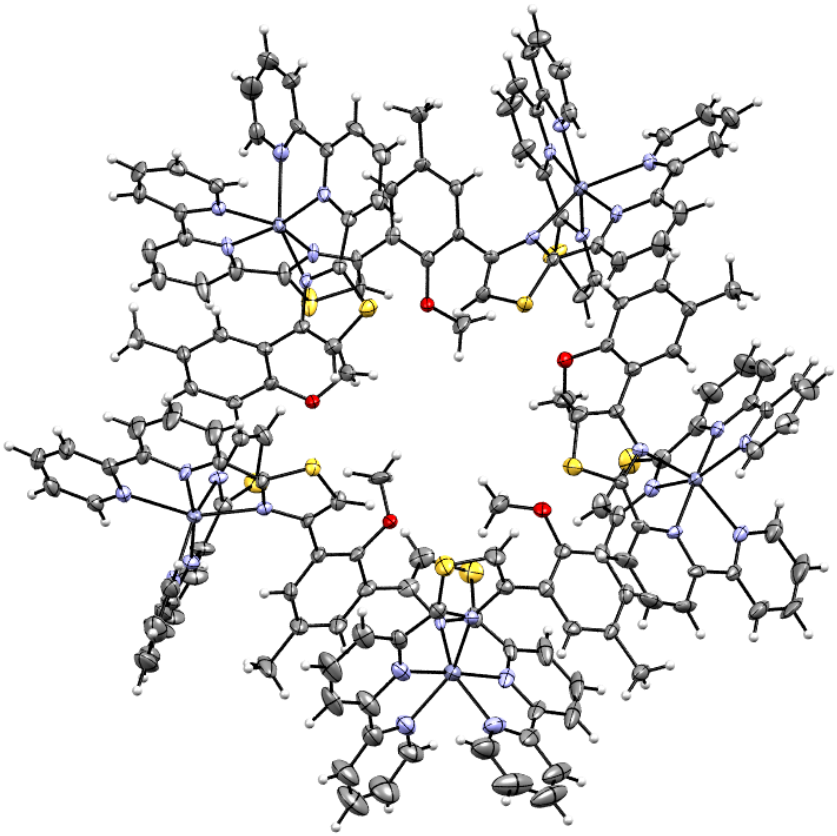

*Fig. 59: The X-ray crystal structure of the pentanuclear circular helicate $[Zn_5(\mathbf{L^3})_5]^{10+}$ formed from reaction of **L^3** with zinc (II) perchlorate. Thermal ellipsoids are shown at 50% probability.*

The five zinc (II) metal centres in the structure are coordinated by one bipyridyl-thiazole binding domain each from two ligand strands and as a result are six coordinate (Fig. 60 a. and b.). Bond lengths from the nitrogen atoms of the bipyridyl-thiazole domains to the metal centres are ave. 2.172 Å. Unlike the $[Zn_4(\mathbf{L^2})_4]^{8+}$ complex there is no -OH···O- hydrogen bonding interactions within the central core, rather this contains five –OMe units which point outwards from the assembly.

a.

b.

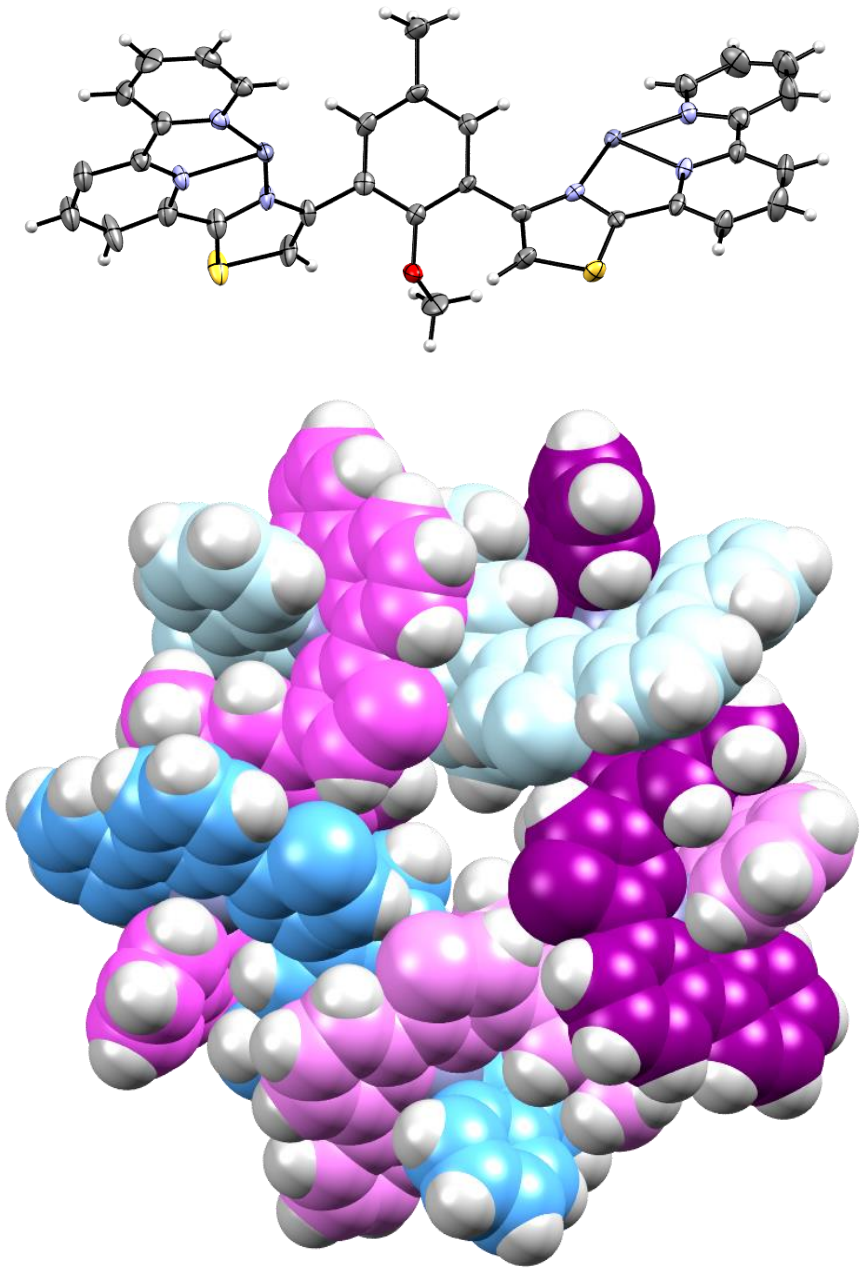

Fig. 60: a. A partial view of the X-ray crystal structure of $[Zn_5(\mathbf{L^3})_5]^{10+}$ showing the partitioning of the ligand strand into its bipyridyl-thiazole domains with a zinc (II) metal ion coordinated in each. Thermal ellipsoids are shown at 50% probability. b. An alternate view of the X-ray Crystal structure of $[Zn_5(\mathbf{L^3})_5]^{10+}$ shown in spacefilling format. The ligand strands are coloured light blue, purple, light pink, blue and pink to better illustrate the helical wrapping of the ligand strands throughout the structure. Hydrogen atoms are coloured silver.

Previously reported work by Rice *et al.* has shown that circular helicates constructed from ligands that contain a central 1,3-phenyl spacer unit result in the formation of pentanuclear assemblies, as a result of the geometry imposed by the substitution pattern of the phenyl ring.[67] However, when this 1,3-phenyl spacer unit was changed to a 1,3-phenol unit a tetranuclear circular helicate was

assembled instead.[91] It was suggested that the driving force behind the formation of the tetranuclear species was the methyl group (present on the back of the spacer phenyl unit) and consequently increased steric bulk on the central aromatic spacer group forced the formation of the lower nuclearity species. However, the complexes $[Zn_4(\mathbf{L^2})_4]^{8+}$ and $[Zn_5(\mathbf{L^3})_5]^{10+}$ strongly suggest that this isn't the case as both the ligand strands **L²** and **L³** possess the same steric bulk on the back of the central aromatic unit (i.e. both contain a methyl substituent) but different nuclearity assemblies are formed. As removal of the –OH units via methylation results in the formation of a pentanuclear species (i.e. $[Zn_5(\mathbf{L^3})_5]^{10+}$), it can instead be inferred that the formation of the lower nuclearity tetranuclear species is a direct result of the hydrogen bonding from the –OH groups of the phenol units and not the steric bulk of the methyl group on the back of the central spacer unit.

In a similar fashion to the previous ligands, **L⁴** was capable of partitioning into two separate binding domains. However unlike **L²** and **L³** and due to the unsymmetrical nature of the ligand strand, **L⁴** would partition into two different binding domains; a tridentate bipyridyl-thiazole domain and a bidentate pyridyl-thiazole domain. Hence reaction of **L⁴** with a metal ion which has a preference for a five coordinate coordination geometry (such as copper (II)), would potentially facilitate the formation of a head-to-tail circular helicate by each metal ion coordinating both binding domains. For example, if a copper (II) metal centre was coordinated by a tridentate bipyridyl-thiazole domain of one **L⁴** ligand strand, then its preferred coordination number of five was completed through the coordination from a bidentate pyridyl-thiazole domain of another **L⁴** ligand strand.

Suspension of **L⁴** in acetonitrile and reaction with copper (II) perchlorate gave a clear blue solution. After slow diffusion of diisopropyl ether, blue crystals suitable for X-ray analysis were obtained and analysis in the solid state revealed the head-to-tail, pentanuclear circular helicate species $[Cu_5(\mathbf{L^4})_5]^{10+}$ is formed (Fig. 61 a.). As predicted, the ligand **L⁴** did partition itself into separate bipyridyl-thiazole and pyridyl-thiazole binding domains and the copper (II) metal ions adopted a coordination number of five to coordinate one of each domain in a head-to-tail conformation.

a.

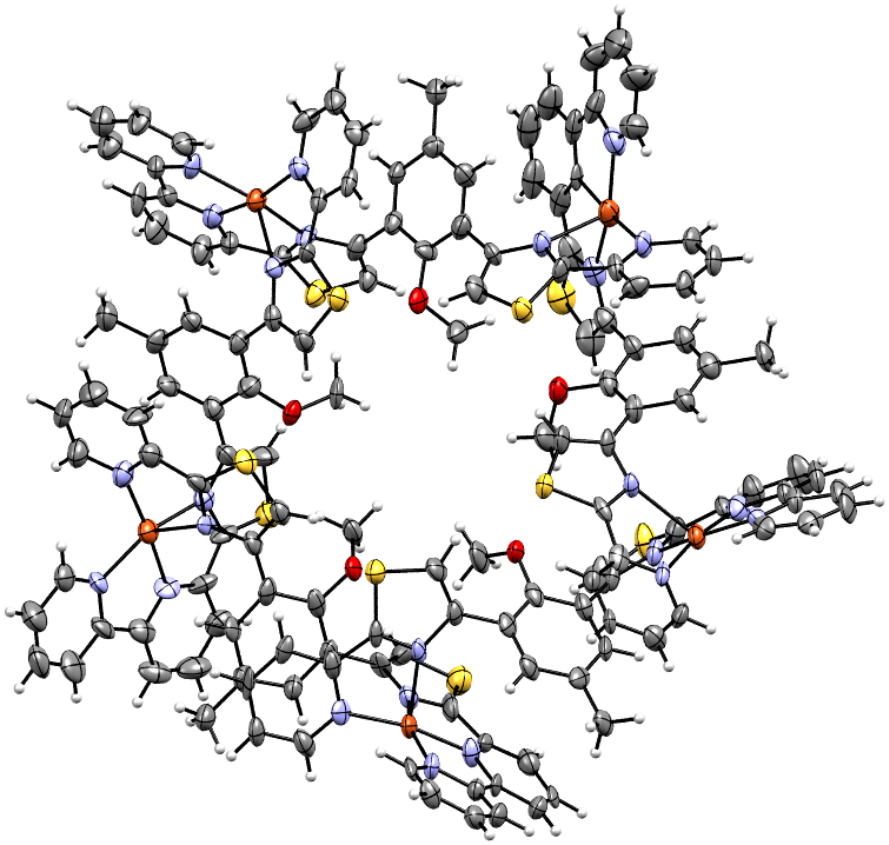

b.

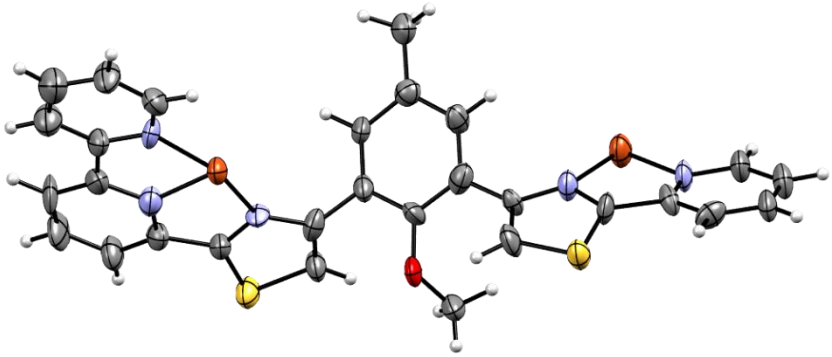

Fig. 61: a. The X-ray crystal structure of the head-to-tail pentanuclear circular helicate complex $[Cu_5(\mathbf{L^4})_5]^{10+}$ formed upon reaction of $\mathbf{L^4}$ with copper (II) perchlorate. b. Partial view of the X-ray crystal structure of $[Cu_5(\mathbf{L^4})_5]^{10+}$ showing one $\mathbf{L^4}$ ligand strand with a copper (II) metal ion partially coordinated in each domain. Thermal ellipsoids are shown at 50% probability.

Bond lengths from the coordinating nitrogen atoms of the binding domains to the copper (II) metal centres are ave. 2.081 Å. The replacement of the inwardly facing –OH groups on the central aromatic spacing group with –OMe groups had prevented the hydrogen bonding that appeared to be a

controlling factor in the tetranuclear nature of the $[Zn_4(\mathbf{L^3})_4]^{8+}$ and consequently resulted in the $[Cu_5(\mathbf{L^4})_5]^{10+}$ assembly being pentanuclear.

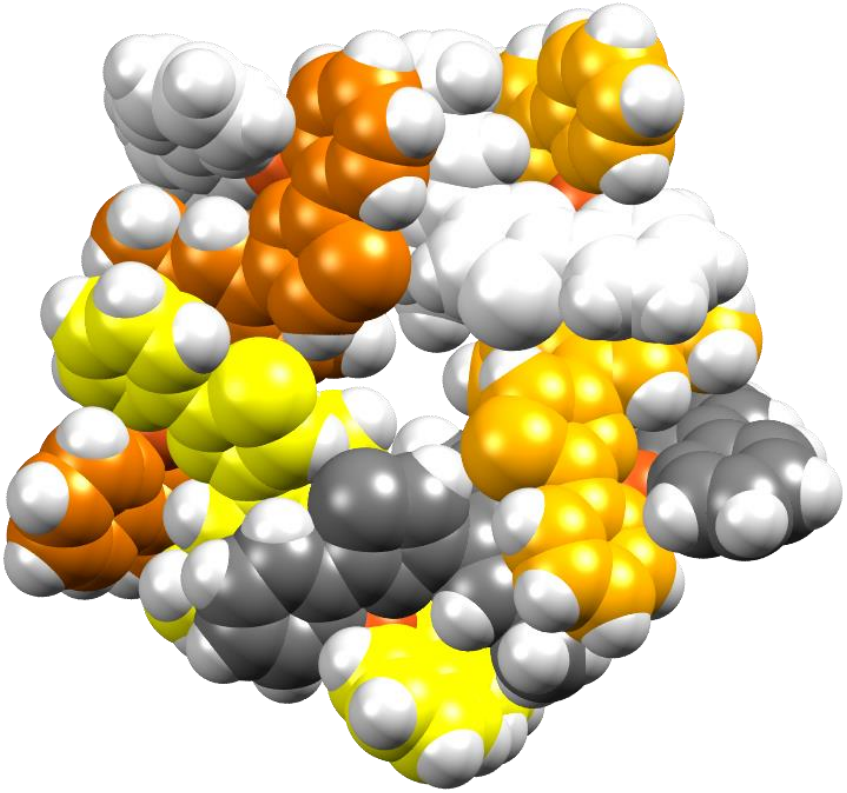

Fig. 62: An alternate view of the crystal structure of $[Cu_5(\mathbf{L^4})_5]^{10+}$ shown in spacefilling view to better show the helical motif of the circular assembly. $\mathbf{L^4}$ ligand strands are coloured white, orange, dark grey, yellow and dark orange for clarity. Hydrogen atoms are coloured silver.

3.3 Conclusions

The work reported in this chapter has demonstrated how the subtle pre-programming of ligand strands can be utilised to control the nuclearity and formation of circular helicate assemblies when reacted with transition metal ions.

Reaction of **L^2** with zinc (II) trifluoromethanesulfonate results in the formation of the tetranuclear circular helicate species $[Zn_4(\mathbf{L^2})_4]^{8+}$. The hydrogen atoms of each –OH group of the central cresol space group hydrogen bond to the oxygen atom of the adjacent –OH group in the core of the assembly and it is this that contributes to the tetranuclear nuclearity.[1]

Reaction of **L^3** with zinc (II) perchlorate results in the formation of the pentanuclear circular helicate species $[Zn_5(\mathbf{L^3})_5]^{10+}$. The change in nuclearity between the $[Zn_4(\mathbf{L^2})_4]^{8+}$ and the $[Zn_5(\mathbf{L^3})_5]^{10+}$ complexes is attributed to the replacement of the –OH group on the central aromatic spacer in **L^2** with the –OMe group in **L^3**. The removal of the –OH group prevents any hydrogen bonding taking place between adjacent ligand strands and this results in the structure adopting a pentanuclear conformation.

Reaction of the unsymmetrical ligand strand **L^4** with copper (II) perchlorate gives the head-to-tail, pentanuclear circular helicate species $[Cu_5(\mathbf{L^4})_5]^{10+}$. Due to the ligand being unsymmetrical with a tridentate bipyridyl-thiazole domain and a bidentate pyridyl-thiazole domain, a head-to-tail conformation was adopted. The copper (II) metal ions are five coordinate in the complex as a result of them coordinating through one binding domain of one **L^4** ligand strand and then the alternate binding domain from a separate **L^4** ligand strand.

4 Chapter 4: The Synthesis of a Series of Bis-bidentate Ligand Strands and their Coordination Chemistry with Ag (I) metal ions

Described in this chapter is the synthesis and coordination chemistry of a series of potentially tetradentate ligands, **L^5**, **L^6** and **L^7** (Fig. 63) all of which possess two pyridyl-thiazole binding domains and a central cresol spacing group. However, the ligands differ from each other through the functionalization of the –OH group of the central spacer. Upon reaction with silver (I) metal ions, **L^5** forms the dinuclear mesocate species $[Ag_2(\mathbf{L^5})_2]^{2+}$ and **L^6** forms the one-dimensional helical polymer species $[Ag_n(\mathbf{L^6})_n]^{n+}$. Reaction of **L^7** with silver (I) gives the three-dimensional infinite honeycomb-like polymer $[Ag_6(\mathbf{L^7})_6]^{6+}]_n$ made up of individual hexanuclear circular helicate units all connected together via inter-assembly Ag···Ag interactions. However, upon reacting **L^7** with copper (I) metal ions, the hexanuclear circular mesocate species $[Cu_6(\mathbf{L^7})_6]^{6+}$ is formed.

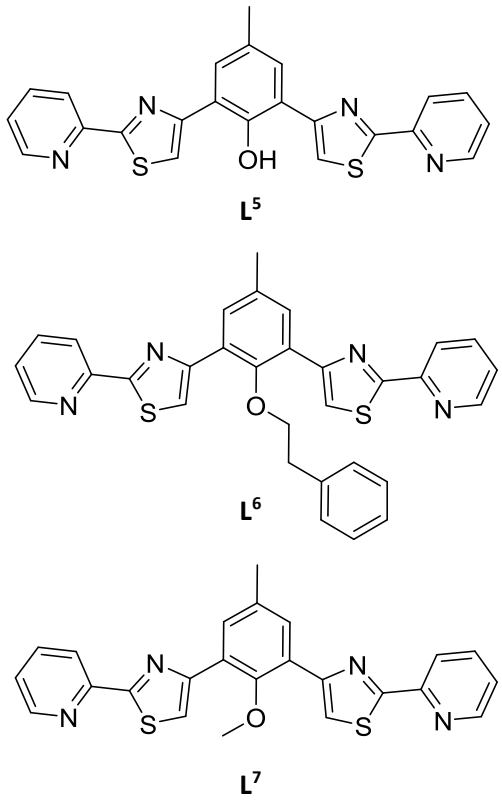

*Fig. 63: The three ligand strands, **L^5**, **L^6** and **L^7** to be reported and discussed in this chapter.*

4.1 Synthesis of L^5, L^6 and L^7

Unless otherwise stated, all solvents and materials were purchased from Sigma Aldrich, Acros Organics and/or Fisher Scientific and were used without further purification. The 1,3-di(α-bromoacetyl)cresol (**5**) was prepared by a previously reported method by bromination of 1,3-di(acetyl)cresol.[91] ^{1}H and/or ^{13}C NMR data was recorded on either a Bruker AV (III) 400MHz NMR spectrometer or a Bruker Advance 500 MHz NMR spectrometer. Mass spectra were obtained on either an Agilent 6210 TOF MS with electrospray ionisation, operating in positive ion mode or a Bruker Micro TOF-q LC mass spectrometer with electrospray ionisation, operating in positive ion mode. Single crystal studies were recorded on a Bruker D8 Venture with Dual IμS Microfocus Sources using either Mo or Cu radiation at 150 (2) K.

4.1.1 Synthesis of 5

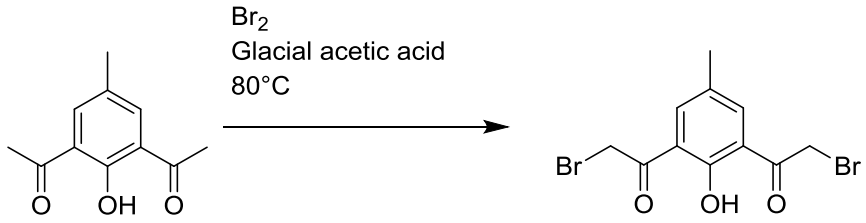

5

1,3-diacetyl cresol (500 mg, 2.6 mmol) was dissolved in glacial acetic acid (20 mL) and set to stir at 80 ˚C. To this was added Br_2 (833 mg, 0.267 mL, 5.2 mmol) in acetic acid (1 mL) over a period of 2 hours. Progress of the reaction was monitored *via* TLC (SiO_2, 1 % hexane in DCM) and once the starting material had been consumed, the solution was evaporated to dryness. Purification was achieved by column chromatography (SiO_2, 1% hexane in DCM) and gave the di-bromo containing product **5** as a yellow solid (350 mg, 1.0 mmol, 38 %). ^{1}H NMR (400 MHz, $CDCl_3$) δ: 12.8 (s, H, -OH); 7.9 (s, 2H, Ar); 4.6 (s, 4H, -CH_2); 2.4 (s, 3H, -CH_3) ppm.

4.1.2 Synthesis of L^5

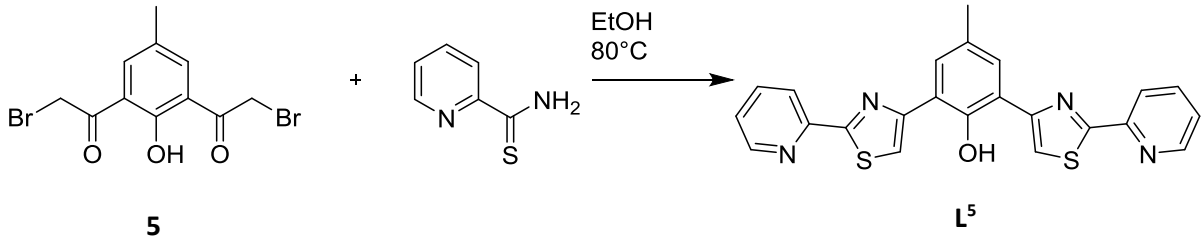

5 **L^5**

To a two-necked round bottom flask containing pyridine-2-thioamide (87 mg, 0.63 mmol) and ethanol (25 mL) was added the dibromo species (**1**) (100 mg, 0.29 mmol) and the reaction heated to 80 ˚C. After 12 hours a precipitate had formed which was isolated by vacuum filtration and washed with ethanol (1 x 5 mL) and diethyl ether (2 x 5 mL) to give the hydrobromide salt of the product as a yellow solid. This solid was then suspended in concentrated aqueous ammonia (0.88 sp. gr., 10 mL) for 12 hours after which time the yellow solid was isolated by vacuum filtration and washed with water (2 x 2 mL), ethanol (2 x 2 mL) and diethylether (2 x 2 mL) giving the free-base ligand **L5** as a yellow powder. (47 mg, 0.11 mmol, 75 %). ^{1}H NMR (400 MHz, $(CD_3)_2SO$) δ: 12.4 (s, -OH, 1H); 8.70 (d, *J*= 4.52, 2H, py); 8.48 (s, 2H, tz); 8.28 (d, *J*= 7.84, 2H, py); 8.05 (td, *J*= 7.68, 1.48, 2H, py); 7.98 (s, 2H, Ar); 7.57 (dd, *J*= 6.94, 5.12, 2H, py); 2.42 (s, $-CH_3$, 3H) ppm. ^{13}C NMR (100 MHz, $CDCl_3$) δ: 167.6, 153.3, 151.5, 150.3, 150.2, 138.5, 129.3, 128.5, 126.0, 120.3, 119.9, 119.4, 20.9 ppm. *HRMS (m/z): $[M+H]^+$ for $C_{23}H_{16}N_4OS_2$ calculated 429.0838, measured 429.0832.*

4.1.3 Synthesis of **L^6**:

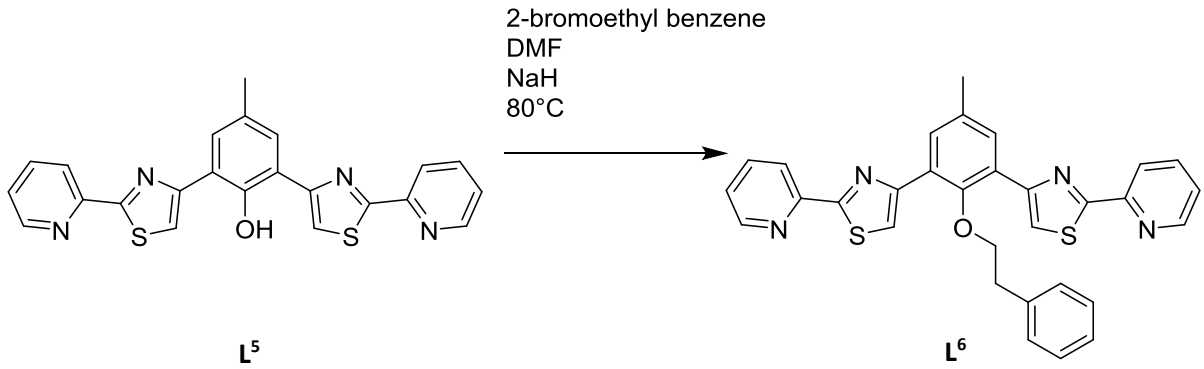

L^5 **L^6**

A two necked round bottom flask containing **L^5** (80 mg, 0.187 mmol) and sodium hydride (60% dispersion in mineral oil, 100 mg, 2.5 mmol) was placed under an atmosphere of N_2 and left to purge for ~ 30 minutes. To this, anhydrous DMF (20 mL) was added and the resulting suspension left to stir at 80 °C for 1 hour. After this time 2-Bromoethyl benzene (0.5 mL, 3.66 mmol) was added and the reaction left to heat and stir for 12 hours. After this time the reaction was allowed to cool and methanol was added whilst under N_2 (to remove any unreacted NaH) and the reaction was evaporated to dryness. Purification *via* column chromatography (SiO_2, 2% MeOH in DCM) gave **L^6** as a white solid (66 mg, 0.124 mmol, 48 %). ^{1}H NMR (400 MHz, $CDCl_3$) δ: 8.68 (d, *J*= 4.8, 2H, py); 8.37 (d, *J*= 7.92, 2H, py); 8.01 (s, 2H, Ar); 7.85 (td, *J*= 7.68, 1.6, 2H, py); 7.71 (s, 2H, tz); 7.39-7.28 (m, overlapping, 5H, Ar) 7.24 (d, *J*= 6.48, 2H, py); 3.85 (t, *J*= 6.28, 2H, -CH_2); 2.96 (t, *J*= 6.2, 2H, -CH_2); 2.49 (s, 3H, -CH_3) ppm. ^{13}C NMR (100 MHz, $CDCl_3$) δ: 167.3, 152.5, 152.2, 151.5, 149.5, 138.5, 137.0, 134.3, 130.7, 129.5, 128.7, 128.5, 126.8, 124.5, 119.9, 119.7, 73.6 (-O*C*$H_2$$CH_2$), 37.3 (-OCH$_2$*C*$H_2$), 21.1 (-$CH_3$) ppm. *HRMS (m/z): [M+H]$^+$ for $C_{31}H_{24}N_4OS_2$ calculated 533.1464, measured 533.1458.*

4.1.4 Synthesis of **L[7]**:

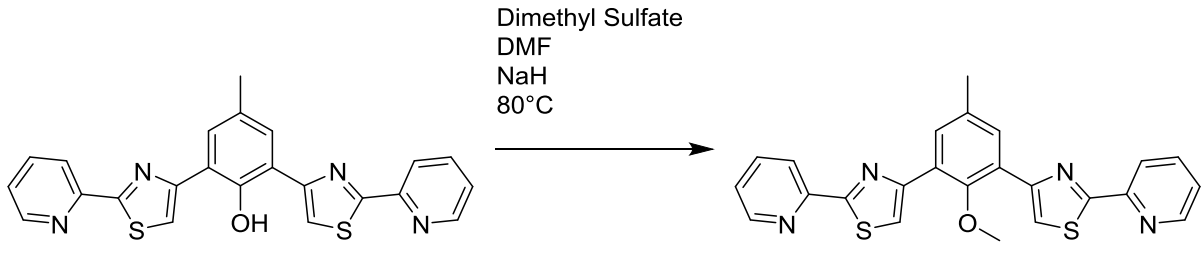

L[5] **L[7]**

A two necked round bottom flask containing **L[5]** (120 mg, 0.27 mmol) and sodium hydride (60% dispersion in mineral oil, 100 mg, 2.5 mmol) was placed under an atmosphere of N_2 and left to purge for 30 minutes. To this, anhydrous DMF (20 mL) was added and left to stir at 80 ^{0}C for 1 hour and after adding dimethyl sulphate (0.5 mL, 5.0 mmol), was heated for a further 12 hours. After this time the reaction was allowed to cool and methanol was added whilst under N_2 (to remove any unreacted NaH) and the reaction was evaporated to dryness. Purification *via* column chromatography (Al_2O_3, DCM) gave the final product **L[7]** as a white solid (55 mg, 0.12 mmol, 45%). ^{1}H NMR (400 MHz, $CDCl_3$) δ: 8.59 (d, J= 4.36, 2H, py); 8.31 (d, J= 7.92, 2H, py); 8.05 (s, 2H, Ar); 7.97 (s, 2H, tz); 7.77 (td, J= 7.68, 1.68, 2H, py); 7.28 (ddd, *J* = 7.4, 4.8, 1.0 Hz, 2H, py); 3.56 (s, 3H, -OCH_3); 2.42 (s, 3H, -CH_3). ^{13}C NMR (100 MHz, $CDCl_3$) δ: 167.4, 153.7, 152.6, 151.5, 149.5, 137.1, 134.3, 130.8, 128.2, 124.5, 119.9, 119.8, 60.1 (-OCH_3), 21.1 (-CH_3) ppm. *HRMS (m/z): $[M+H]^+$ for $C_{24}H_{18}N_4OS_2$ calculated 443.0995, measured 443.0986.*

4.1.5 Synthesis of $[Ag_2(\mathbf{L^5})_2]^{2+}$:

To a suspension of $\mathbf{L^5}$ (0.01 g 0.023 mmol) in MeCN (2 mL), $Ag(ClO_4)$ (0.005 g, 0.024 mmol) was added and the reaction briefly heated and sonicated until all the ligand dissolved to give a yellow solution. Chloroform was allowed to slowly diffuse into the solution and after a few days, yellow crystals had formed (0.009g, 66%). ^{1}H NMR (400 MHz, CD_3CN) δ (ppm) 12.45 (s, 1H, OH), 8.62 (d, *J* = 4.8, 2H, py), 8.09 (d, *J* = 8.5, 2H, py), 8.08 (s, 2H, tz), 7.95 (dt, *J* = 7.8, 1.5, 2H, py), 7.77 (s, 2H, Ph), 7.51 (ddd, *J* = 7.5, 4.8, 0.8 Hz, 2H, py), 2.31 (s, 3H, $-CH_3$). ESI-MS *m/z* = 1171 corresponding to $\{[Ag_2(\mathbf{L^5})_2](ClO_4)\}^+$.

4.1.6 Synthesis of $[Ag_n(\mathbf{L^6})_n]^{n+}$:

To a suspension of $\mathbf{L^6}$ (0.01 g 0.019 mmol) in $MeNO_2$ (2 mL), $Ag(BF_4)$ (0.004 g, 0.024 mmol) was added and the reaction briefly heated and sonicated until all the ligand dissolved to give a colourless solution. Diisopropyl ether was allowed to slowly diffuse into the solution giving colourless crystals after a few days (0.01 g 73%). ^{1}H NMR (400 MHz, CD_3NO_2) δ (ppm) 8.63 (brs, 2H), 8.25 (brs, 5H overlapping), 7.85 (brs, 2H), 7.75 (brs, 2H), 7.09 (brs, 3H, overlapping), 6.86 (brs, 2H), 3.81 (brs, 2H), 2.81 (brs, 2H) and 1.81 (brs, 3H). ESI-MS *m/z* = 897 corresponding to $\{[Ag_2(\mathbf{L^6})](CF_3SO_3)\}^+$, 1173 corresponding to $\{[Ag(\mathbf{L^6})_2]\}^+$, 1429 corresponding to $\{[Ag_2(\mathbf{L^6})_2](CF_3SO_3)\}^+$ and 1687 corresponding to $\{[Ag_3(\mathbf{L^6})_2(CF_3SO_3)_2\}^+$.

4.1.7 Synthesis of $[[Ag_6(\mathbf{L^7})_6]^{6+}]_n$:

To a suspension of $\mathbf{L^7}$ (0.01 g 0.23 mmol) in $MeNO_2$ (2 mL), $Ag(BF_4)$ (0.0045 g, 0.24 mmol) was added and the reaction briefly heated and sonicated until all the ligand dissolved to give a colourless solution. Diisopropyl ether was allowed to slowly diffuse into the solution giving pale yellow crystals after a few days which were isolated by filtration and dried under vacuum (0.009 g, 62 %). Found: C, 44.7; H, 2.8; N, 8.7%; $C_{24}H_{18}N_4OS_2AgBF_4$ requires C, 45.2; H, 2.8; N, 8.8%. ^{1}H NMR (400 MHz, CD_3CN) δ

(ppm) 8.62 (d, *J* = 4.8, 2H, py), 8.22 (d, *J* = 7.9, 2H, py), 8.04 (s, 2H, tz), 7.99 (dt, *J* = 7.7, 1.6, 2H, py), 7.89 (s, 2H, Ph), 7.51 (ddd, *J* = 7.5, 5.0, 0.7 Hz, 2H), 3.48 (s, 3H, $-OCH_3$), 2.24 (s, 3H, $-CH_3$). ESI-MS *m/z* = 3735 corresponding to $\{[Ag_6(\mathbf{L^7})_6](BF_4)_5\}^+$ along with lower molecular weight species e.g. $\{[Ag_n(\mathbf{L^7})_n](BF_4)_{n-1}\}^+$ where n = 1 to 5.

4.1.8 Synthesis of $[Cu_6(\mathbf{L^7})_6]^{6+}$:

To a suspension of $\mathbf{L^7}$ (0.01 g 0.23 mmol) in MeCN (2 mL), $Cu(CF_3SO_3)$ (0.013 g, 0.025 mmol) was added and the reaction briefly heated and sonicated until all the ligand dissolved to give a dark red solution. Dichloromethane was allowed to slowly diffuse into the solution giving dark red crystals after a few days (2 mg, 14%).

4.2 Results and Discussion

The ligand **L**^{5} was prepared by reaction of pyridine-2-thioamide with 2,6-di(2-bromoethanone)cresol which can be functionalised at the oxygen atom by deprotonation and reaction of 2-bromoethyl benzene giving **L**^{6} or dimethyl sulfate to give **L**^{7}.

Suspension of **L**^{5} in nitromethane and reaction with silver (I) perchlorate gave a clear yellow solution which after slow diffusion of $CHCl_3$ gave crystals suitable for X-ray analysis. Analysis in the solid state shows that a dinuclear mesocate is formed e.g. $[Ag_2(\mathbf{L}^{5})_2]^{4+}$ (Fig. 64).

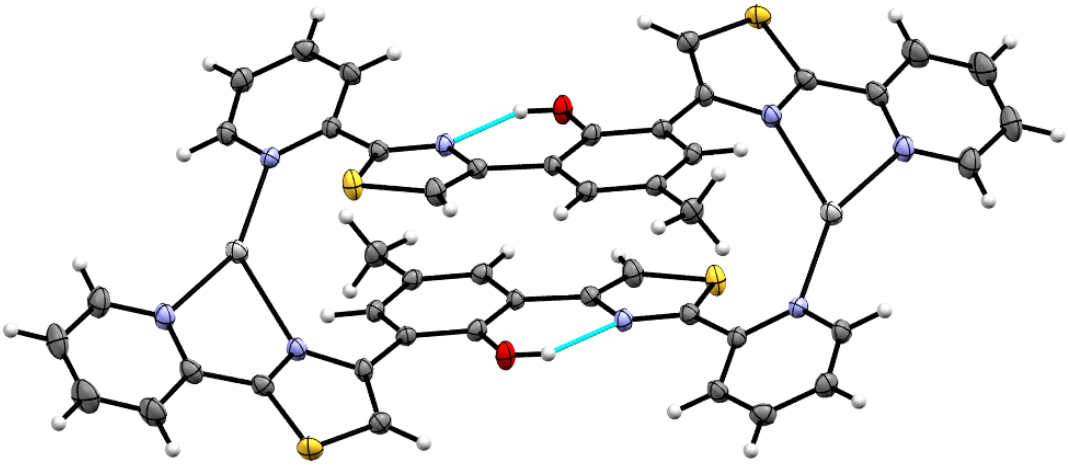

Fig. 64: X-ray crystal structure of the dinuclear mesocate complex $[Ag_2(\mathbf{L}^{5})_2]^{2+}$ showing hydrogen bonding between the nitrogen atom of the thiazole group and the hydrogen atom of the hydroxyl group (dashed blue lines). Thermal ellipsoids shown at 50% probability.

In this structure the ligand partitions into a bidentate pyridyl-thiazole domain and a monodentate pyridyl domain each of which coordinates a different metal ion resulting in a three coordinate Ag (I) centre. The Ag-N bond lengths range from 2.196 (3) Å to 2.359 (3) Å with the longest bonds arising from the thiazole-metal interactions with the remaining uncoordinated thiazole unit forming a hydrogen bond to the cresol hydroxyl unit. Quite why the ligand does not act as a bis-bidentate donor isn't clear. It is possible using all the nitrogen domains to coordinate the sliver ion would require the formation of a higher nuclearity species (see later) as the steric constraints of the central phenol oxygen prevent the formation of a helicate/mesocate with four-coordinate Ag (I) metal ions.

As a result the entropically favoured mesocate is formed with the ligand acting as a mono- and bidentate donor with the uncoordinated thiazole unit forming a hydrogen bond to the phenolic hydrogen atom.

a.

b.

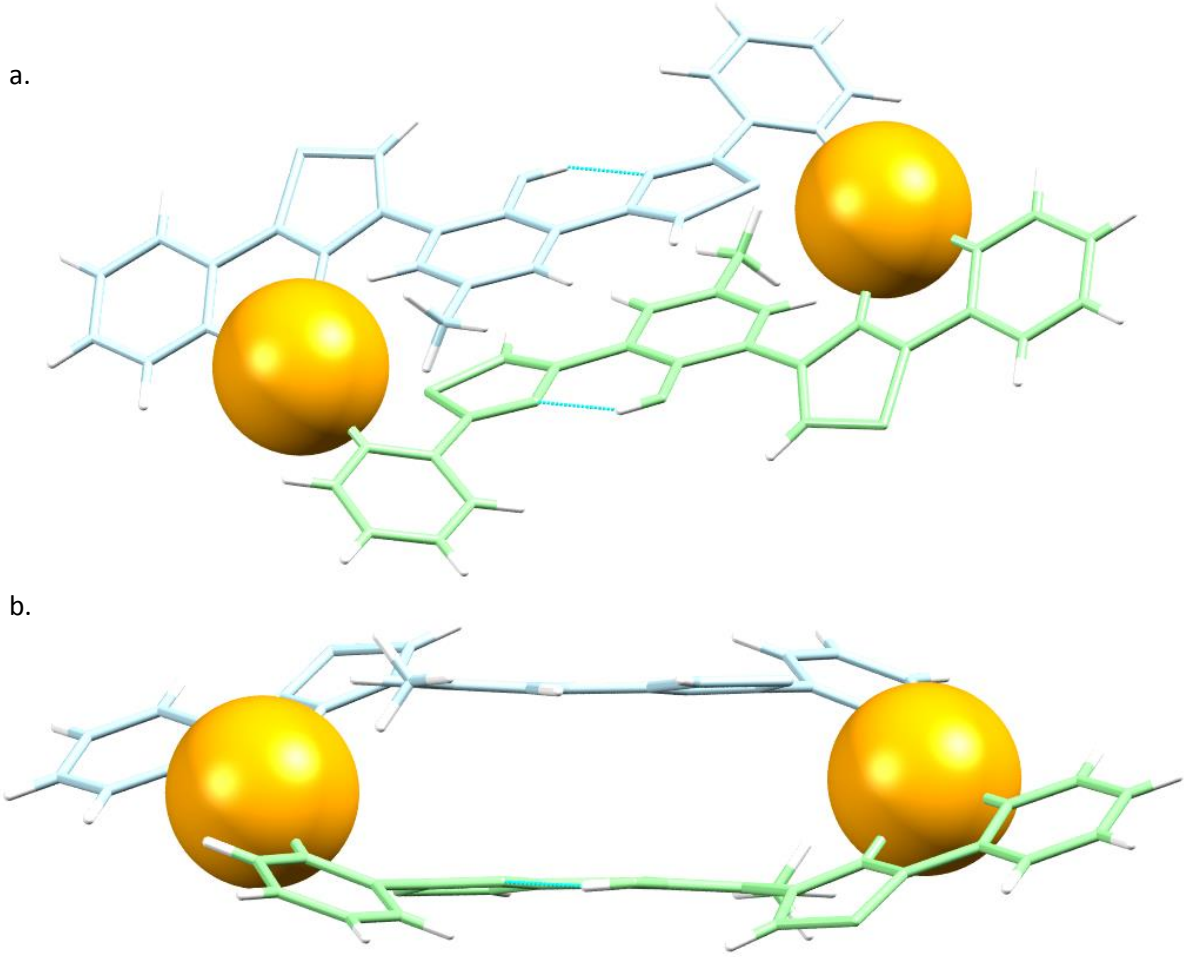

Fig. 65: Alternate views of the X-ray crystal structure of the dinuclear mesocate complex $[Ag_2(\mathbf{L^5})_2]^{2+}$. Ligands have been coloured blue and green for clarity and Ag (I) metal ions coloured orange and shown in spacefilling view. In b. the dinuclear mesocate $[Ag_2(\mathbf{L^5})_2]^{2+}$ is viewed from the side to illustrate the absence of the helical twist in the structure required for the conventional helicate motif.

This dinuclear species also occurs in solution as an ion at m/z 1171 corresponding to $\{[Ag_2(\mathbf{L^5})_2](ClO_4)\}^+$ is observed in the ESI-MS. However, in the ^{1}H NMR six aromatic signals are observed which indicates that a symmetrical ligand species is present which isn't the case in the solid state as the ligand partitions into different binding domains. The symmetry observed in solution is probably a result of fluxional behaviour, as the bidentate and monodentate domains can

easily interchange. Regardless, it is clear the dinuclear nature of the complex is observed in both the solid and solution state.

Reaction of $\mathbf{L^6}$ with Ag (BF_4) in $MeNO_2$ gave a colourless solution from which colourless crystals were deposited by slow diffusion of diisopropyl ether. In the solid state (in an analogous fashion to $\mathbf{L^5}$) the ligand partitions into two donor units but in this example the ligand acts as a bis-bidentate donor with each end of the ligand coordinating a different metal ion via pyridyl-thiazole donor units. The silver (I) metal ions are further coordinated by a different ligand resulting in the 1-dimensional helical metal-containing polymer, $[Ag_n(\mathbf{L^6})_n]^{n+}$ (Fig. 66).

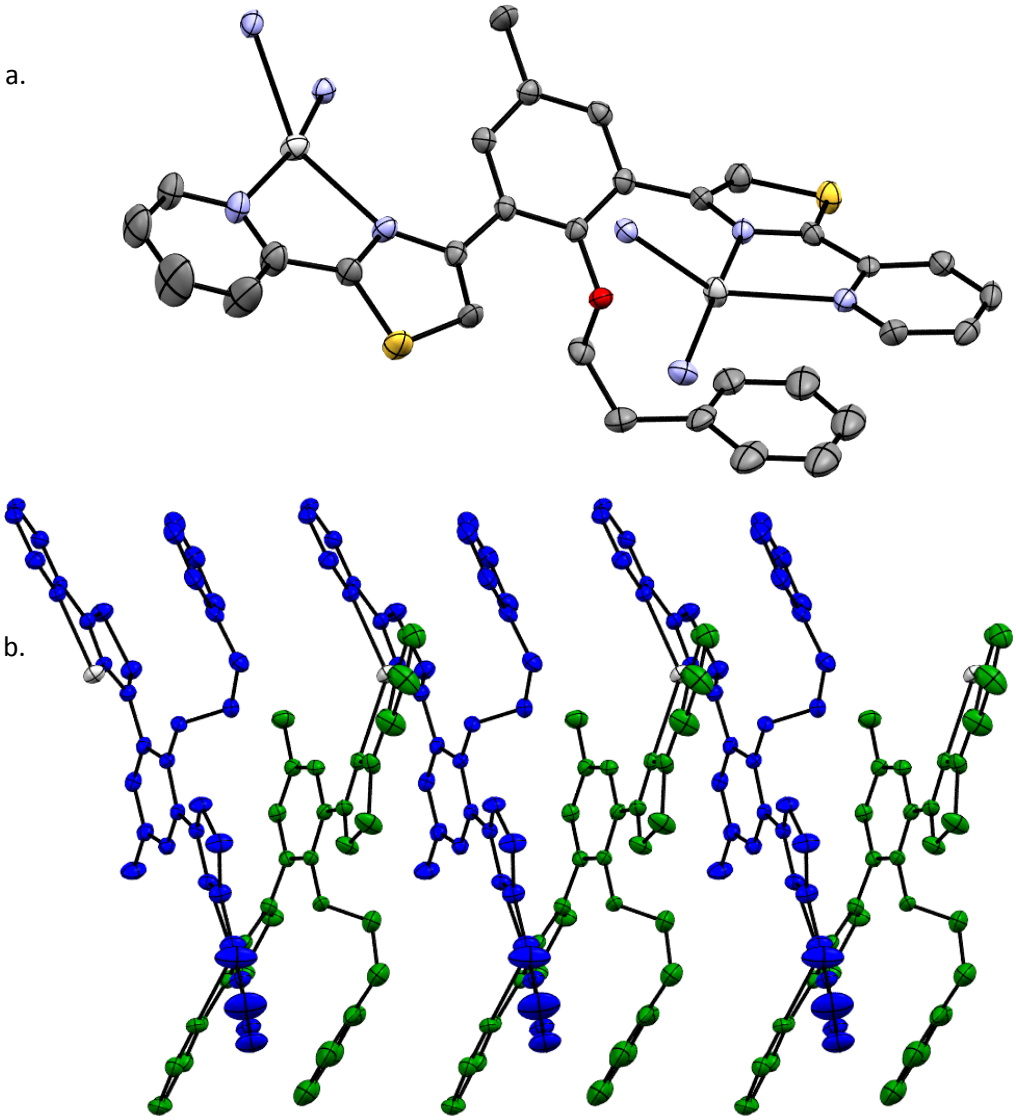

Fig. 66: Crystal structure of the $[Ag_n(\mathbf{L^6})_n]^{n+}$ polymer a. Partial view showing the $[Ag_2(\mathbf{L^6})]^{2+}$ unit and b. the polymeric complex $[Ag_n(\mathbf{L^6})_n]^{n+}$ with alternating ligand strands coloured blue and green and hydrogen atoms omitted for clarity. Thermal ellipsoids shown at 50% probability.

As would be expected, ESI-MS analysis shows fragments of the polymeric structure with ions corresponding to $\{[Ag_2(\mathbf{L^6})]CF_3SO_3\}^+$, $\{[Ag(\mathbf{L^6})_2]\}^+$, $\{[Ag_2(\mathbf{L^6})_2]CF_3SO_3\}^+$ and $\{[Ag_3(\mathbf{L^6})_2](CF_3SO_3)_2\}^+$ being observed (Fig. 67). In the ^1H NMR (CD_3NO_2) the corresponding signals are observed in the aromatic region but these are broadened which is again to be expected for a polymeric species.

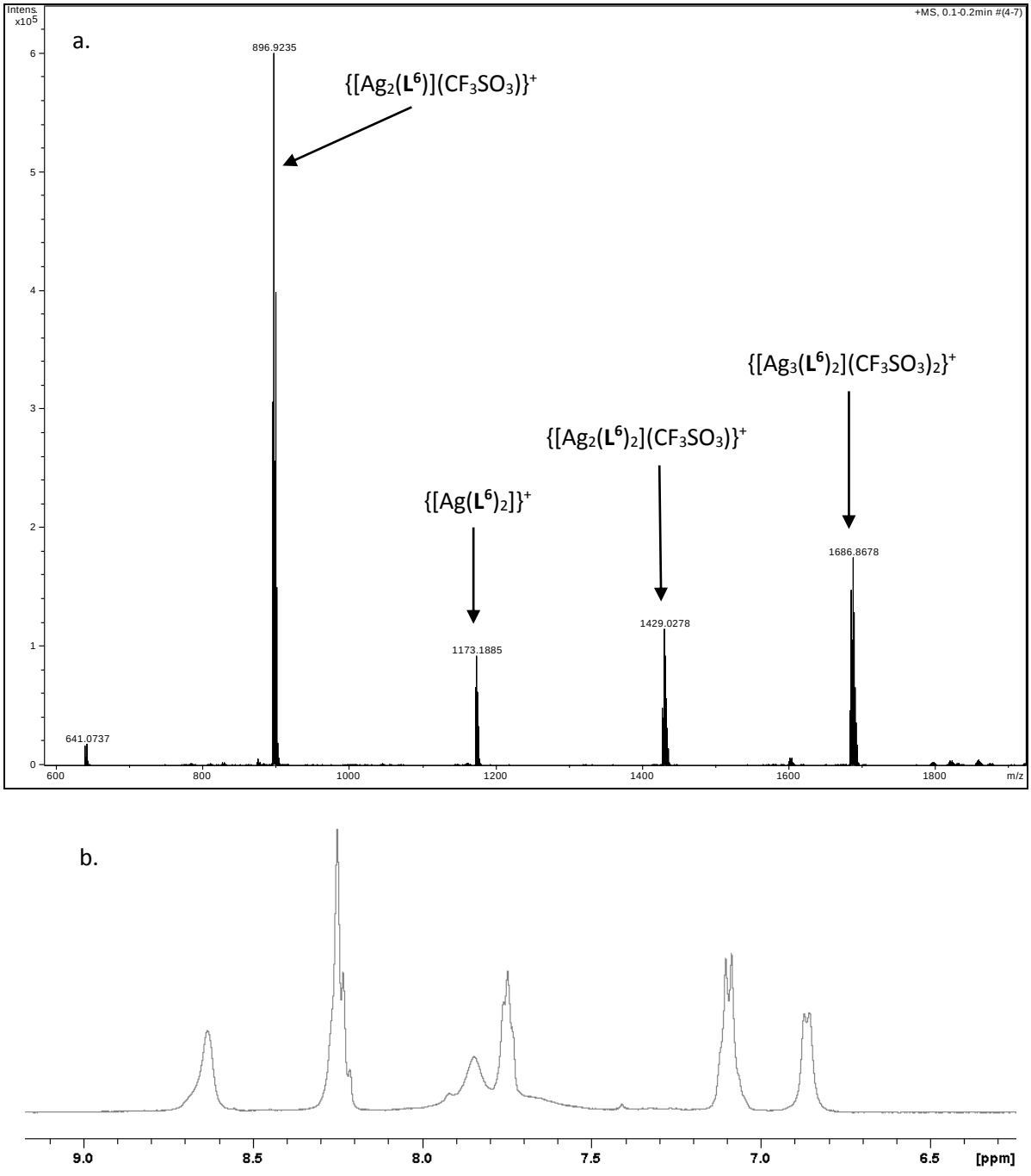

Fig. 67: a. ESI-MS spectrum for the complex $[Ag_n(\mathbf{L^6})_n]^{n+}$ showing various molecular weight components of the polymeric species and b. the aromatic region of the ^1H NMR spectrum for $[Ag_n(\mathbf{L^6})_n]$ showing the broadened signals indicative of a polymeric species.

The formation of this species is the result of two factors. Firstly, the removal of the phenol hydrogen atom prevents the formation of the intramolecular hydrogen bond leaving all four nitrogen atoms to act as metal donors. Secondly the inclusion of the ethyl phenyl unit forms intramolecular π-stacking interactions between itself and the planar pyridyl thiazole domain, promoting the formation of the polymeric unit. It can be seen that the ethyl phenyl units only exhibit intermolecular π-stacking interactions with one of the pyridyl thiazole units not with its nearest neighbour but in a 1,3 alternate fashion (Fig. 68 a.).

Also π-stacking interactions can be seen down the central spine of the polymer, through the central aromatic rings found in the spacer units (Fig. 68 b.). Conversely to the π-stacking interactions between the pyridyl-thiazole and the ethyl phenyl domains, the interactions are observed directly between alternating ligand strands.

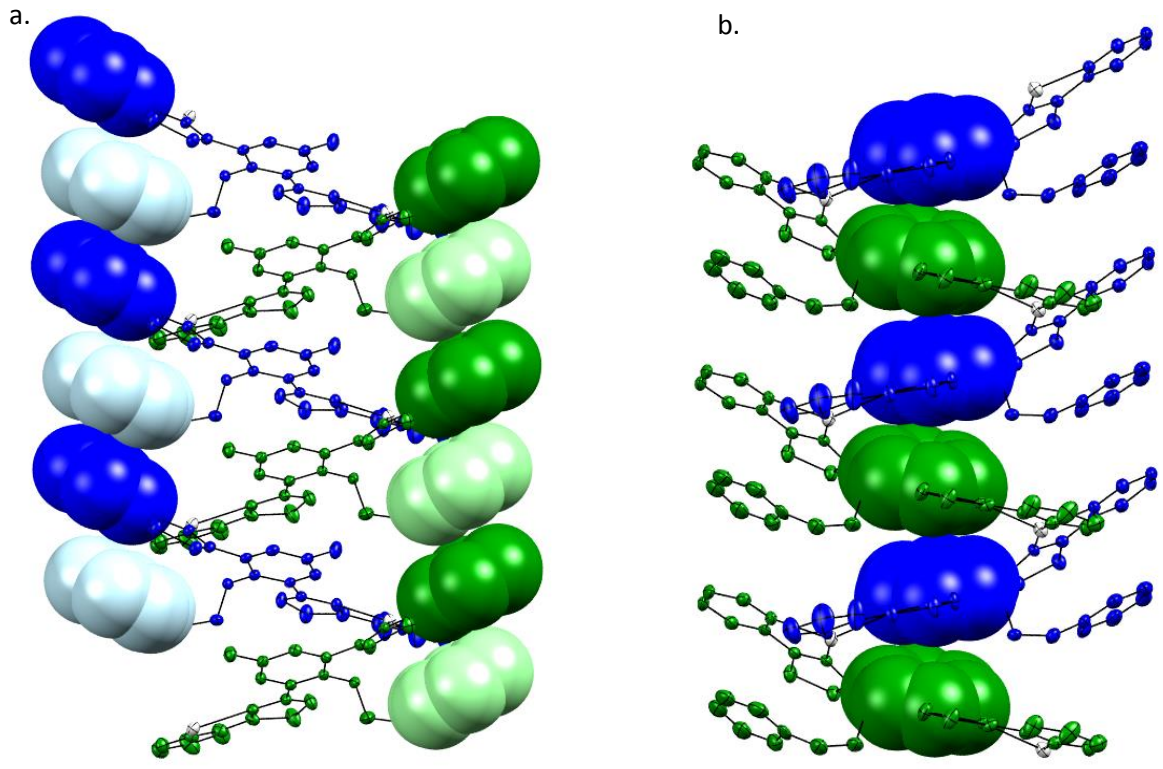

Fig. 68: Crystal structure of the polymeric complex $[Ag_n(\mathbf{L^6})_n]^{n+}$ with alternating ligand strands coloured blue and green. a. The phenyl rings of the phenyl ethyl domain of the ligand strands (light blue and light green when a part of the blue and green ligands respectively) exhibit π-stacking interactions between the terminal pyridyl domains necessitating the formation of the helical polymer. The phenyl rings of the ethyl phenyl and the terminal pyridyl-thiazole domains are shown in spacefilling view. b. π-stacking interactions can be seen between the aromatic rings of the spacer group (shown in spacefilling view) of alternating ligands down the centre of the polymer chain. All thermal ellipsoids are shown at 50% probability and hydrogen atoms have been omitted for clarity.

The Ag-N bond lengths range from 2.271 (4) – 2.576 (3) Å. However it could be argued that this coordination sphere is further supplemented by an additional interaction as the phenol ether oxygen atom lies relatively close to the silver cation (ave. 2.727 Å) (Fig. 69). Although this is a relatively long distance, it is still within the sum of the van der Waals radii and suggests that whilst this interaction isn't a major contributor to the formation of the polymer, it is likely to be a further stabilizing effect.

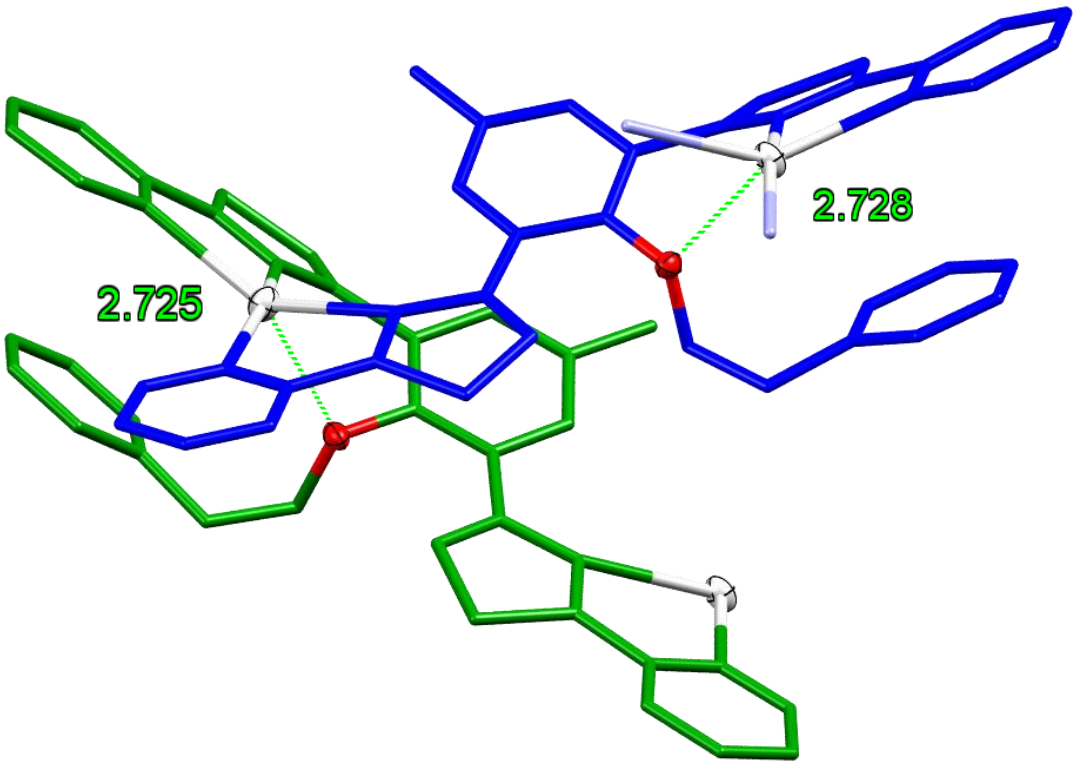

Fig. 69: Partial view of the X-ray crystal structure of $[Ag_n(\mathbf{L^6})_n]^{n+}$ showing only a section of the polymeric species. The Ag (I) metal ions and the phenol ether oxygen atoms are shown as ellipsoids. Distances between the atoms are shown in Å and shown by the dashed green lines. Thermal ellipsoids are shown at 50% probability and hydrogen atoms are omitted for clarity. Alternate ligand strands have been coloured blue and green also for clarity.

Reaction of $\mathbf{L^7}$ with $Ag(BF_4)$ in MeCN gave a colourless solution from which crystals were obtained either by slow diffusion of diisopropyl ether or slow evaporation. Analysis by X-ray crystallography showed that the asymmetric unit cell contained one ligand coordinated to one silver (I) metal ion via a bidentate pyridyl-thiazole domain (Fig. 70). The remaining bidentate pyridyl-thiazole domain coordinates a different silver metal ion with the two sites bridged by the central anisole spacer and the bidentate domains arrange themselves in an 'over and under' conformation giving rise to a hexanuclear circular helicate e.g. $[Ag_6(\mathbf{L^7})_6]^{6+}$ (Fig. 71).

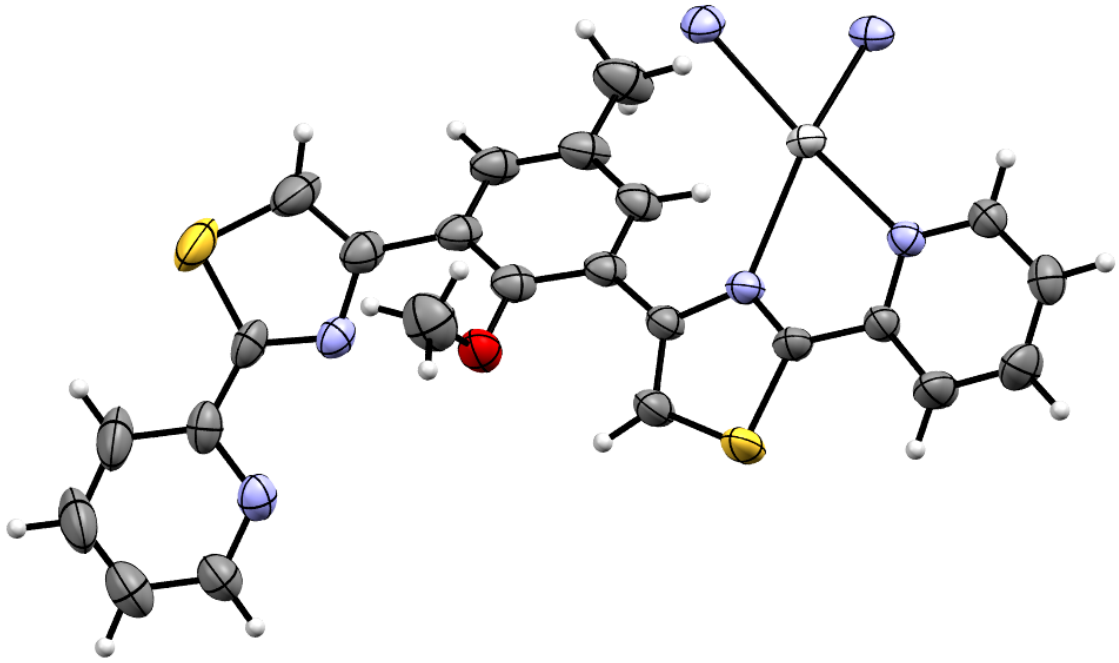

Fig. 70: Partial view of the crystal structure of $[Ag_6(\mathbf{L^7})_6]^{6+}$ showing an $[Ag(\mathbf{L^7})]^{+}$ unit. Thermal ellipsoids are shown at 50% probability.

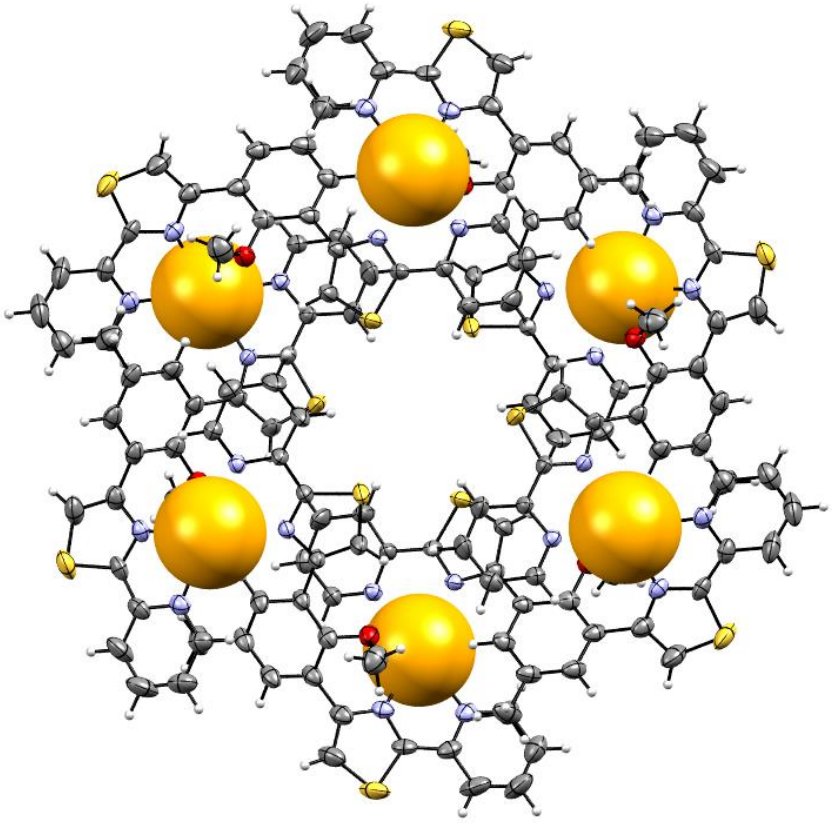

Fig. 71: Crystal structure of the hexanuclear circular helicate $[Ag_6(\mathbf{L^7})_6]^{6+}$. Ag(I) atoms have been coloured orange and shown in spacefilling view. Thermal ellipsoids are shown at 50% probability.

However, this coordination motif is further supplemented by Ag···Ag interactions and it is through these argentophilic interactions that a 3-dimensional polymer develops. Each of the Ag (I) metal ions interacts with a separate Ag (I) ion of a different $[[(Ag)_6(\mathbf{L^7})_6]^{6+}]$ unit and connects them together into a 3-dimensional infinite honeycomb-like structure of hexanuclear circular helicates. The direction of the Ag···Ag interaction from each Ag (I) ion alternates around the circular helicate pointing 'up and down' with respect to one another in a crown-like fashion (Fig. 72 a). This results in one Ag (I) ion connecting to a Ag (I) ion of a $[[Ag_6(\mathbf{L^7})_6]^{6+}]$ unit above its corresponding unit and the next Ag (I) ion in the circular helicate connects to a Ag (I) ion of a $[[Ag_6(\mathbf{L^7})_6]^{6+}]$ unit below it. As a result, the connectivity of each $[[Ag_6(\mathbf{L^7})_6]^{6+}]$ unit comprises of three alternating interactions with three circular helicates above and three below (Fig. 72 b).

a.

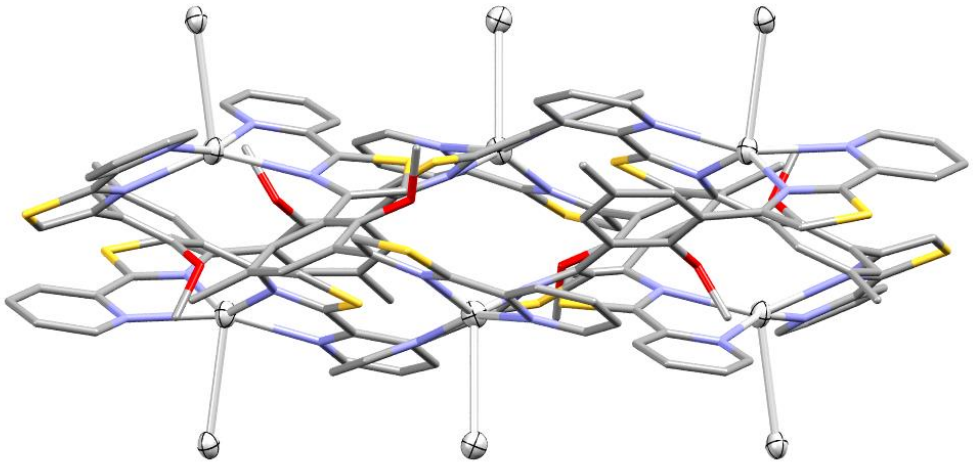

b.

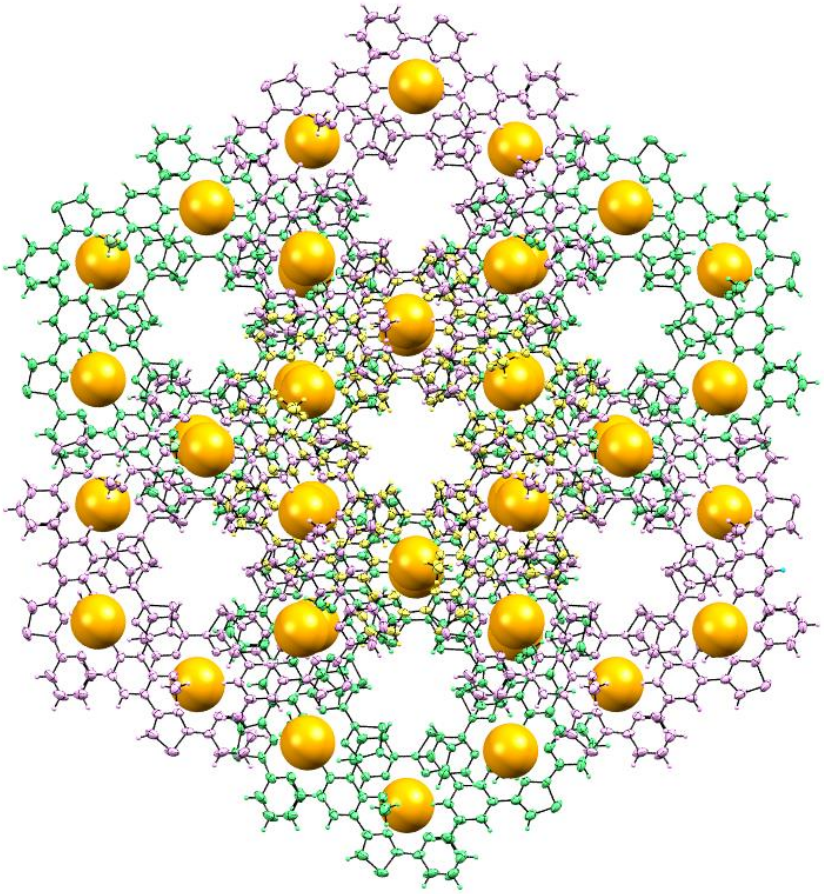

Fig. 72: a. Side view of the hexanuclear circular helicate $[Ag_6(\mathbf{L^7})_6]^{6+}$ with Ag (I) atoms shown as thermal ellipsoids to better highlight the Ag···Ag interactions. Hydrogen atoms have been removed for clarity. b. Crystal structure showing seven circular helicates of the polymeric assembly $[[Ag_6(\mathbf{L^7})_6]^{6+}]_n$ formed as a result of Ag···Ag interactions between circular helicates. Ag (I) atoms have been coloured orange and shown in spacefilling view. Units connected through argentophilic interactions 'above' the central circular helicate (yellow), are coloured pink and those 'below' are coloured green. Thermal ellipsoids in all above figures are shown at 50% probability.

a.

b.

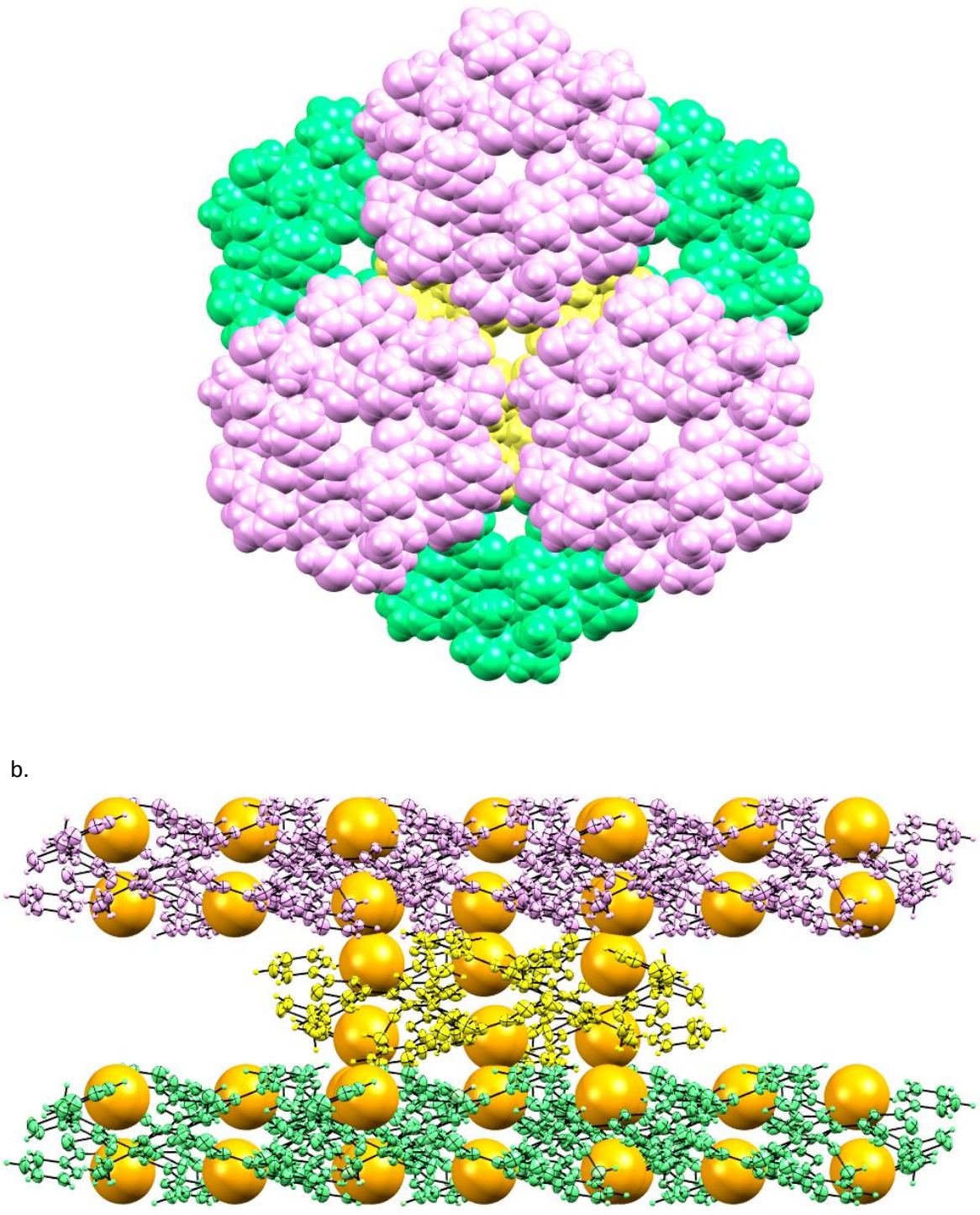

Fig. 73: Alternate views of the crystal structure of the polymeric assembly $[[Ag_6(\mathbf{L^7})_6]^{6+}]_n$ in its polymeric form showing seven circular helicates connected through Ag···Ag interactions. a. The assembly is shown entirely in spacefilling view and units connected through argentophilic interactions 'above' the central circular helicate (yellow), are coloured pink and those 'below' are coloured green. b. Side view of the polymeric assembly showing how circular helicates in the same plane as one another remain unconnected and how Ag···Ag interactions only connect circular helicate units above and below one another in different planes. Ag(I) metal ions are coloured orange and shown in spacefilling view whilst the central circular helicate is coloured yellow, circular units 'above' are coloured pink and those 'below' are coloured green. Thermal ellipsoids are shown at 50% probability.

Arguably a final interaction observed in this supramolecular structure can be found between the oxygen atom of the methyl ether branch of $\mathbf{L^7}$ and the Ag (I) metal centre. The methyl ether branches of the six $\mathbf{L}^7$ ligands in the structure appear to have direction with the oxygen atom of the methyl ether tending towards the silver metal centre from the opposite side to where the Ag···Ag interaction connects (Fig. 74). This gives a similar crown like fashion to what is observed with the alternating argentophilic interactions. Whilst the distance between these two atoms is a longer 3.138 Å compared to the ave. 2.727 Å seen in $[Ag_n(\mathbf{L^6})_n]^{n+}$ it is still within the expected range of the van der Waals radii indicating a possible sixth interaction to the Ag (I) metal centre.

However, this interaction could arise from a steric effect rather than an electronic effect. Due to the space constraints of the circular helicate the methyl ether substituent cannot lie close to the silver centre as the methyl ether branch would be unable to fit into the space near the Ag (I) atom. Hence the branch would be sterically favoured to lie away from the Ag (I) ion and give an apparent oxygen-silver interaction (Fig. 74).

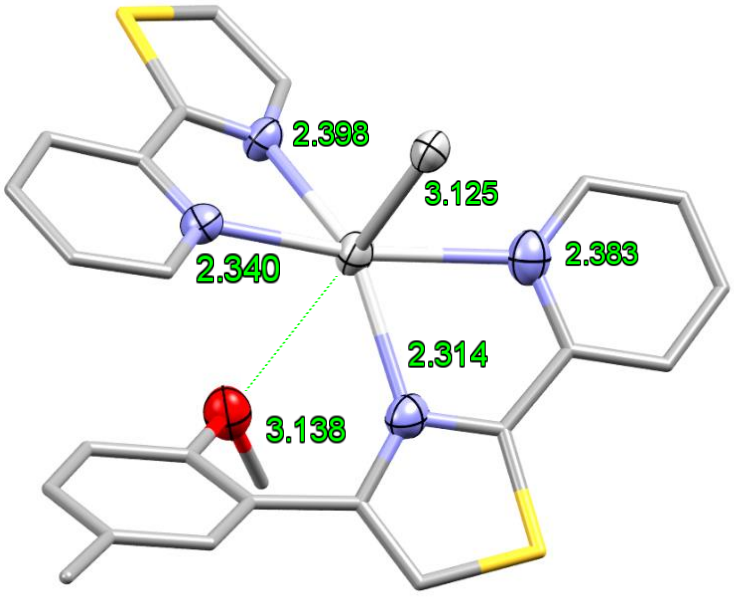

Fig. 74: Crystal structure of a partial view of the $[Ag_6(\mathbf{L^7})_6]^{6+}$ polymer showing the distances between all atoms connected to the Ag (I) metal centre in Å and the apparent interaction between the methyl ether oxygen atom and the Ag (I) centre. Thermal ellipsoids are shown at 50% probability and hydrogen atoms are omitted for clarity.

This 3-dimensional polymer could also be considered to be a metal organic framework. A dried sample (which still gave a high quality X-ray diffraction pattern) did contain voids of approximately 3500 $Å^3$ in the unit cell. However, these voids do not seem readily accessible as a BET (Brunauer-Emmett-Teller) isotherm obtained using N_2 at 77K showed no appreciable surface area. A contributing factor to the absence of an appreciable surface area can be found with the presence of the anions in the crystal structure. Whilst the reaction of $\mathbf{L^7}$ with Ag (I) (BF_4) gives rise to the honeycomb-like polymer in the solid state, it is nevertheless a charged species and so will require the presence of six tetrafluoroborate anions per circular helicate to neutralize this charge. Their location in the crystal structure (above and below the central cavity of, and in the spaces in between, each circular helicate) would heavily reduce any available surface area and prevent access for any other gases or solvents amongst the cavities (Fig. 75).

a.

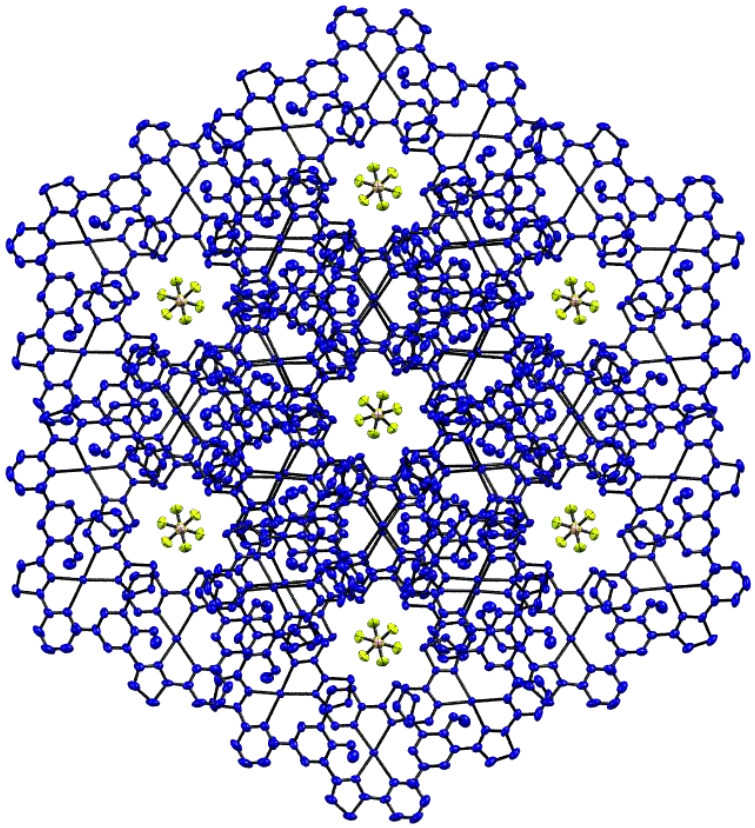

b.

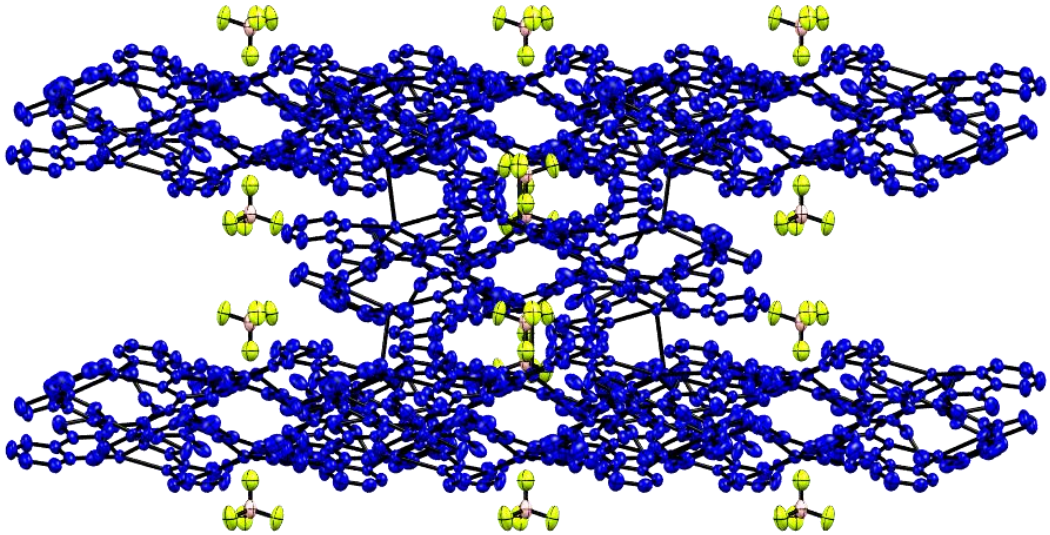

Fig. 75: Partial views of the X-ray crystal structure of the polymeric assembly $[[Ag_6(\mathbf{L^7})_6]^{6+}]_n$ showing seven circular helicates (blue). The tetrafluoroborate $(BF_4)^-$ anions can be seen occupying the cavities throughout the crystal structure potentially contributing to the low surface area. Hydrogen atoms have been omitted for clarity and thermal ellipsoids are shown at 50% probability.

Analysis of $[Ag_6(\mathbf{L^7})_6]^{6+}$ in CD_3CN by ^1H NMR showed the presence of one major product containing eight different proton environments, indicating a symmetrical ligand as would be expected by the solid-state structure. Analysis by ESI-MS gave an ion at *m/z* 3735 corresponding to $\{[Ag_6(\mathbf{L^7})_6](BF_4)_5\}^+$ along with lower molecular weight species e.g. $\{[Ag_n(\mathbf{L^7})_n](BF_4)_{n-1}\}^+$ where n = 1 to 5 (Fig. 76). This would suggest that in the solution state a reaction of Ag(I) metal ions with $\mathbf{L^7}$ forms the circular helicate species $[Ag_6(\mathbf{L^7})_6]^{6+}$ and that the polymeric effect of the Ag···Ag interactions is only observed as an artefact of the solid state. This would be expected as the Ag···Ag bonds would be easily solvated in solution.

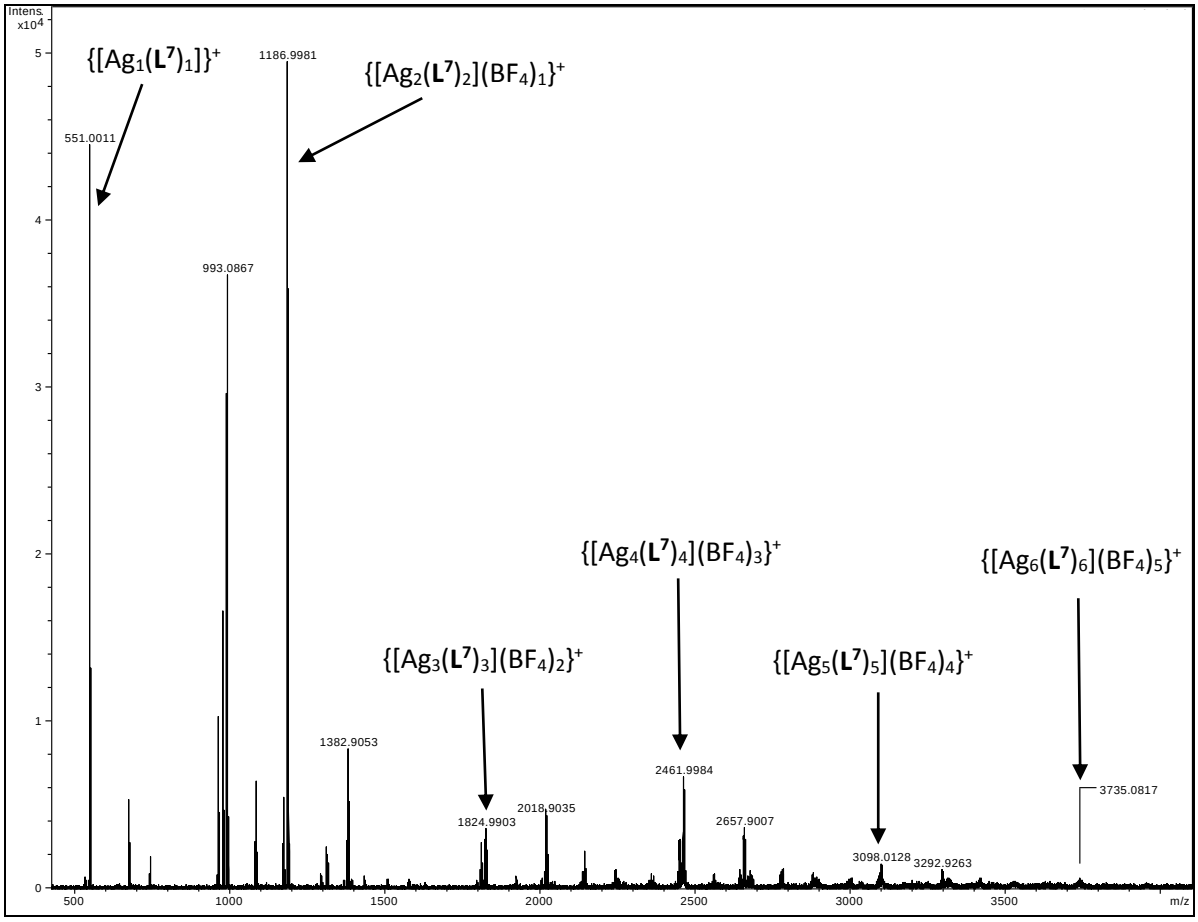

Fig. 76: ESI-MS spectrum for the complex $\{[Ag_6(\mathbf{L^7})_6](BF_4)_5\}^+$ showing an ion at m/z 3735 corresponding to $\{[Ag_6(\mathbf{L^7})_6](BF_4)_5\}^+$ along with lower molecular weight species e.g. $\{[Ag_n(\mathbf{L^7})_n](BF_4)_{n-1}\}^+$ where n = 1 to 5.

Reaction of $\mathbf{L^7}$ with copper (I) trifluromethanesulfonate (as the benzene complex) in MeCN gave a dark red solution from which X-ray quality crystals were obtained by slow diffusion of diisopropyl ether. In the solid-state a hexanuclear circular assembly has formed e.g. $[Cu_6(\mathbf{L^7})_6]^{6+}$ (Fig. 77).

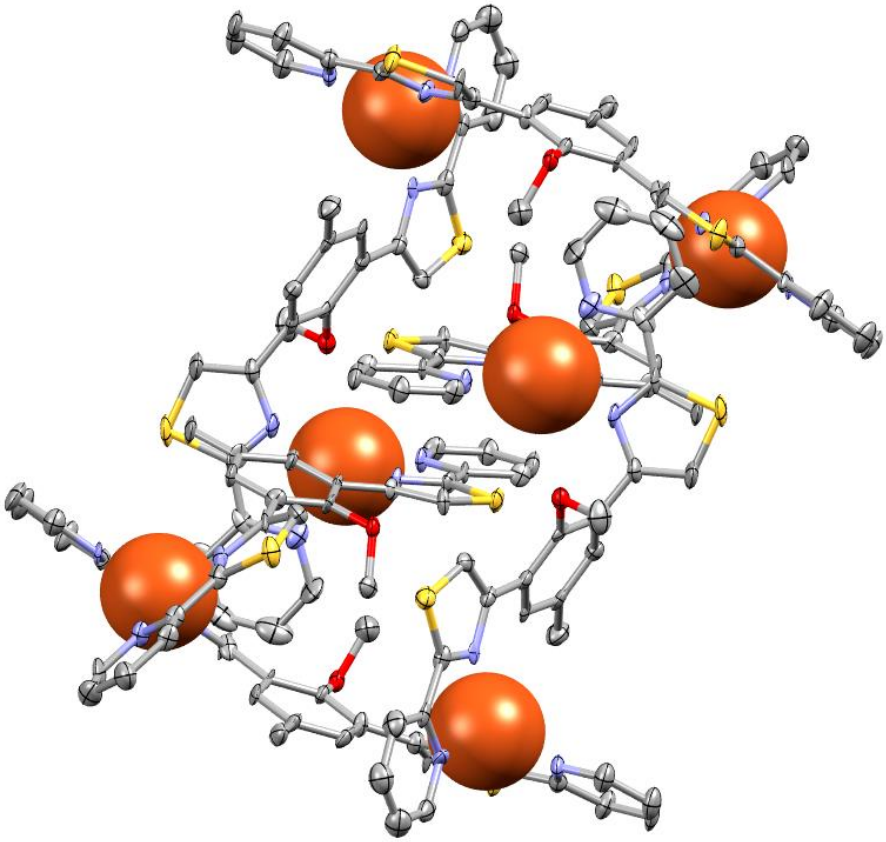

Fig. 77: The X-ray crystal structure of the hexanuclear circular species $[Cu_6(\mathbf{L^7})_6]^{6+}$. Cu(I) atoms are shown in spacefilling view and hydrogen atoms are omitted for clarity. Thermal ellipsoids are shown at 50% probability.

As would be expected the ligand partitions into two bidentate units each of which coordinates a different Cu (I) ion and the remaining two coordination sites on the metal centre are coordinated by a bidentate unit of a different ligand. This gives a circular arrangement containing six ligand strands and six metal ions. In the structure there is significant π-stacking interactions which, to some degree, contribute to the formation of this hexanuclear species (Fig. 78).

a.

b.

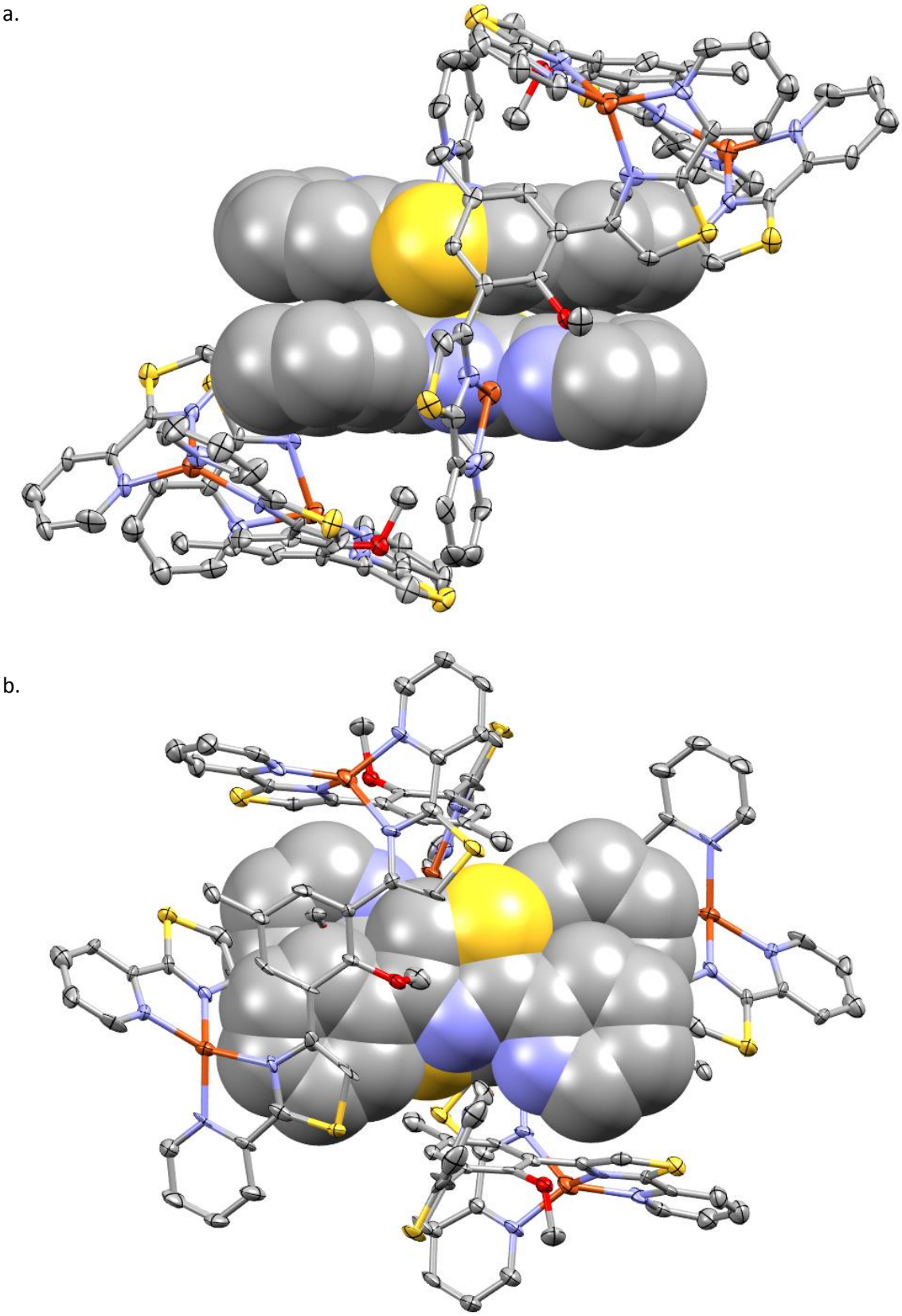

Fig. 78: X-ray crystal structure of $[Cu_6(\mathbf{L^7})_6]^{6+}$ with the π-stacking interactions between the pyridyl-thiazole-aromatic rings of the central ligands strands shown within the centre of the assembly in spacefilling view. a. Side view of the assembly and b. a birds eye view. Thermal ellipsoids are shown at 50% probability and hydrogen atoms have been omitted for clarity.

It is of no real surprise that a distinct species is formed in the solid-state as although Cu (I) ··· Cu (I) interactions are known[92] unlike argentophilic interactions they are much less common in metallosupramolecular chemistry. As a result and in contrast to the 3-dimensional infinite honeycomb-like assembly found in $[[Ag_6(\mathbf{L^7})_6]^{6+}]_n$, the $[Cu_6(\mathbf{L^7})_6]^{6+}$ assembly was an individual hexanuclear circular helicate and didn't display any polymeric characteristics to any other circular units. It should be noted that the $[Cu_6(\mathbf{L^7})_6]^{6+}$ assembly is believed to be just one product of at least two that occur upon reaction of Cu (I) trifluromethanesulfonate benzene complex with $\mathbf{L^7}$. Whilst dark red crystals of this complex were successfully grown, green crystals had also formed (however not of X-ray quality) which would indicate a change in the oxidation state of Cu (I) to Cu (II) and would point to a separate species being formed. Unfortunately, attempts to characterise the other species were unsuccessful.

4.3 Conclusions

The work reported in this chapter has demonstrated the control and selective formation of multiple silver (I) ion containing metallosupramolecular complexes based on the same ligand framework (e.g a bidentate domain consisting of a pyridyl and a thiazole unit separated by a 1,3-cresol spacer) via a combination of non-covalent interactions. The formation of the dinuclear double mesocate species $[Ag_2(\mathbf{L^5})_2]^{2+}$ was shown to be a result of the hydrogen bonding of the cresol hydroxyl unit to the uncoordinated thiazole unit of the ligand strand, preventing the bis-bidentate coordination of the donor and increasing the π-stacking effects within the structure.

The formation of the helical polymer $[Ag_n(\mathbf{L^6})_n]^{n+}$ was a direct result of replacing the phenol unit with an ethyl phenyl ether. The absence of the phenol hydrogen unit prevents the hydrogen bonding to the thiazole ring and allows for all four nitrogen donor atoms to coordinate the metal ion, whilst π-stacking interactions between the ethyl phenyl unit and the terminal pyridines of the ligands helps promote the π-stacking of the polymeric structure.

The formation of the hexanuclear circular helicate $[Ag_6(\mathbf{L^7})_6]^{6+}$ was a result of the anisole spacer not undergoing hydrogen bonding to the adjacent thiazole unit preventing formation of the mesocate and hence not contributing to π-stacking, preventing the linear helicate polymer. Finally, Ag···Ag interactions between the circular helicate units allowed for the 3-dimensional infinite honeycomb-like structure consisting of hexanuclear circular helicates species $[[Ag_6(\mathbf{L^7})_6]^{6+}]_n$ to be formed.

By replacing the silver (I) ions with copper (I) ions in the reaction with $\mathbf{L^7}$, a hexanuclear circular assembly $[Cu_6(\mathbf{L^7})_6]^{6+}$ was formed yet no polymerisation was observed in the structure. The lack of polymerisation in the assembly was a result of the removal of the silver (I) ions preventing any possibility for argentophilic interactions to take place and thus stopping any way for the individual circular units to connect to one another. It is remarkable that such subtle changes in the ligand framework can give rise to substantially different self-assembled species.

References

1 S. J. Bullock, PhD Thesis, University of Huddersfield, 2014.

2 M. McCarty, *J. Exp. Med.*, 1946, **83**, 89–96.

3 J. D. Watson and F. H. C. Crick, *Nature*, 1953, **171**, 737–738.

4 R. E. Franklin and R. G. Gosling, *Nature*, 1953, **172**, 156–157.

5 R. E. Franklin and R. G. Gosling, *Nature*, 1953, **171**, 740–741.

6 J. D. Watson and F. H. C. Crick, *Nature*, 1953, **171**, 964–967.

7 M. H. F. Wilkins, A. R. Stokes and H. R. Wilson, *Nature*, 1953, **171**, 738–740.

8 D. J. Cram, *J. Incl. Phenom.*, 1988, **6**, 397–413.

9 P. J. Cragg, *Supramolecular Chemistry*, VCH, 2006.

10 D. J. Cram and J. M. Cram, *Science*, 1974, **183**, 803–809.

11 E. P. Kyba, R. C. Helgeson, K. Madan, G. W. Gokel, T. L. Tarnowski, S. S. Moore and D. J. Cram, *J. Am. Chem. Soc.*, 1977, **99**, 2564–2571.

12 C. J. Pedersen, *J. Am. Chem. Soc.*, 1967, **89**, 7017–7036.

13 E. B. Kyba, K. Koga, L. R. Sousa, M. G. Sigel and D. J. Cram, *J. Am. Chem. Soc.*, 1973, **97**, 2692–2693.

14 E. P. Kyba, M. G. Siegel, L. R. Sousa, G. D. Y. Sogah and D. J. Cram, *J. Am. Chem. Soc.*, 1972, **95**, 2691–2692.

15 R. C. Helgeson, K. Koga, J. M. Timko and D. J. Cram, *J. Am. Chem. Soc.*, 1973, **95**, 3021–3023.

16 R. Helgeson, J. Timko and D. Cram, *J. Am. Chem. Soc.*, 1973, **95**, 3023–3025.

17 G. W. Gokel and D. J. Cram, *J. Chem. Soc. Chem. Commun.*, 1973, 481–482.

18 T. Kaneda, S. Umeda, H. Tanigawa, S. Misumi, Y. Kai, H. Morii, K. Miki and N. Kasai, *J. Am. Chem. Soc.*, 1985, **107**, 4802–4803.

19 B. Dietrich, J. M. Lehn and J. P. Sauvage, *Tetrahedron Lett.*, 1969, **10**, 2889–2892.

20 J.-M. Lehn, *Pure Appl. Chem*, 1980, **52**, 2441–2459.

21 C. A. Hunter and J. K. M. Sanders, *J. Am. Chem. Soc.*, 1990, **112**, 5525–5534.

22 C. Janiak, *Dalton Trans.*, 2000, 3885–3896.

23 E. T. Kool, *Annu. Rev. Biophys. Biomol. Struct.*, 2001, **30**, 1–22.

24 A. Sygula, F. R. Fronczek, R. Sygula, P. W. Rabideau and M. M. Olmstead, *J. Am. Chem. Soc.*, 2007, **129**, 3842–3843.

25 M. Albrecht, *J. Incl. Phenom.*, 2000, **36**, 127–151.

26 J. Steed, D. Turner and K. Wallace, *Core Concepts in Supramolecular Chemistry and Nanochemistry*, John Wiley, 2008.

27 J. W. Steed and J. L. Atwood, *Supramolecular Chemistry*, Oxford University Press, 2009.

28 S. Zhang, D. M. Marini, W. Hwang and S. Santoso, *Curr. Opin. Chem. Biol.*, 2002, **6**, 865–871.

29 K. Rajagopal and J. P. Schneider, *Curr. Opin. Struct. Biol.*, 2004, **14**, 480–486.

30 S. I. Stupp and L. C. Palmer, *Chem. Mater.*, 2014, **26**, 507–518.

31 V. Georgakilas, *Functionalization of Graphene*, Wiley-VCH Verlag GmbH & Co. KGaA, Weinheim, Germany, 2014.

32 N. Patra, Y. Song and P. Král, *ACS Nano*, 2011, **5**, 1798–1804.

33 W. Jin, T. Fukushima, M. Niki, A. Kosaka, N. Ishii and T. Aida, *Proc. Natl. Acad. Sci. U. S. A.*, 2005, **102**, 10801–10806.

34 M. J. Winter, *d-Block Chemistry*, Oxford University Press, 1994.

35 C.-H. Zhang, Y.-G. Chen, Q. Tang and S.-X. Liu, *Dalt. Trans.*, 2012, **41**, 9971–9978.

36 M. Dudev, J. Wang, T. Dudev and C. Lim, *J. Phys. Chem. B*, 2006, **110**, 1889–1895.

37 Daniela Belli Dell' Amico, F. Calderazzo, Matteo Curiardi, A. Luca Labella and F. Marchetti, *Inorg. Chem.*, 2004, **43**, 5459–5465.

38 C. R. Rice, S. Wörl, J. C. Jeffery, R. L. Paul and M. D. Ward, *Chem. Commun.*, 2000, **97**, 1529–1530.

39 H. Wu, Y. Zhang, C. Chen, J. Zhang, Y. Bai, F. Shi and X. Wang, *New J. Chem*, 2014, 3688–3698.

40 I. A. Popov, T. Jian, G. V Lopez, A. I. Boldyrev and L.-S. Wang, *Nat. Commun.*, 2015, **6**, 8654.

41 Moeller T, in *Advances in Chemistry*, 1967, **62**, 306–317.

42 S. Cotton, *Lanthanide and Actinide Chemistry*, Wiley, 2006.

43 C. Boucher, M. G. . Drew, P. Giddings, L. M. Harwood, M. J. Hudson, P. B. Iveson and C. Madic, *Inorg. Chem. Commun.*, 2002, **5**, 596–599.

44 S. Z. Vatsadze, I. A. Vatsadze, M. A. Manaenkova, N. V. Zyk, A. V. Churakov, M. Y. Antipin, J. A. K. Howard and H. Lang, *Russ. Chem. Bull.*, 2007, **56**, 1775–1781.

45 W. Wong, L. Zhang and T. C. W. Mak, *Chem. Commun.*, 1997, **429**, 1525–1526.

46 R. W. Turner and E. L. Amma, *J. Am. Chem. Soc.*, 1966, **88**, 3243–3247.

47 V. Chaurin, E. C. Constable and C. E. Housecroft, *New J. Chem.*, 2006, **30**, 1740–1744.

48 J. M. Lehn, A. Rigault, J. Siegel, J. Harrowfield, B. Chevrier and D. Moras, *Proc. Natl. Acad. Sci. USA*, 1987, **84**, 2565–2569.

49 C. J. Baylies, L. P. Harding, J. C. Jeffery, T. Riis-Johannessen and C. R. Rice, *Angew. Chemie - Int. Ed.*, 2004, **43**, 4515–4518.

50 T. Riis-Johannessen, L. P. Harding, J. C. Jeffery, R. Moon and C. R. Rice, *Dalton Trans.*, 2007, **3**, 1577–1587.

51 J. C. Jeffery, C. R. Rice, L. P. Harding, C. J. Baylies and T. Riis-Johannessen, *Chem. - A Eur. J.*, 2007, **13**, 5256–5271.

52 C.-S. Tsang, H.-L. Yeung, W.-T. Wong and H.-L. Kwong, *Chem. Commun.*, 2009, **27**, 1999–2001.

53 D. J. Cooke, J. M. Cross, R. V Fennessy, L. P. Harding, C. R. Rice and C. Slater, *Chem. Commun.*, 2013, **49**, 7785–7787.

54 M. Albrecht, *Chem. Rev.*, 2001, **101**, 3457–3497.

55 M. Albrecht and S. Kotila, *Angew. Chemie Int. Ed.*, 1995, **34**, 2134–2137.

56 J. Xu, T. N. Parac and K. N. Raymond, *Angew. Chemie Int. Ed.*, 1999, **38**, 2878–2882.

57 Z. Zhang and D. Dolphin, *Chem. Commun.*, 2009, 6931–6933.

58 M. Meyer, B. Kersting, R. E. Powers and K. N. Raymond, *Inorg. Chem.*, 1997, **36**, 5179–5191.

59 M. Albrecht, *Chem. - A Eur. J.*, 2000, **6**, 3485–3489.

60 F. Cui, S. Li, C. Jia, J. S. Mathieson, L. Cronin, X. J. Yang and B. Wu, *Inorg. Chem.*, 2012, **51**, 179–187.

61 P. A. Gale and T. Gunnlaugsson, *Chem. Soc. Rev.*, 2010, **39**, 3595–3596.

62 S. Li, C. Jia, B. Wu, Q. Luo, X. Huang, Z. Yang, Q. S. Li and X. J. Yang, *Angew. Chemie - Int. Ed.*, 2011, **50**, 5721–5724.

63 R. L. Paul, Z. R. Bell, J. C. Jeffery, J. A. McCleverty and M. D. Ward, *Proc. Natl. Acad. Sci. USA*, 2002, **99**, 4883–4888.

64 R. A. Faulkner, L. P. Harding, J. Higginson, C. R. Rice and C. Slater, *Angew. Chemie Int. Ed.*, 2014, **53**, 13540–13543.

65 B. Hasenknopf, J. M. Lehn, N. Boumediene, A. Dupont-Gervais, A. Van Dorsselaer, B. Kneisel and D. Fenske, *J. Am. Chem. Soc.*, 1997, **119**, 10956–10962.

66 L. Bain, S. Bullock, L. Harding, T. Riis-Johannessen, G. Midgley, C. R. Rice and M. Whitehead, *Chem. Commun. (Camb).*, 2010, **46**, 3496–3498.

67 K. E. Allen, R. A. Faulkner, L. P. Harding, C. R. Rice, T. Riis-Johannessen, M. L. Voss and M. Whitehead, *Angew. Chemie - Int. Ed.*, 2010, **49**, 6655–6658.

68 H. B. Tanh Jeazet, K. Gloe, T. Doert, O. N. Kataeva, A. Jäger, G. Geipel, G. Bernhard, B. Büchner and K. Gloe, *Chem. Commun.*, 2010, **46**, 2373.

69 O. Mamula, A. von Zelewsky and G. Bernardinelli, *Angew. Chemie Int. Ed.*, 1998, **37**, 289–293.

70 Z.-S. Wu, J.-T. Hsu, C.-C. Hsieh and Y.-C. Horng, *Chem. Commun. (Camb).*, 2012, **48**, 3436–8.

71 A. Winter and U. S. Schubert, *Chem. Soc. Rev.*, 2016, **45**, 5311–5357.

72 R. W. Seidel, R. Goddard, B. Zibrowius and I. M. Oppel, *Polymers (Basel).*, 2011, **3**, 1458–1474.

73 R. W. Seidel, R. Goddard and I. M. Oppel, *Polymers (Basel).*, 2013, **5**, 527–575.

74 M. Vázquez, A. Taglietti, D. Gatteschi, L. Sorace, C. Sangregorio, A. M. González, M. Maneiro, R. M. Pedrido and M. R. Bermejo, *Chem. Commun. (Camb).*, 2003, **2**, 1840–1841.

75 M. Vázquez, M. R. Bermejo, M. Fondo, A. M. Gonzalez, J. Mahia, L. Sorace and D. Gatteschi, *Eur. J. Inorg. Chem.*, 2001, **2001**, 1863–1868.

76 M. Vázquez, M. R. Bermejo, J. Sanmartín, A. M. García-Deibe, C. Lodeiro and J. Mahía, *J. Chem. Soc. Dalt. Trans.*, 2002, **38**, 870–877.

77 M. R. Bermejo, M. Vázquez, J. Sanmartín, A. M. García-Deibe, M. Fondo and C. Lodeiro, *New J. Chem.*, 2002, **26**, 1365–1370.

78 A. Stephenson and M. D. Ward, *Chem. Commun.*, 2012, **48**, 3605–3607.

79 W. L. Leong and J. J. Vittal, *Chem. Rev.*, 2011, **111**, 688–764.

80 A. M. Stadler, N. Kyritsakas, G. Vaughan and J. M. Lehn, *Chem. - A Eur. J.*, 2007, **13**, 59–68.

81 G. Baum, E. C. Constable, D. Fenske, C. E. Housecroft and T. Kulke, *Chem. Commun.*, 1998, 2659–2660.

82 L. Valencia, R. Bastida, A. Macias, M. Vicente and P. Perez-Lourido, *New J. Chem.*, 2005, **29**, 424–426.

83 A. Galet, M. C. Muñoz, A. B. Gaspar and J. A. Real, *Inorg. Chem.*, 2005, **44**, 8749–8755.

84 H. Schmidbaur and A. Schier, *Angew. Chemie Int. Ed.*, 2015, **54**, 746–784.

85 D. A. Leigh, R. G. Pritchard and A. J. Stephens, *Nat. Chem.*, 2014, **6**, 978–982.

86 S. Xu, S. L. Li and Q. Xu, *Energy Environ. Sci.*, 2013, **66**, 1754–5692.

87 M. D. Ward, C. G. P. Taylor and J. R. Piper, *Chem. Commun.*, 2016, **52**, 6199–6338.

88 E. R. Kay and D. A. Leigh, *Angew. Chemie - Int. Ed.*, 2015, **54**, 10080–10088.

89 G. Vlád and I. T. Horváth, *J. Org. Chem.*, 2002, **67**, 6550–6552.

90 A. J. Amoroso, A. Banu, M. P. Coogan, P. G. Edwards, G. Hossain and K. M. A. Malik, *Dalton Trans.*, 2010, **39**, 6993–7003.

91 S. J. Bullock, L. P. Harding, M. P. Moore, A. Mills, S. A. F. Piela, C. R. Rice, L. Towns-Andrews and M. Whitehead, *Dalton Trans.*, 2013, **42**, 5805–5811.

92 W. F. Fu, X. Gan, C. M. Che, Q. Y. Cao, Z. Y. Zhou and N. Nian-Yong Zhu, *Chem. - A Eur. J.*, 2004, **10**, 2228–2236.

93 O. V. Dolomanov, L. J. Bourhis, R. J. Gildea, J. A. K. Howard and H. Puschmann, *J. Appl. Crystallogr.*, 2009, **42**, 339–341.

Appendices: Crystal Data Tables

Crystal Structure Information for $[Cu_2(\mathbf{L^1})_1]^{2+}$:

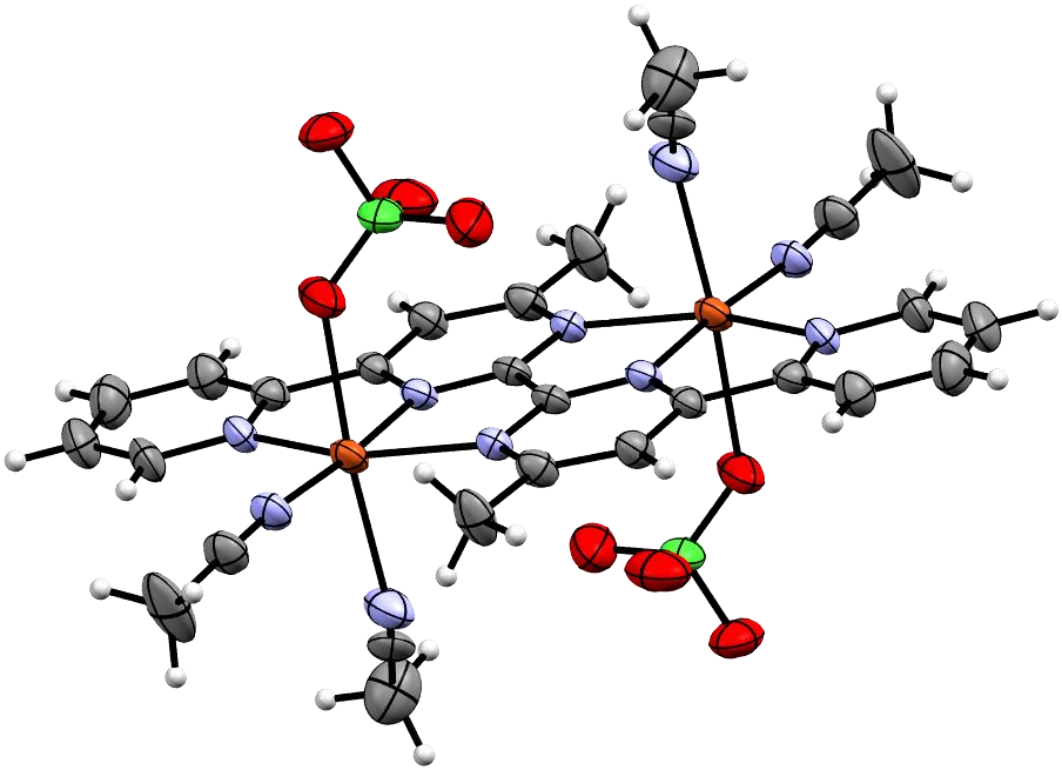

Compound Reference	$[Cu_2(\mathbf{L^1})_1]^{2+}$
Chemical Formula	$C_{28}H_{28}Cl_4Cu_2N_{10}O_{16}$
Formula Mass	1029.48
Crystal System	monoclinic
a/Å	10.1974(3)
b/Å	11.8760(4)
c/Å	16.7845(5)
α/°	90
β/°	96.0357(18)
γ/°	90
Unit cell volume/Å^3	2021.41(11)
Temperature/K	150(2)
Space group	P 21/c
No. of formula units per unit cell, *Z*	2
Radiation type	Cu K\α
Absorption coefficient, μ/mm^{-1}	4.455
No. of reflections measured	16007

No. of independent reflections	3693
R_{int}	0.1056
Final R_1 values ($I>2\sigma(I)$)	0.0819
Final $wR(F^2)$ values ($I>2\sigma(I)$)	0.2182
Final R_1 values (all data)	0.1123
Final $wR(F^2)$ values (all data)	0.2444
Goodness of fit on F^2	1.050

In $[Cu_2(\mathbf{L^1})_1]^{2+}$, the coordinated perchlorate counter anions and acetonitrile molecules were disordered and as a consequence refined poorly. The disordered atoms were all constrained using *DELU* and *SIMU* and the disordered perchlorate anions, were modelled in two positions using the *PART* instruction. Afterwards the molecule refined to an acceptable level.

Crystal Structure Information for $[Cu_2(\mathbf{L^1})_3]^{4+}$:

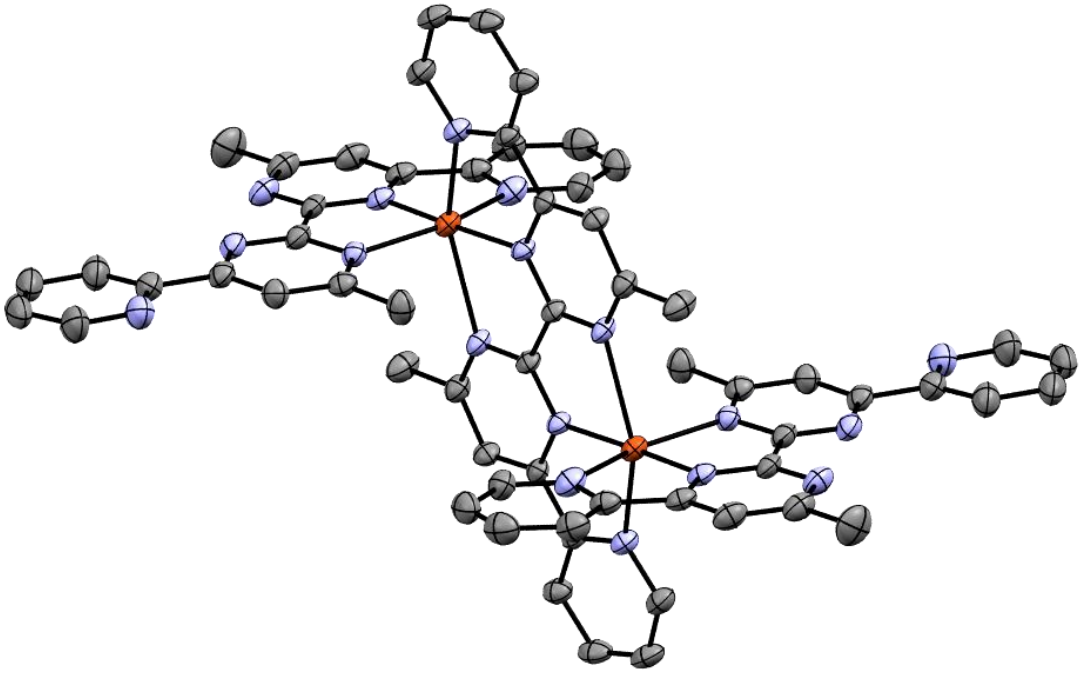

Compound Reference	$[Cu_2(\mathbf{L^1})_3]^{4+}$
Chemical Formula	$C_{68}H_{60}Cu_2F_{12}N_{22}O_{20}S_4$
Formula Mass	1988.70
Crystal System	monoclinic
a/Å	12.9783(9)
b/Å	20.1247(13)
c/Å	15.7915(9)
α/°	90
β/°	103.3377(17)
γ/°	90
Unit cell volume/Å^3	4013.2(4)
Temperature/K	150(2)
Space group	P 21/n
No. of formula units per unit cell, *Z*	2
Radiation type	Mo K\α
Absorption coefficient, μ/mm^{-1}	0.748
No. of reflections measured	64338
No. of independent reflections	9999

R_{int}	0.0695
Final R_1 values ($I>2\sigma(I)$)	0.0733
Final $wR(F^2)$ values ($I>2\sigma(I)$)	0.1418
Final R_1 values (all data)	0.1392
Final $wR(F^2)$ values (all data)	0.1793
Goodness of fit on F^2	1.051

For $[Cu_2(\mathbf{L}^1)_3]^{4+}$, the trifluoromethansulfonate counter anions and a molecule of nitromethane were disordered. As a result of this, the disordered atoms and molecules were constrained using *DELU*, *SIMU*, *SADI* and *ISOR* and the constraints were used in the least-squares refinement. In the case of the disordered nitromethane molecule, one nitrogen atom was particularly disordered and so was constrained using *EADP* in the least-squares refinement. Furthermore, the disordered counter anions and nitromethane molecule were modelled in two positions using the *PART* instruction. Afterwards, the crystal structure refined to an acceptable level.

Crystal Structure Information for $[Cd(\mathbf{L^1})_2]^{2+}$:

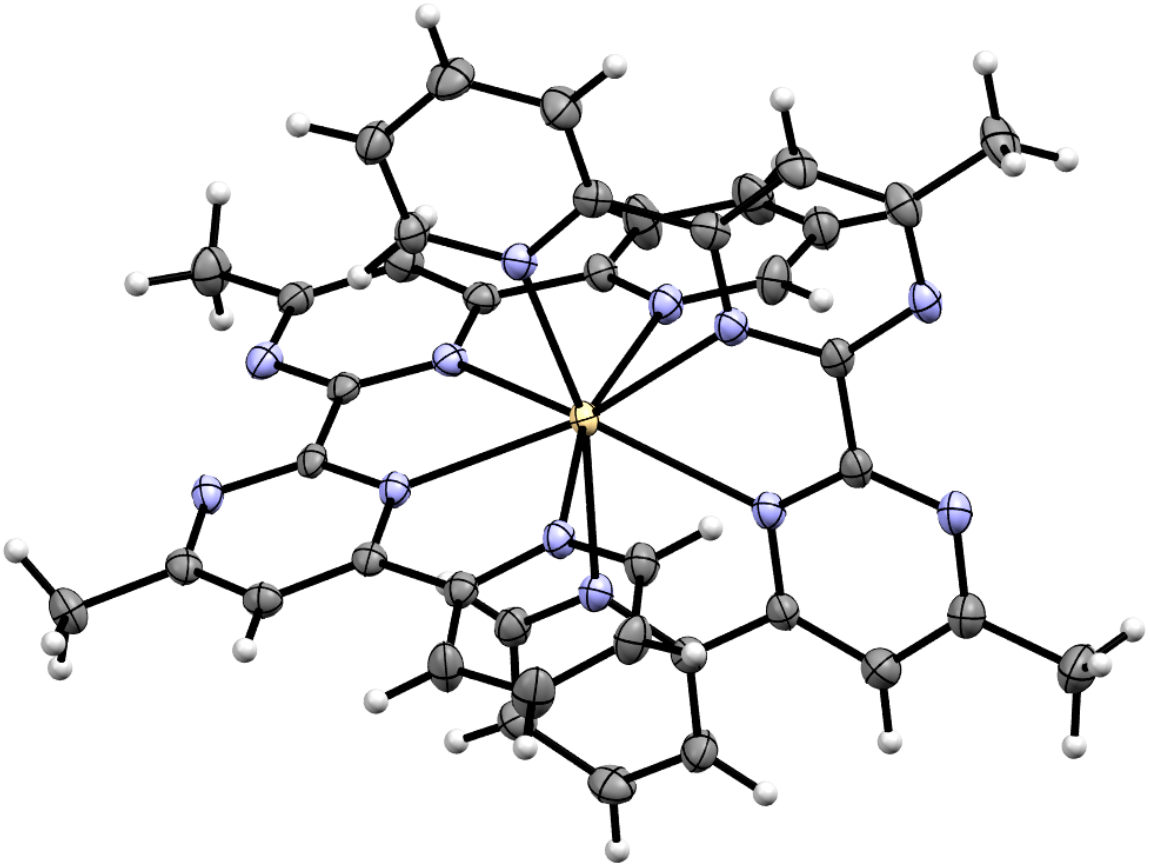

Compound Reference	$[Cd(\mathbf{L^1})_2]^{2+}$
Chemical Formula	$C_{42}H_{35}CdCl_2N_{13}O_8$
Formula Mass	1033.13
Crystal System	Triclinic
a/Å	11.1843(6)
b/Å	11.6083(6)
c/Å	17.3177(9)
α/°	79.7070(10)
β/°	72.2700(10)
γ/°	79.1440(10)
Unit cell volume/Å^3	2085.49(19)
Temperature/K	150(2)
Space group	P-1
No. of formula units per unit cell, *Z*	2
Radiation type	Mo K\α
Absorption coefficient, μ/mm^{-1}	0.725

No. of reflections measured	25444
No. of independent reflections	6612
R_{int}	0.0458
Final R_1 values ($I>2\sigma(I)$)	0.0303
Final $wR(F^2)$ values ($I>2\sigma(I)$)	0.0649
Final R_1 values (all data)	0.0440
Final $wR(F^2)$ values (all data)	0.0704
Goodness of fit on F^2	1.052

No additional restraints, constraints or additional solvent masking was required for the $[Cd(\mathbf{L^1})_2]^{2+}$ crystal structure.

Crystal Structure Information for $[Eu(\mathbf{L^1})_2]^{2+}$:

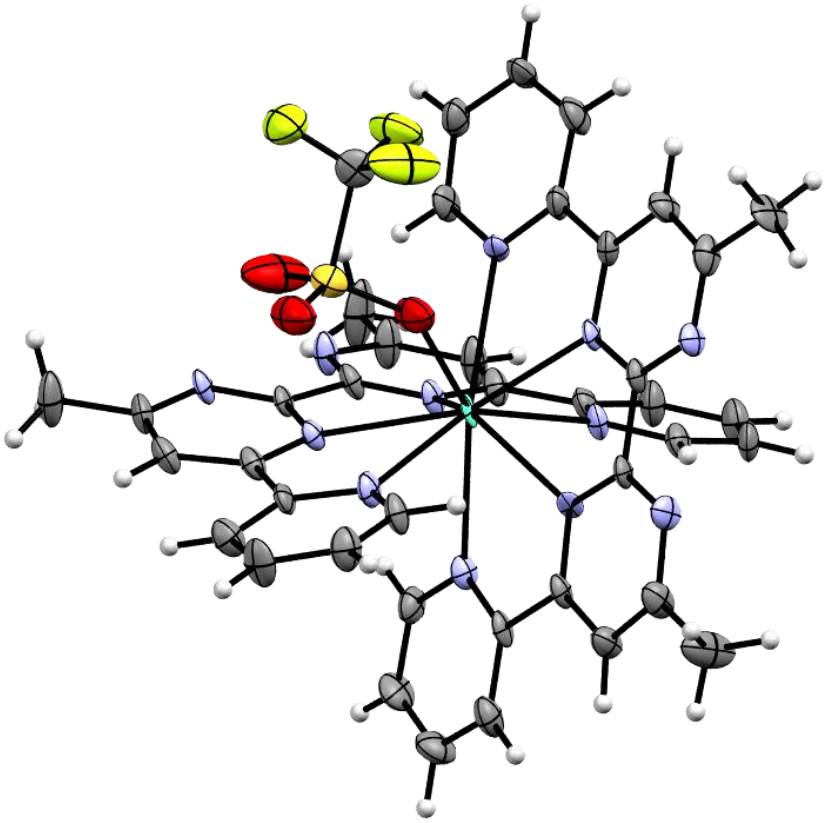

Compound Reference	$[Eu(\mathbf{L^1})_2]^{2+}$
Chemical Formula	$C_{43}H_{32}EuF_9N_{12}O_9S_3$
Formula Mass	1279.94
Crystal System	Triclinic
a/Å	10.3993(3)
b/Å	12.6702(3)
c/Å	20.4630(5)
α/°	101.2282(12)
β/°	104.2036(13)
γ/°	103.0068(12)
Unit cell volume/Å^3	2455.96(11)
Temperature/K	150(2)
Space group	P-1
No. of formula units per unit cell, *Z*	2
Radiation type	Cu K\α

Absorption coefficient, μ/mm^{-1}	11.245
No. of reflections measured	27722
No. of independent reflections	8748
R_{int}	0.0793
Final R_1 values ($I>2\sigma(I)$)	0.0772
Final $wR(F^2)$ values ($I>2\sigma(I)$)	0.2019
Final R_1 values (all data)	0.0926
Final $wR(F^2)$ values (all data)	0.2207
Goodness of fit on F^2	1.047

In $[Eu(\mathbf{L^1})_2(CF_3SO_3)]^{2+}$, a carbon atom from the pyridyl ring was disordered. The disordered atom was constrained using *DELU* and *SIMU* using the least-squares refinement and afterwards the structure refined to an acceptable level.

Crystal Structure Information for $[Eu_2Ag_2(\mathbf{L^1})_2(CF_3SO_3)_8]$:

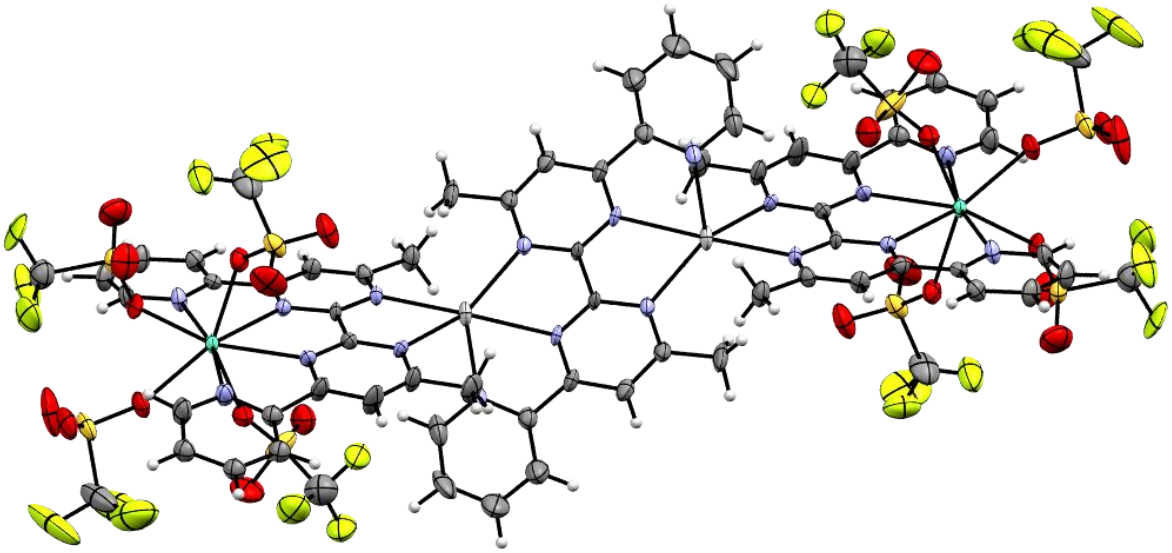

Compound Reference	$[Eu_2Ag_2(\mathbf{L^1})_2(CF_3SO_3)_8]$
Chemical Formula	$C_{72}H_{54}Ag_2Eu_2F_{24}N_{20}O_{24}S_8$
Formula Mass	2815.49
Crystal System	Orthorhombic
a/Å	30.7962(7)
b/Å	16.8129(4)
c/Å	18.6268(5)
α/°	90
β/°	90
γ/°	90
Unit cell volume/Å^3	9644.5(4)
Temperature/K	150(2)
Space group	P c c n
No. of formula units per unit cell, *Z*	4
Radiation type	Cu K\α
Absorption coefficient, μ/mm^{-1}	15.154
No. of reflections measured	55354
No. of independent reflections	8769
R_{int}	0.1047

Final R_1 values ($I>2\sigma(I)$)	0.0544
Final $wR(F^2)$ values ($I>2\sigma(I)$)	0.1352
Final R_1 values (all data)	0.0811
Final $wR(F^2)$ values (all data)	0.1517
Goodness of fit on F^2	1.060

In $[Eu_2Ag_2(\mathbf{L^1})_2(CF_3SO_3)_8]$, the trifluoromethanesulfonate anions, one of the pyridyl rings and an acetonitrile molecule were all considerably disordered and consequently refined poorly. All disordered atoms and molecules were constrained using *DELU*, *SIMU*, *SADI* and *ISOR* using the least-squares refinement. One disordered carbon atom in a trifluoromethanesulfonate counter ion was constrained using *EADP*. In some cases, disordered atoms and molecules were modelled over two positions using the *PART* instruction. After these constraints had been applied, the crystal data refined to an acceptable level.

Crystal Structure Information for *ter*-**L**^{1}ReCl(CO)$_3$:

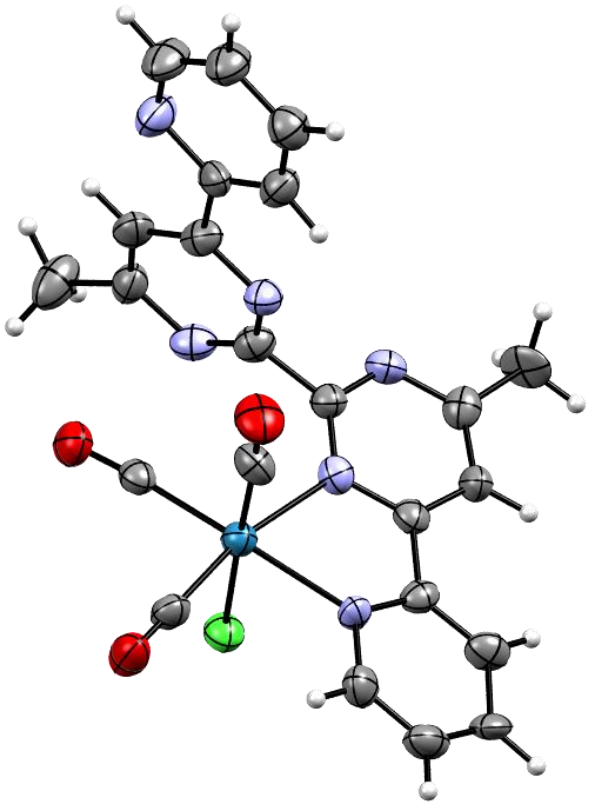

Compound Reference	*ter*-**L**^{1}ReCl(CO)$_3$
Chemical Formula	$C_{23}H_{16}ClN_6O_3Re$
Formula Mass	646.07
Crystal System	Monoclinic
a/Å	10.3654(7)
b/Å	12.3394(9)
c/Å	17.8326(12)
α/°	90
β/°	101.273(2)
γ/°	90
Unit cell volume/Å^3	2236.8(3)
Temperature/K	150(2)
Space group	P 21/n
No. of formula units per unit cell, *Z*	4
Radiation type	Mo K\α

Absorption coefficient, μ/mm^{-1}	5.591
No. of reflections measured	20856
No. of independent reflections	6515
R_{int}	0.0688
Final R_1 values (I>2σ(I))	0.0771
Final $wR(F^2)$ values (I>2σ(I))	0.1939
Final R_1 values (all data)	0.1365
Final $wR(F^2)$ values (all data)	0.2338
Goodness of fit on F^2	0.970

No additional restraints, constraints or additional solvent masking was required for the *ter*-**L**^{1}ReCl(CO)$_3$ crystal structure.

Crystal Structure Information for *cent*-**L**^{1}ReCl(CO)$_3$:

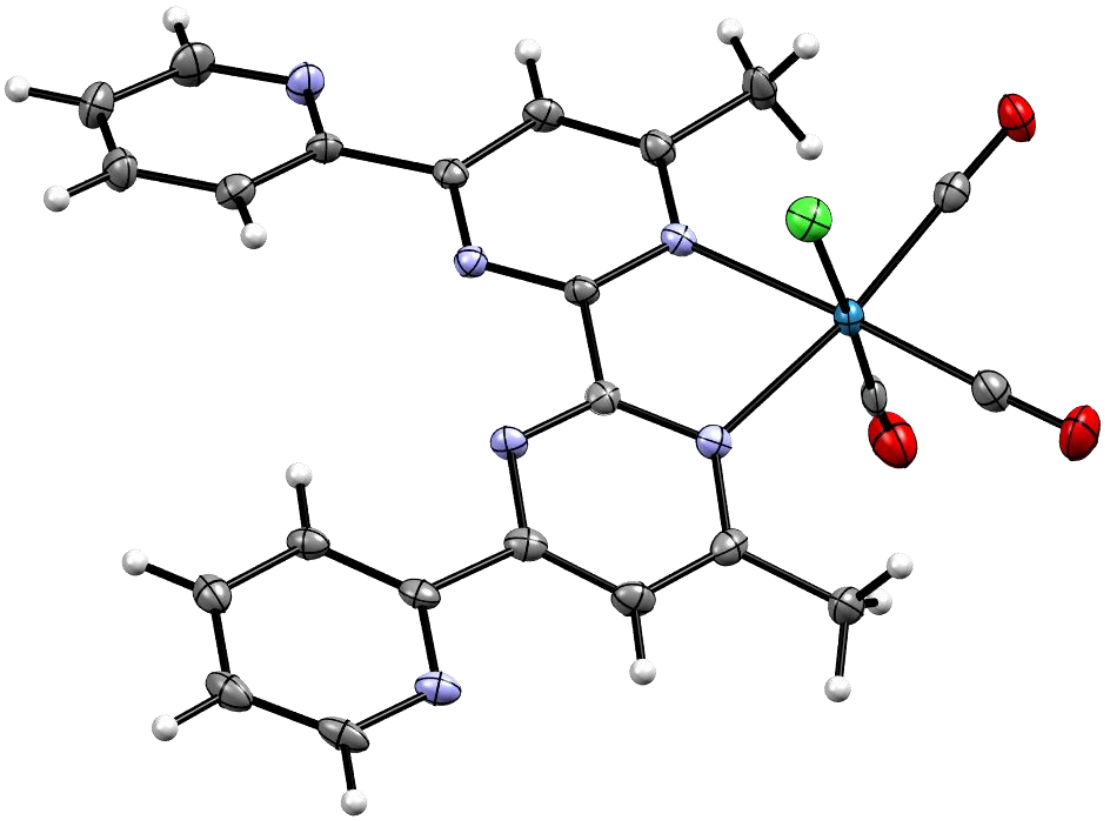

Compound Reference	*cent*-**L**^{1}ReCl(CO)$_3$
Chemical Formula	$C_{23}H_{16}ClN_6O_3Re$
Formula Mass	646.07
Crystal System	Monoclinic
a/Å	7.1109(3)
b/Å	24.9643(10)
c/Å	12.4718(5)
α/°	90
β/°	99.1873(12)
γ/°	90
Unit cell volume/Å^3	2185.57(15)
Temperature/K	150(2)
Space group	P 21/c
No. of formula units per unit cell, *Z*	4
Radiation type	Mo K\α

Absorption coefficient, μ/mm^{-1}	5.723
No. of reflections measured	27292
No. of independent reflections	6694
R_{int}	0.0589
Final R_1 values ($I>2\sigma(I)$)	0.0413
Final $wR(F^2)$ values ($I>2\sigma(I)$)	0.0640
Final R_1 values (all data)	0.0712
Final $wR(F^2)$ values (all data)	0.0699
Goodness of fit on F^2	1.055

No additional restraints, constraints or additional solvent masking was required for the *cent*-**L**^{1}ReCl(CO)$_3$ crystal structure.

Crystal Structure Information for *ter*-**L**^{1}Re(CO)$_3$(H$_2$O).(CF$_3$SO$_3$):

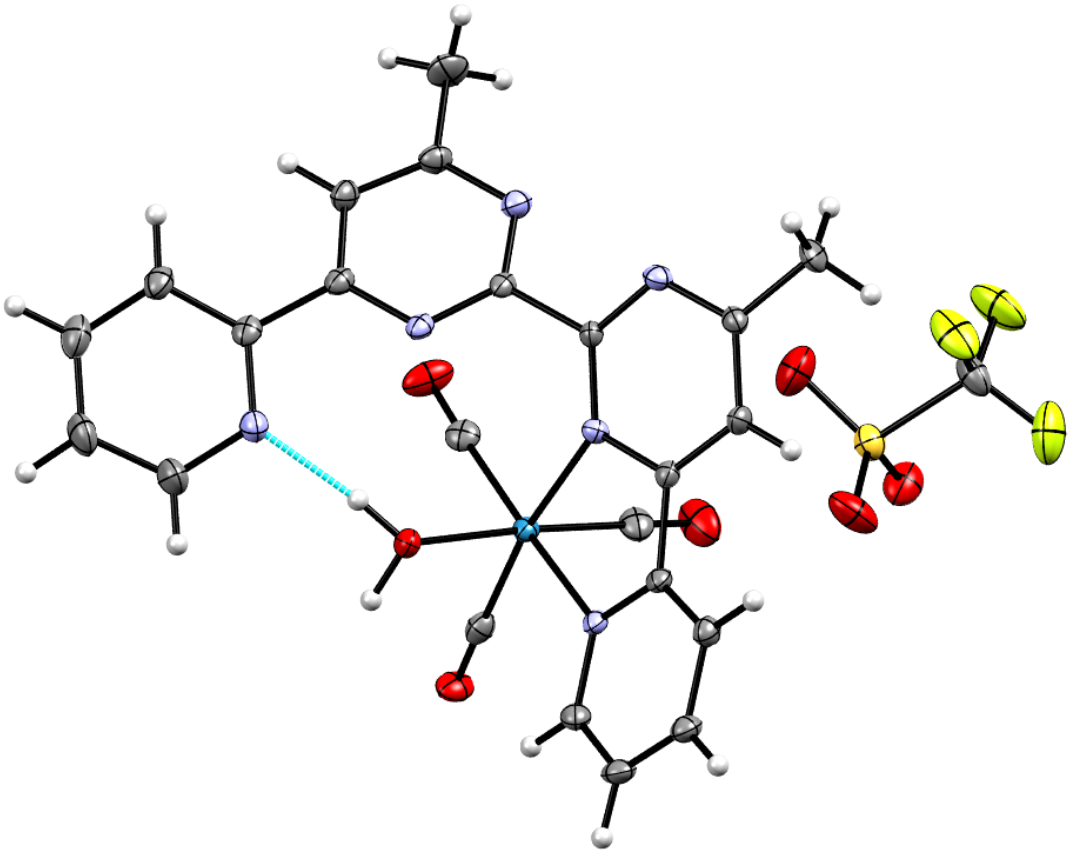

Compound Reference	*ter*-**L**^{1}Re(CO)$_3$(H$_2$O).(CF$_3$SO$_3$)
Chemical Formula	$C_{25}H_{20}Cl_2F_3N_6O_7ReS$
Formula Mass	862.65
Crystal System	Triclinic
a/Å	9.9806(6)
b/Å	12.1603(8)
c/Å	14.2155(9)
α/°	109.3121(18)
β/°	106.6643(15)
γ/°	96.8151(17)
Unit cell volume/Å^3	1515.71(17)
Temperature/K	150(2)
Space group	P-1
No. of formula units per unit cell, *Z*	2
Radiation type	Mo K\α

Absorption coefficient, μ/mm^{-1}	4.327
No. of reflections measured	44815
No. of independent reflections	11017
R_{int}	0.0833
Final R_1 values ($I>2\sigma(I)$)	0.0492
Final $wR(F^2)$ values ($I>2\sigma(I)$)	0.1002
Final R_1 values (all data)	0.0694
Final $wR(F^2)$ values (all data)	0.1121
Goodness of fit on F^2	1.0135

No additional restraints, constraints or additional solvent masking was required for the *ter*-**L**^{1}Re(CO)$_3$(H$_2$O).(CF$_3$SO$_3$) crystal structure.

Crystal Structure Information for *cent*-**L**^{1}ReCl(CO)$_3$.[CuCl$_4$]$^-$:

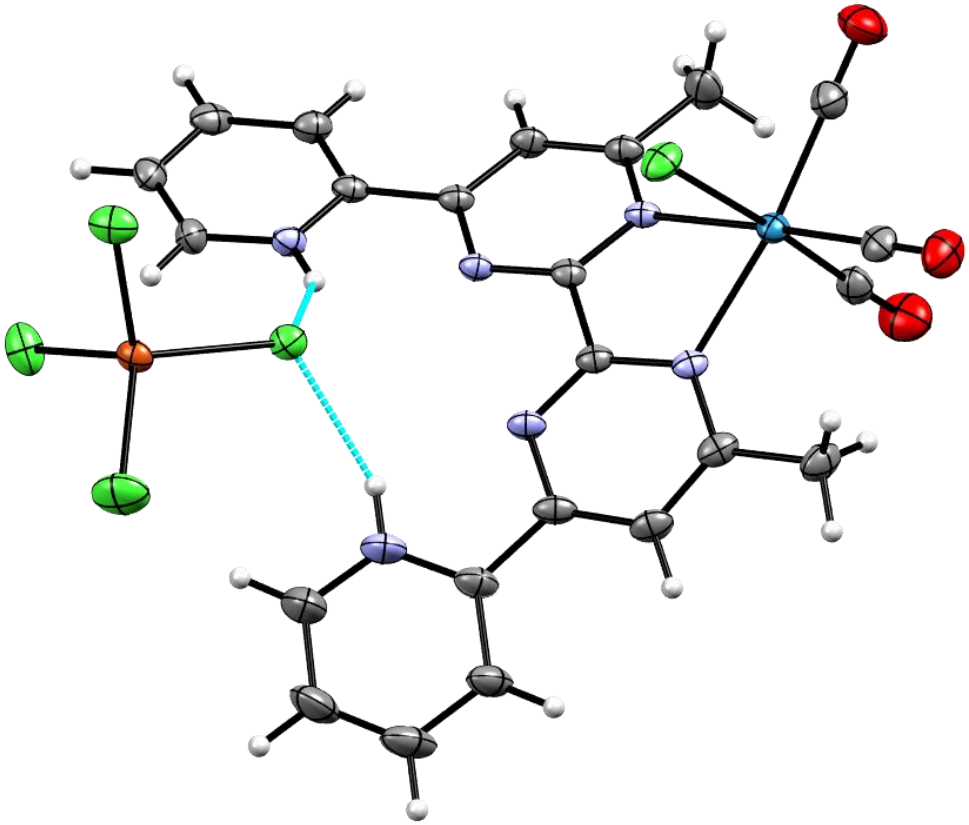

Compound Reference	*cent*-**L**^{1}ReCl(CO)$_3$.[CuCl$_4$]$^-$
Chemical Formula	$C_{25}H_{22}Cl_8CuN_7O_5Re$
Formula Mass	1033.83
Crystal System	Monoclinic
a/Å	8.4427(2)
b/Å	23.1556(7)
c/Å	18.1885(4)
α/°	90
β/°	97.2172(11)
γ/°	90
Unit cell volume/Å^3	3527.60(16)
Temperature/K	150(2)
Space group	P 21/n
No. of formula units per unit cell, *Z*	4
Radiation type	Mo K\α

Absorption coefficient, μ/mm^{-1}	4.684
No. of reflections measured	50332
No. of independent reflections	13479
R_{int}	0.0713
Final R_1 values ($I>2\sigma(I)$)	0.0559
Final $wR(F^2)$ values ($I>2\sigma(I)$)	0.0870
Final R_1 values (all data)	0.1059
Final $wR(F^2)$ values (all data)	0.1010
Goodness of fit on F^2	1.067

No additional restraints, constraints or additional solvent masking was required for the *ter*-**L**^{1}Re(CO)$_3$(H$_2$O).(CF$_3$SO$_3$) crystal structure.

Crystal structure information for $[Zn_4(\mathbf{L^2})_4]^{8+}$:

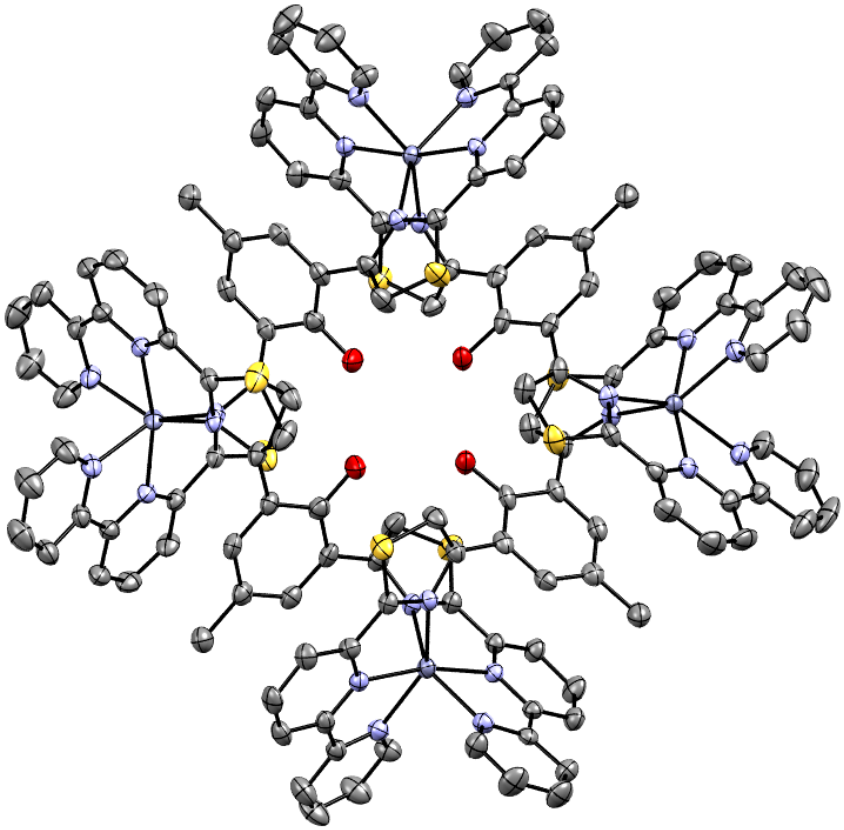

Compound Reference	$[Zn_4(\mathbf{L^2})_4]^{8+}$
Chemical Formula	$C_{156}H_{112}F_{24}N_{32}O_{28}S_{16}Zn_4$
Formula Mass	4113.22
Crystal System	Monoclinic
a/Å	32.2354(15)
b/Å	21.4761(10)
c/Å	24.9500(11)
α/°	90
β/°	98.9450(10)
γ/°	90
Unit cell volume/Å^3	17062.6(14)
Temperature/K	150(2)
Space group	C 1 2/c 1
No. of formula units per unit cell, *Z*	4
Radiation type	Mo K\α

Absorption coefficient, μ/mm^{-1}	0.858
No. of reflections measured	81406
No. of independent reflections	21309
R_{int}	0.0764
Final R_1 values ($I>2\sigma(I)$)	0.0705
Final $wR(F^2)$ values ($I>2\sigma(I)$)	0.1658
Final R_1 values (all data)	0.1460
Final $wR(F^2)$ values (all data)	0.2002
Goodness of fit on F^2	1.031

In $[[Zn_4(\mathbf{L^2})_4]^{8+}$, the trifluoromethanesulfonate counter ions and acetonitrile solvent molecules were disordered and consequently refined poorly. As a result they were constrain using *DELU*, *SIMU*, *SADI* and *ISOR*. In some cases, the trifluoromethanesulfonate counter ions were also modelled over two positions using the *PART* instruction. After wards, the crystal structure refined to an acceptable level.

Crystal structure information for $[Zn_5(\mathbf{L^3})_5]^{10+}$:

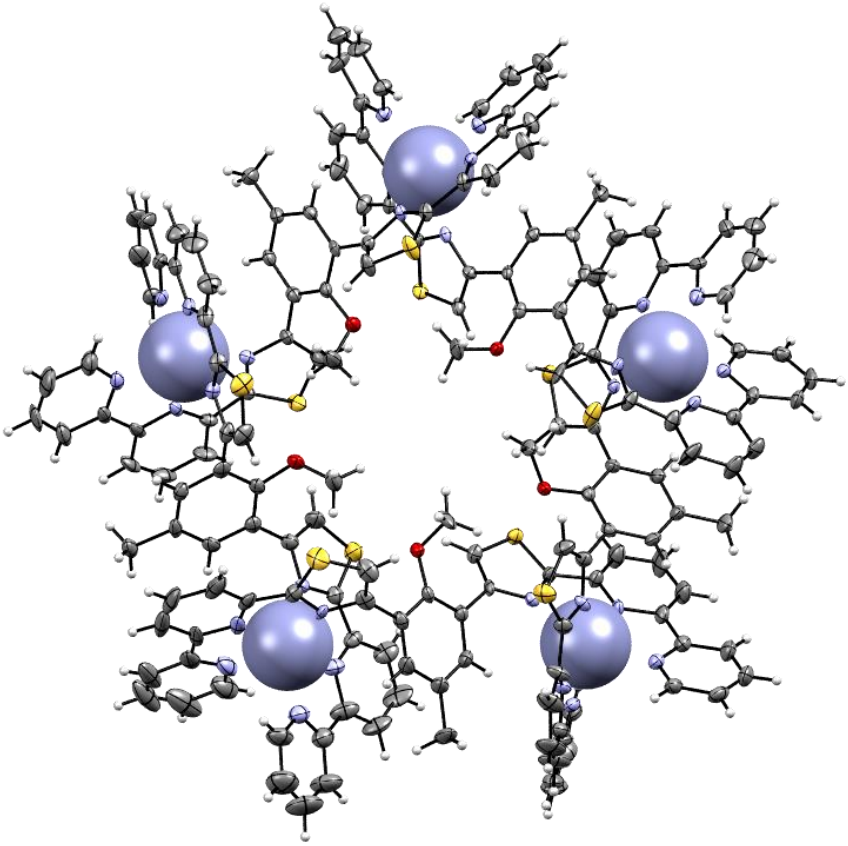

Compound Reference	$[Zn_5(\mathbf{L^3})_5]^{10+}$
Chemical Formula	$C_{182}H_{134}Cl_{10}N_{36}O_{45}S_{10}Zn_5$
Formula Mass	4547.47
Crystal System	Triclinic
a/Å	12.3813(3)
b/Å	25.0840(7)
c/Å	34.1153(9)
α/°	82.1769(13)
β/°	83.8251(13)
γ/°	81.9354(14)
Unit cell volume/Å^3	10350.5(5)
Temperature/K	150(2)
Space group	P -1
No. of formula units per unit cell, *Z*	2

Radiation type	Cu K\α
Absorption coefficient, μ/mm^{-1}	3.477
No. of reflections measured	133646
No. of independent reflections	35980
R_{int}	0.0979
Final R_1 values (I>2σ(I))	0.1098
Final wR(F^2) values (I>2σ(I))	0.2977
Final R_1 values (all data)	0.1333
Final wR(F^2) values (all data)	0.3228
Goodness of fit on F^2	1.2704

In $[[Zn_5(\mathbf{L^3})_5]^{10+}$, the perchlorate counter ions and acetonitrile solvent molecules were disordered and consequently refined poorly. As a result they were constrained using *DELU*, *SIMU*, *SADI* and *ISOR*. In some cases, the perchlorate counter ions were also modelled over two positions using the *PART* instruction. Furthermore, the structure contained disorder that could not be satisfactorily modelled and as a result the diffuse electron density was removed using the solvent mask facility in Olex2, resulting in voids in the crystal structure.[93] The solvent mask removed a total of 348.5 electrons in the unit cell (174.25 per asymmetric unit) which corresponds to 8 molecules of acetonitrile in the asymmetric unit (16 in the unit cell).

Crystal structure information for $[Cu_5(\mathbf{L^4})_5]^{10+}$:

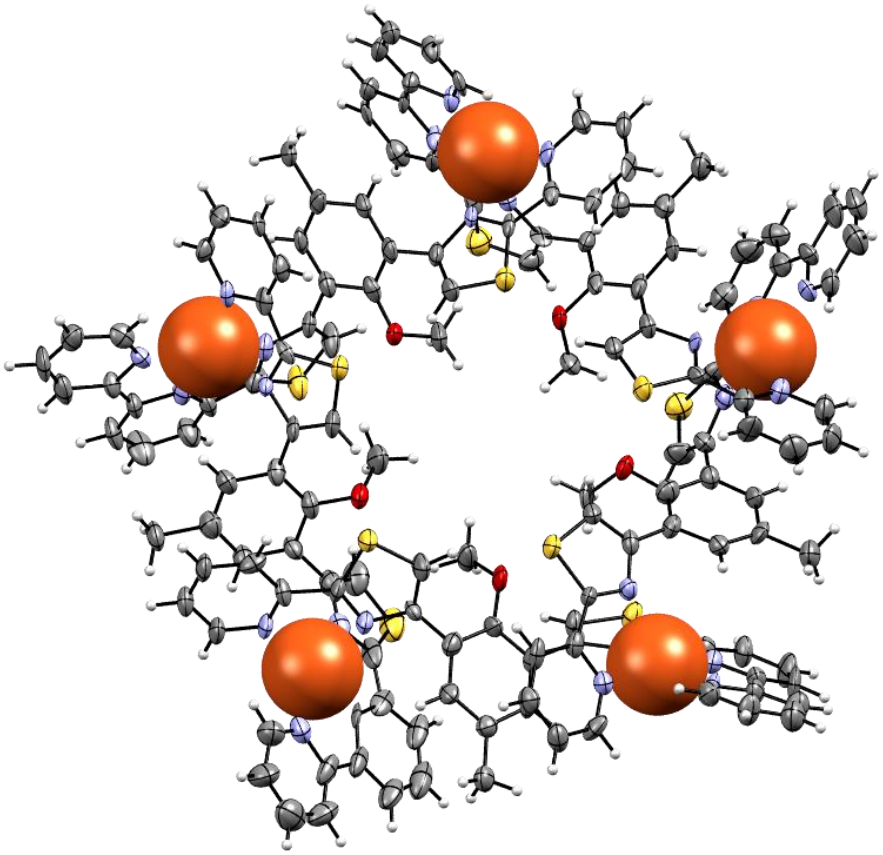

Compound Reference	$[Cu_5(\mathbf{L^4})_5]^{10+}$
Chemical Formula	$C_{152}H_{104}Cl_9Cu_5N_{27}O_{41}S_{10}$
Formula Mass	3922.54
Crystal System	Monoclinic
a/Å	21.1788(4)
b/Å	21.9244(5)
c/Å	39.9063(7)
α/°	90
β/°	103.826(1)
γ/°	90
Unit cell volume/Å^3	17992.9(6)
Temperature/K	150(2)
Space group	P 1 21/n 1
No. of formula units per unit cell, *Z*	4

Radiation type	Cu K\α
Absorption coefficient, μ/mm^{-1}	3.648
No. of reflections measured	49839
No. of independent reflections	18482
R_{int}	0.0805
Final R_1 values (I>2σ(I))	0.1160
Final wR(F^2) values (I>2σ(I))	0.3007
Final R_1 values (all data)	0.1447
Final wR(F^2) values (all data)	0.3265
Goodness of fit on F^2	1.2934

In $[[Cu_5(\mathbf{L}^4)_5]^{10+}$, the perchlorate counter ions and acetonitrile solvent molecules were disordered and consequently refined poorly. As a result they were constrained using *DELU*, *SIMU*, *SADI* and *ISOR*. In some cases, the perchlorate counter ions were also modelled over two positions using the *PART* instruction. Furthermore, the structure contained disorder that could not be satisfactorily modelled and as a result the diffuse electron density was removed using the solvent mask facility in Olex2, resulting in voids in the crystal structure.[93] The solvent mask removed a total of 784 electrons in the unit cell (196 per asymmetric unit) which corresponds to 36 molecules of acetonitrile in the asymmetric unit (9 in the unit cell).

Crystal structure information for $[Ag_2(\mathbf{L^5})_2]^{2+}$:

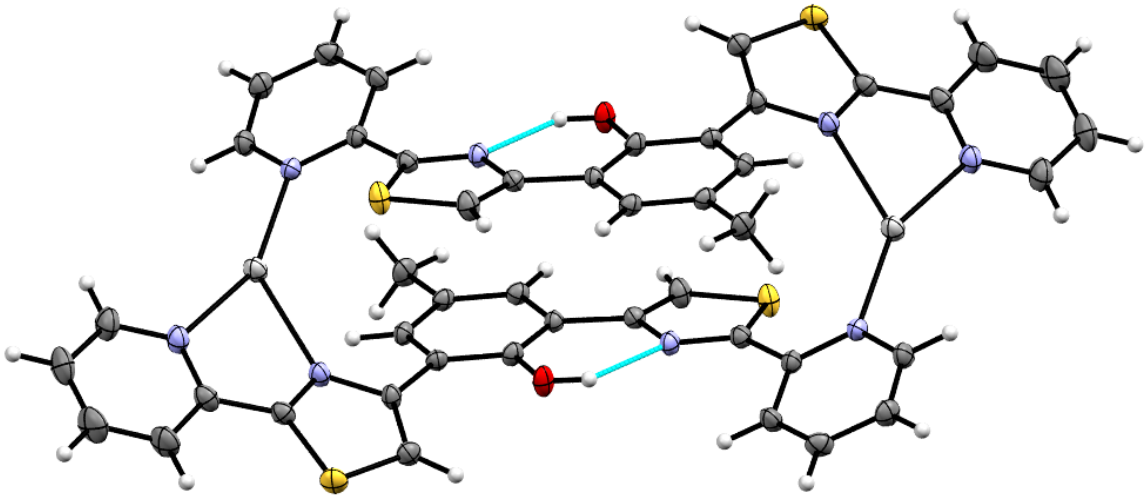

Compound Reference	$[Ag_2(\mathbf{L^5})_2]^{2+}$
Chemical Formula	$C_{48}H_{34}Ag_2Cl_8N_8O_{10}S_4$
Formula Mass	1510.47
Crystal System	Triclinic
a/Å	7.5797(2)
b/Å	10.6965(3)
c/Å	17.3538(5)
α/°	103.551(1)
β/°	101.676(1)
γ/°	90.482(1)
Unit cell volume/Å^3	1337.20(7)
Temperature/K	150(2)
Space group	P -1
No. of formula units per unit cell, *Z*	1
Radiation type	Mo K\α
Absorption coefficient, μ/mm^{-1}	1.356
No. of reflections measured	31041
No. of independent reflections	8127
R_{int}	0.0438
Final R_1 values ($I>2\sigma(I)$)	0.0502

Final $wR(F^2)$ values ($I>2\sigma(I)$)	0.1506
Final R_1 values (all data)	0.0717
Final $wR(F^2)$ values (all data)	0.1692
Goodness of fit on F^2	1.1530

No added restraints, constraints or additional solvent masking was required for the $[Ag_2(L^1)_2]^{2+}$ crystal structure.

Crystal structure information for $[Ag_n(\mathbf{L^6})_n]^{n+}$:

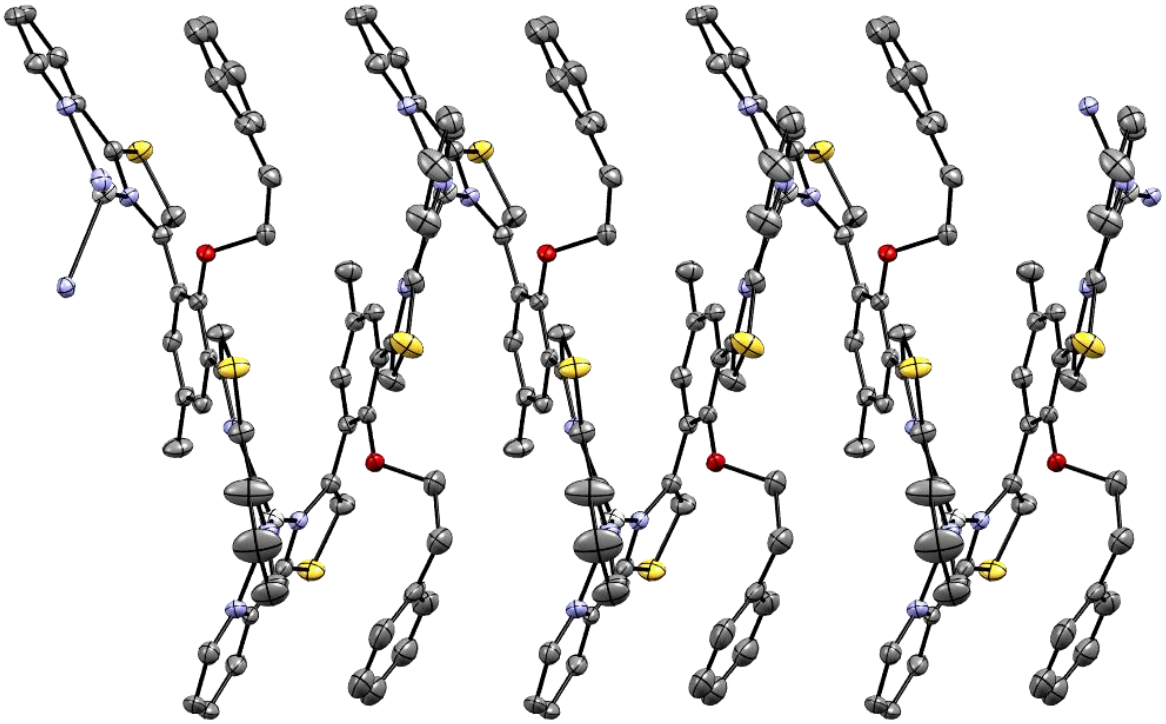

Compound Reference	$[Ag_n(\mathbf{L^6})_n]^{n+}$
Chemical Formula	$C_{127}H_{105}Ag_4B_4F_{16}N_{19}O_{10}S_8$
Formula Mass	3092.64
Crystal System	Triclinic
a/Å	7.820(4)
b/Å	18.768(9)
c/Å	25.836(12)
α/°	80.419(16)
β/°	82.135(19)
γ/°	83.58(3)
Unit cell volume/Å^3	3688(3)
Temperature/K	150
Space group	P -1
No. of formula units per unit cell, *Z*	1
Radiation type	Mo K\α

Absorption coefficient, μ/mm^{-1}	0.715
No. of reflections measured	101583
No. of independent reflections	18387
R_{int}	0.0990
Final R_1 values ($I>2\sigma(I)$)	0.0616
Final $wR(F^2)$ values ($I>2\sigma(I)$)	0.1758
Final R_1 values (all data)	0.0989
Final $wR(F^2)$ values (all data)	0.1933
Goodness of fit on F^2	1.1969

For $[Ag_n(\mathbf{L^6})_n]^{n+}$ the tetrafluoroborate counter anions were disordered and these were modelled in two positions using the *PART* instruction. In all cases of disordered atoms/molecules *DELU*, *SIMU*, *SADI*, and in some cases *ISOR*, constraints were used in the lest-squares refinement. Furthermore, the structure contained disorder that could not be satisfactorily modelled and as a result the diffuse electron density was removed using the solvent mask facility in Olex2, resulting in voids in the crystal structure.[93] The solvent mask removed a total of 208.9 electrons in the unit cell which corresponds to five molecules of nitromethane and a molecule of diisopropyl ether in the unit cell.

Crystal structure information for $[[Ag_6(\mathbf{L^7})_6]^{6+}]_n$:

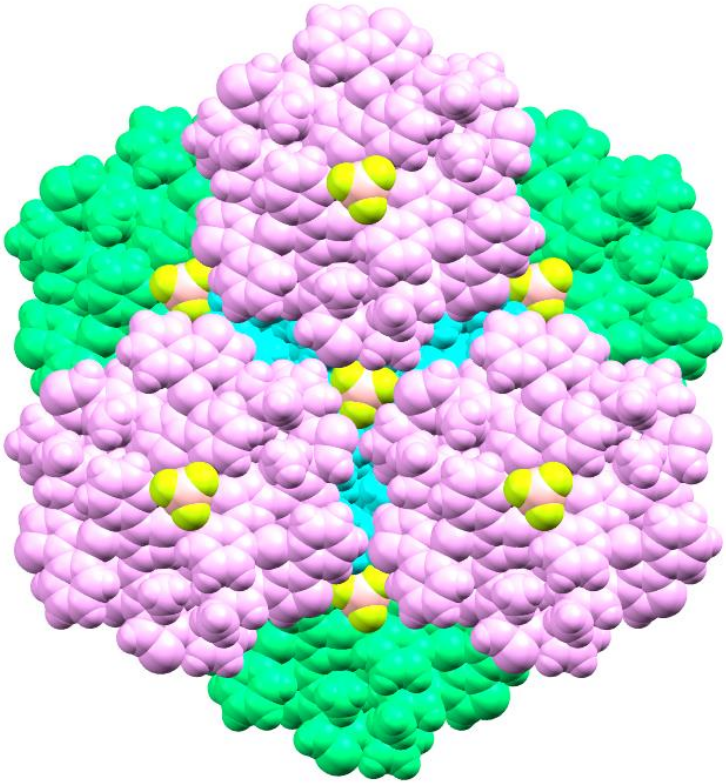

Compound Reference	$[Ag_6(\mathbf{L^7})_6]^{6+}$
Chemical Formula	$C_{144}H_{108}Ag_6B_5F_{20}N_{24}O_6S_{12}$
Formula Mass	3736.71
Crystal System	Trigonal
a/Å	26.047(11)
b/Å	26.047(11)
c/Å	41.751(2)
α/°	90
β/°	90
γ/°	120
Unit cell volume/Å^3	24530.9(19)
Temperature/K	150(2)
Space group	R -3 c
No. of formula units per unit cell, *Z*	6
Radiation type	Mo K\α
Absorption coefficient, μ/mm^{-1}	0.939

No. of reflections measured	41376
No. of independent reflections	8294
R_{int}	0.0510
Final R_1 values ($I>2\sigma(I)$)	0.0548
Final $wR(F^2)$ values ($I>2\sigma(I)$)	0.1450
Final R_1 values (all data)	0.0983
Final $wR(F^2)$ values (all data)	0.1712
Goodness of fit on F^2	1.0673

In $[[Ag_6(\mathbf{L^7})_6]^{6+}]_n$, one of the tetrafluoroborate counter anions was disordered and as a consequence refined poorly. It was constrained using *DELU*, *SIMU*, *SADI* and *ISOR* and its occupancy was fixed to 10.50. Using this, the molecule refined reasonably well. Due to this the occupancy of the counter anions is low (e.g. six silver ions and five tetrafluoroborate anions) however, the valence of the cation is not in any doubt and the structure refined well using this value. Furthermore, the structure contained disorder that could not be satisfactorily modelled and as a result the diffuse electron density was removed using the solvent mask facility in Olex2, resulting in voids in the crystal structure.[93] The solvent mask removed a total of 644.3 electrons in the unit cell (107.4 per asymmetric unit) which corresponds to five molecules of acetonitrile in the asymmetric unit (30 in the unit cell).

Crystal structure information for $[Cu_6(\mathbf{L^7})_6]^{6+}$:

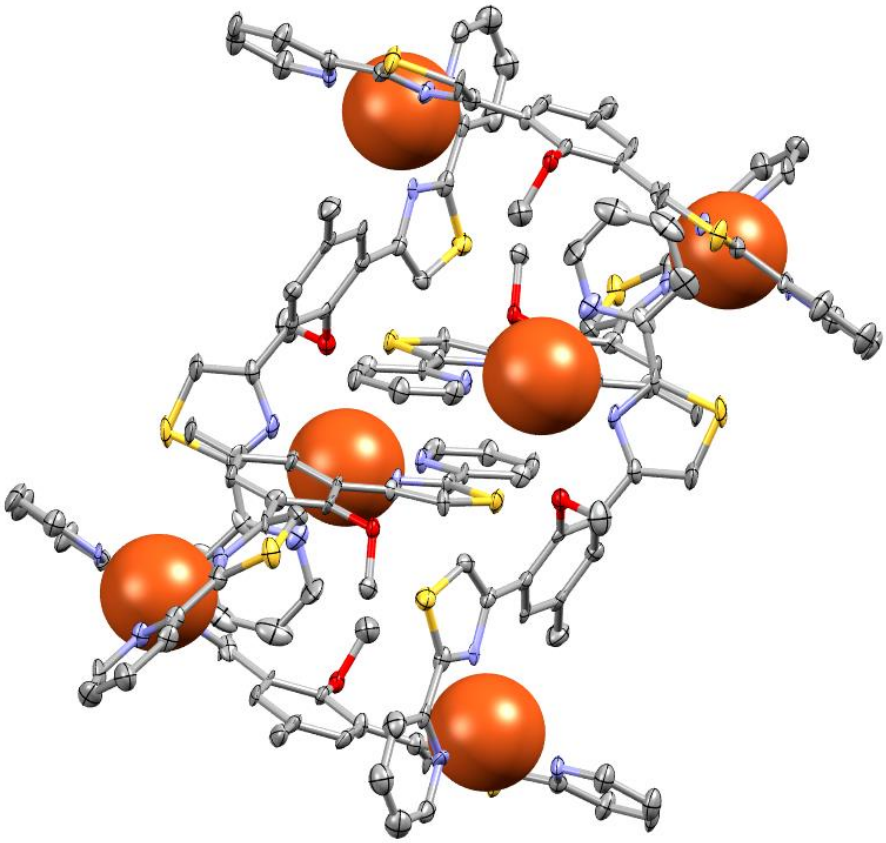

Compound Reference	$[Cu_6(\mathbf{L^7})_6]^{6+}$
Chemical Formula	$C_{144}H_{108}Cu_6N_{24}O_6S_{12}$
Formula Mass	578.55
Crystal System	monoclinic
a/Å	20.535(8)
b/Å	16.370(4)
c/Å	26.427(8)
α/°	90
β/°	99.04(2)
γ/°	90
Unit cell volume/Å^3	8773(5)
Temperature/K	150(2)
Space group	P 1 21/c 1
No. of formula units per unit cell, Z	14

Radiation type	Cu K\α
Absorption coefficient, μ/mm^{-1}	3.586
No. of reflections measured	47709
No. of independent reflections	9348
R_{int}	0.1166
Final R_1 values (I>2σ(I))	0.1010
Final $wR(F^2)$ values (I>2σ(I))	0.2063
Final R_1 values (all data)	0.1481
Final $wR(F^2)$ values (all data)	0.2315
Goodness of fit on F^2	1.1106

In $[Cu_6(\mathbf{L^7})_6]^{6+}$, one of the trifluoromethanesulfonate counter anions was disordered and as a consequence refined poorly. The disordered atoms were constrained using *DELU*, *SIMU* and *ISOR* and as a result, the molecule refined to an acceptable level.